

# MEASURING THE SUPERMASSIVE BLACK HOLE PARAMETERS FROM SPACE

• Александр Федорович Захаров  
(Alexander Fyodorovich Zakharov)

E-mail: zakharov@itep.ru

- (1) *Institute of Theoretical and Experimental Physics, Moscow;*  
(2) *Astro Space Center of Lebedev Physics Institute of Russian Academy  
of Sciences, Moscow;*

**12th Regional Conference on Mathematical Physics**  
**Islamabad, Pakistan, April 1, 2006**

SEARCH

Go

Advanced search

MY ACCOUNT E-ALERT

Home

News

Features

Columns & blogs

Archive

Archive

Specials

In focus

- X chromosome
- Future computing
- Stem cells
- Bird flu
- Mars
- GM crops

Stories by subject

NEWS CHANNELS

- My news
- Biotechnology
- Careers
- Drug discovery
- Earth and environment
- Medical Research
- Physical Sciences

Feedback

About this site

About us

For librarians

TOP STORIES

Air pollution influences crop disease  
04 April 2005

Hunters win hike in polar bear quota  
04 April 2005

Genetic patch treats 'bubble-boy' disease  
03 April 2005

Transgenic cows have

## NEWS

Published online: 31 March 2005; | doi:10.1038/news050328-8

### Black holes 'do not exist'

Philip Ball

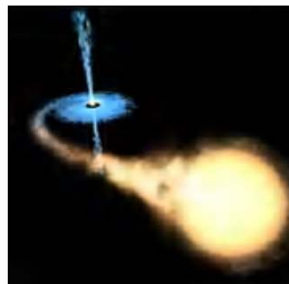
#### These mysterious objects are dark-energy stars, physicist claims.

Black holes are staples of science fiction and many think astronomers have observed them indirectly. But according to a physicist at the Lawrence Livermore National Laboratory in California, these awesome breaches in space-time do not and indeed cannot exist.

Over the past few years, observations of the motions of galaxies have shown that some 70% the Universe seems to be composed of a strange 'dark energy' that is driving the Universe's accelerating expansion.

George Chapline thinks that the collapse of the massive stars, which was long believed to generate black holes, actually leads to the formation of stars that contain dark energy. "It's a near certainty that black holes don't exist," he claims.

Black holes are one of the most celebrated predictions of Einstein's general theory of relativity, which explains gravity as the warping of space-time caused by massive objects. The theory suggests that



Black holes, such as the one pictured in this artist's impression, may in fact be pockets of 'dark energy'.

© ESA/NASA

a sufficiently massive star, when it dies, will collapse under its own gravity to a single point.

But Einstein didn't believe in black holes, Chapline argues. "Unfortunately", he adds, "he couldn't articulate why." At the root of the problem is the other revolutionary theory of twentieth-century physics, which Einstein also helped to formulate: quantum mechanics.

**“It's a near certainty that black holes don't exist.”**

George Chapline  
Lawrence Livermore National Laboratory

In general relativity, there is no such thing as a 'universal time' that makes clocks tick at the same rate everywhere. Instead, gravity makes clocks run at different rates in

different places. But quantum mechanics, which describes physical phenomena at infinitesimally small scales, is meaningful only if time is universal; if not, its equations make no sense.

This problem is particularly pressing at the boundary, or event horizon, of a black hole. To a far-off observer, time seems to stand still here. A spacecraft falling into a black hole would seem, to someone watching it from afar, to be stuck forever at the event horizon, although the astronauts in the spacecraft would feel as if they were continuing to fall. "General relativity predicts that nothing happens at the event horizon," says Chapline.

### Quantum transitions

However, as long ago as 1975 quantum physicists argued that strange things do happen at an event horizon: matter governed by quantum laws becomes hypersensitive to slight disturbances. "The result was quickly forgotten," says Chapline, "because it didn't agree with the prediction of general relativity. But actually, it was absolutely correct."

This strange behaviour, he says, is the signature of a 'quantum phase transition' of space-time. Chapline argues that a star doesn't simply collapse to form a black hole; instead, the space-time inside it becomes filled with dark energy and this has some intriguing gravitational effects.

Outside the  
'surface' of a

ADVERTISEMENT

dark-energy star, it behaves much like a black hole, producing a strong gravitational tug. But inside, the 'negative' gravity of dark energy may cause matter to bounce back out again.

If the dark-energy star is big enough, Chapline predicts, any electrons bounced out will have been converted to positrons, which then annihilate other electrons in a burst of high-energy radiation. Chapline says that this could explain the radiation observed from the centre of our galaxy, previously interpreted as the signature of a huge black hole.

He also thinks that the Universe could be filled with 'primordial' dark-energy stars. These are formed not by stellar collapse but by fluctuations of space-time itself, like blobs of liquid condensing spontaneously out of a cooling gas. These, he suggests, could be stuff that has the same gravitational effect as normal matter, but cannot be seen: the elusive substance known as dark matter.



Register now for HUGO's 10th annual human genome meeting  
Deadline for abstracts  
January 21st 2005



[Click here for information on HGM2005](#)

## References

1. Chapline G. Arxiv,  
<http://xxx.arxiv.org/abs/astro-ph/0503200>  
(2005).

[▲ Top](#)

[▲ Top](#)

# Outline of my talk

- History
- Black holes in astrophysics
- The iron  $K_{\alpha}$  -line as a tool for BH characteristics
- Movies

# Outline of my talk

- Wrong pictures of black holes
- Mirages around BHs and retro-lensing
- Black Hole Images
- Conclusions

Rev. John Michell: *Phil. Trans. R. Soc. London*, 74, 35–57 (1784):

VII. *On the Means of discovering the Distance, Magnitude, &c.  
of the Fixed Stars, in consequence of the Diminution of the  
Velocity of their Light, in case such a Diminution should be  
found to take place in any of them, and such other Data should be  
procured from Observations, as would be farther necessary for  
that Purpose.* By the Rev. John Michell, B. D. F. R. S.  
*In a Letter to Henry Cavendish, Esq. F. R. S. and A. S.*

Read November 27, 1783.

Rev. John Michell: *Phil. Trans. R. Soc. London*, **74**, 35–57 (1784):

42

*Mr. MICHELL on the Means of discovering the*

16. Hence, according to article 10, if the semi-diameter of a sphære of the same density with the sun were to exceed that of the sun in the proportion of 500 to 1, a body falling from an infinite height towards it, would have acquired at its surface a greater velocity than that of light, and consequently, supposing light to be attracted by the same force in proportion to its vis inertiarum, with other bodies, all light emitted from such a body would be made to return towards it, by its own proper gravity.

# Black hole history (I)

- 1783 : The Reverend John Michell (invisible sphere)
- 1798,1799 : P.S. Laplace (Exposition du Systeme du Monde Part II, p. 305, Allgemeine Geographifche Ephemeriden, 4, S.1, 1799)
- 1915 : K. Schwarzschild
- 1928 : Ya.I Frenkel (EOS for degenerate electron Fermi-gas with arbitrary relativistic degree and typical WD masses)
- 1930 : E. Stoner (the upper limit for masses of white dwarfs for uniform mass distribution)
- 1931 : S. Chandrasekhar (the upper limit for masses of white dwarfs for polytrope mass distribution)
- 1932 : E. Stoner (EOS for degenerate electron Fermi-gas with arbitrary relativistic degree)
- 1934, 1935 : S. Chandrasekhar (the upper limit for masses of white dwarfs for arbitrary relativistic degree)
- 1935 : A.Eddington (rejections of the upper limit for WDs)
- 1939 : R.Oppenheimer & G.Volkoff (the upper limit for NSs and the GR approach)
- 1939 : R.Oppenheimer & R.Snyder (the collapse of pressureless stars and the GR approach) “Every statement of this paper is in accordance with ideas that remain valid today”(Novikov & Frolov, 2001)

# Black hole history (II)

- 1939: Einstein considered a possibility “to create a field having Schwarzschild singularity by gravitating masses”;
- Einstein (1939): “The main result of this investigation is a clear understanding that Schwarzschild singularities do not exits in real conditions”;
- 1942: Bergmann:” In reality, mass has no possibility to concentrate by the following way that the Schwarzschild singular surface would be in vacuum”
- 1958 : D. Finkelstein & 1960 M.Kruskal (causal structure of Schwarzschild metric)
- 1962 : R. Feynman “Lectures on gravitation” (“it would be interesting to investigate dust collapse” (23 years later OS paper!))
- 1967 : J.A. Wheeler: black holes predicted to result from “continued gravitational collapse of over-compact masses” (the birth of the BH concept)

Таблица 5. Параметры двойных систем с ЧД

Система	Спектр оптической звезды	$P_{\text{орб}}$ , сут	$f_v(m)$ , в $M_\odot$	$m_x$ , в $M_\odot$	$m_v$ , в $M_\odot$	$V_{\text{pec}}$ , км с $^{-1}$	Примечание
Cyg X-1	O 9,7 Iab	5,6	$0,24 \pm 0,01$	$16 \pm 5$	$33 \pm 9$	$2,4 \pm 1,2$	Стационарная
V 1357 Cyg							
LMC X-3	B3 Ve	1,7	$2,3 \pm 0,3$	$9 \pm 2$	$6 \pm 2$	—	Стационарная
LMC X-1	O (7–9) III	4,2	$0,14 \pm 0,05$	$7 \pm 3$	$22 \pm 4$	—	Стационарная
A0 620–00 (V616 Mon)	K5 V	0,3	$2,91 \pm 0,08$	$10 \pm 5$	$0,6 \pm 0,1$	$-15 \pm 5$	Транзиентная
GS 2023+338 (V404 Cyg)	K0 IV	6,5	$6,08 \pm 0,06$	$12 \pm 2$	$0,7 \pm 0,1$	$8,5 \pm 2,2$	Транзиентная
GRS 1124–68 (GU Mus)	K2 V	0,4	$3,01 \pm 0,15$	$6(+5 - 2)$	$0,8 \pm 0,1$	$25 \pm 5$	Транзиентная
GS 2000+25 (QZ Vul)	K5 V	0,3	$4,97 \pm 0,10$	$10 \pm 4$	$0,5 \pm 0,1$	—	Транзиентная
GRO J0422+32 (V518 Per)	M2 V	0,2	$1,13 \pm 0,09$	$10 \pm 5$	$0,4 \pm 0,1$	—	Транзиентная
GRO J1655–40 (XN Sco 1994)	F5 IV	2,6	$2,73 \pm 0,09$	$6,3 \pm 0,5$	$2,4 \pm 0,4$	$-114 \pm 19$	Транзиентная
H 1705–250 (V2107 Oph)	K5 V	0,5	$4,86 \pm 0,13$	$6 \pm 1$	$0,4 \pm 0,1$	$38 \pm 20$	Транзиентная
4U 1543–47 (HL Lup)	A2 V	1,1	$0,22 \pm 0,02$	$4,0 - 6,7$	$\sim 2,5$	—	Транзиентная
GRS 1009–45 (MM Vel)	(K6–M0) V	0,3	$3,17 \pm 0,12$	$3,6 - 4,7$	$0,5 - 0,7$	—	Транзиентная
SAX J1819.3–2525 (V4641 Sgr)	B9 III	2,8	$2,74 \pm 0,12$	$9,61(+2,08 - 0,88)$	$6,53(+1,6 - 1,03)$	—	Транзиентная
XTE J1118+480	(K7–M0) V	0,17	$6,1 \pm 0,3$	$6,0 - 7,7$	$0,09 - 0,5$	$145^*$	Транзиентная
GRS 1915+105	(K–M) III	33,5	$9,5 \pm 3,0$	$14 \pm 4$	$1,2 \pm 0,2$		Транзиентная

**Таблица 6.** Микреквазары в нашей Галактике

Название источника	Компактный объект	$V_{\text{джета}}$
GRS 1915 + 105	ЧД	$0,92c - 0,98c$
GRO J1655 - 40	ЧД	$0,92c$
XTE J1748 - 288	ЧД	$0,93c - 0,23c$
SS 433	ЧД	$0,26c$
Cyg X-3	ЧД	$\sim 0,3c - \geq 0,8c$
CI Cam	НЗ?	$\sim 0,15c$
Sco X-1	НЗ	$\sim 0,5c$
Cir X-1	НЗ	$\geq 0,1c$
1E 1740.7 - 2942	ЧД	
GRS 1758 - 258	ЧД	
SAX J1819.3 - 2525	ЧД	$\geq 0,95c$
LS 5039	?	$\geq 0,15c$
Cyg X-1	ЧД	$> 0,6c$
XTE J1550 - 564	ЧД	

• •  
Ho2

Black holes in centers of galaxies

(L.Ho,ApJ 564,120 (2002))

TABLE 1: GALAXIES WITH BLACK HOLE MASSES

Galaxy Name (1)	Hubble Type (2)	<i>T</i> (3)	Spectral Class (4)	<i>cz</i> (km s <sup>-1</sup> ) (5)	<i>D</i> (Mpc) (6)	Ref. (7)	<i>M</i> <sub>BH</sub> ( <i>M</i> <sub>⊙</sub> ) (8)	Method (9)	Ref. (10)
3C 120 (Mrk 1506)	S0:	-1.0	S1	9896	137.8	1	$2.3 \times 10^7$	R	1
3C 390.3 (VII w 838)	E?	-5.0	S1	16818	241.2	1	$3.4 \times 10^8$	R	1
Ark 120 (Mrk 1095)	S0/a	0.0	S1	9682	134.6	1	$1.84 \times 10^8$	R	1
Arp 102B	E0	-5.0	L1.8	7245	99.7	1	$2.2 \times 10^8$	G	2
Circinus	Sb:	3.0	S2	449	4.0	2	$1.3 \times 10^6$	M	3
Fairall 9	S?	...	S1	14095	199.8	1	$8.0 \times 10^7$	R	1
IC 342	SABcd	6.0	H	31	1.8	3	$<5.0 \times 10^5$	S	4
IC 1459	E3	-5.0	L2	1691	29.2	4	$3.7 \times 10^8$	G	5
IC 4329A	S0+	-1.0	S1	4813	65.5	1	$5.0 \times 10^6$	R	1
Milky Way	Sbc	3.0	...	...	0.008	5	$2.95 \times 10^6$	S	6
Mrk 79 (UGC 3973)	SBb	3.0	S1.5	6652	91.3	1	$5.2 \times 10^7$	R	1
Mrk 110	Pair?	...	S1	10580	147.7	1	$5.6 \times 10^6$	R	1
Mrk 279 (UGC 8823)	S0	-1.0	S1.5	9129	126.6	1	$4.2 \times 10^7$	R	1
Mrk 335	S0/a	0.0	S1.0	7730	106.6	1	$6.3 \times 10^6$	R	7
Mrk 509	comp	...	S1	10312	143.8	1	$5.78 \times 10^7$	R	1
Mrk 590 (NGC 863)	Sa:	1.0	S1.2	7910	109.2	1	$1.78 \times 10^7$	R	1
Mrk 817 (UGC 9412)	S?	...	S1.5	9430	131.0	1	$4.4 \times 10^7$	R	1
NGC 205 (M110)	dE5	-5.0	A	-241	0.74	6	$<9.3 \times 10^4$	S	8
NGC 221 (M32)	E2	-6.0	A	-145	0.81	4	$3.9 \times 10^6$	S	9
NGC 224 (M31)	Sb	3.0	A	-300	0.76	4	$3.3 \times 10^7$	S	10

NGC 224 (M31)	Sb	3.0	A	-300	0.76	4	$3.3 \times 10^7$	S	10
NGC 598 (M33)	Scd	6.0	H	-179	0.87	6	$<1.5 \times 10^3$	S	11
NGC 821	E6?	-5.0	A	1735	24.1	4	$5.0 \times 10^7$	S	12
NGC 1023	SB0-	-3.0	A	637	11.4	4	$3.9 \times 10^7$	S	13
NGC 1068 (M77)	Sb	3.0	S1.9	1137	14.4	7	$1.6 \times 10^7$	M	14
NGC 2778	E	-5.0	...	2049	22.9	4	$2.0 \times 10^7$	S	12
NGC 2787	SB0+	-1.0	L1.9	696	7.5	4	$3.9 \times 10^7$	G	15
NGC 3031 (M81)	Sab	2.0	S1.5	-34	3.9	4	$6.3 \times 10^7$	S	16
NGC 3115	S0-	-3.0	A	720	9.7	4	$9.1 \times 10^8$	S	17
NGC 3227	SABa	1.0	S1.5	1157	20.6	7	$3.9 \times 10^7$	R	1
NGC 3245	S0?	-2.0	T2	1358	20.9	4	$2.1 \times 10^8$	G	18
NGC 3377	E5+	-5.0	A	665	11.2	4	$1.0 \times 10^8$	S	12
NGC 3379 (M105)	E1	-5.0	L2/T2:	911	10.6	4	$1.0 \times 10^8$	S	19
NGC 3384	SB0-:	-3.0	A	704	11.6	4	$1.8 \times 10^7$	S	12
NGC 3516	SB0:	-2.0	S1.2	2649	38.9	7	$2.3 \times 10^7$	R	7
NGC 3608	E2	-5.0	L2/S2:	1253	22.9	4	$1.1 \times 10^8$	S	12
NGC 3783	SBa	1.0	S1	2917	38.5	7	$9.4 \times 10^6$	R	1
NGC 3998	S0?	-2.0	L1.9	1040	14.1	4	$5.6 \times 10^8$	S	16
NGC 4051	SABbc	4.0	S1.2	725	17.0	7	$1.3 \times 10^6$	R	1
NGC 4151	SABab	2.0	S1.5	995	20.3	7	$1.53 \times 10^7$	R	1
NGC 4203	SAB0	-3.0	L1.9	1086	14.1	4	$<1.2 \times 10^7$	G	15
NGC 4258 (M106)	SABbc	4.0	S1.9	448	7.3	4	$4.1 \times 10^7$	M	20
NGC 4261 (3C 270)	E2+	-5.0	L2	2238	31.6	4	$5.2 \times 10^8$	G	21
NGC 4291	E	-5.0	A	1757	26.2	4	$1.5 \times 10^8$	S	12
NGC 4342	S0-	-3.0	...	751	16.8	7	$3.4 \times 10^8$	S	22
NGC 4374 (M84, 3C 272.1)	E1	-5.0	L2	1060	18.4	4	$1.6 \times 10^9$	G	23
NGC 4395	Sm:	9.0	S1.5	319	3.6	7	$<1.1 \times 10^5$	S	24
NGC 4459	S0+	-1.0	T2:	1210	16.1	4	$6.5 \times 10^7$	G	15
NGC 4473	E5	-5.0	A	2244	15.7	4	$1.0 \times 10^8$	S	12
NGC 4486 (M87, 3C 274)	E0+	-4.0	L2	1307	16.1	4	$3.4 \times 10^9$	G	25

Galaxy Name (1)	Hubble Type (2)	<i>T</i> (3)	Spectral Class (4)	<i>cz</i> (km s <sup>-1</sup> ) (5)	<i>D</i> (Mpc) (6)	Ref. (7)	<i>M</i> <sub>BH</sub> ( <i>M</i> <sub>⊙</sub> ) (8)	Method (9)	Ref. (10)
NGC 4486B	E0	-6.0	...	1555	16.1	8	6.0 ×10 <sup>8</sup>	S	26
NGC 4564	E	-5.0	A	1142	15.0	4	5.7 ×10 <sup>7</sup>	S	12
NGC 4593	SBb	3.0	S1	2698	39.5	7	8.1 ×10 <sup>6</sup>	R	7
NGC 4594 (M104)	Sa	1.0	L2	1024	9.8	4	1.1 ×10 <sup>9</sup>	S	27
NGC 4596	SB0	-1.0	L2::	1874	16.8	7	5.8 ×10 <sup>7</sup>	G	15
NGC 4649 (M60)	E2	-5.0	A	1117	16.8	4	2.0 ×10 <sup>9</sup>	S	12
NGC 4697	E6	-5.0	...	1241	11.7	4	1.2 ×10 <sup>8</sup>	S	12
NGC 4945	SBcd	6.0	S2	560	4.2	9	1.1 ×10 <sup>6</sup>	M	28
NGC 5548	S0/a	0.0	S1.5	5149	70.2	1	1.23×10 <sup>8</sup>	R	1
NGC 5845	E	-5.0	...	1456	25.9	4	3.2 ×10 <sup>8</sup>	S	12
NGC 6251	E0	-5.0	S2	6900	94.8	1	5.4 ×10 <sup>8</sup>	G	29
NGC 7052	E4	-5.0	...	4672	63.6	1	3.6 ×10 <sup>8</sup>	G	30
NGC 7457	S0-?	-3.0	A	812	13.2	4	3.4 ×10 <sup>6</sup>	S	12
NGC 7469	SABa	1.0	S1.0	4892	66.6	1	6.5 ×10 <sup>6</sup>	R	1
PG 0026+129	...	...	QSO	0.142	627.4	1	5.4 ×10 <sup>7</sup>	R	1
PG 0052+251	S	...	QSO	0.155	690.4	1	2.2 ×10 <sup>8</sup>	R	1
PG 0804+761	...	...	QSO	0.100	429.9	1	1.89×10 <sup>8</sup>	R	1
PG 0844+349	...	...	QSO	0.064	268.4	1	2.16×10 <sup>7</sup>	R	1
PG 0953+414	S	...	QSO	0.239	1118	1	1.84×10 <sup>8</sup>	R	1
PG 1211+143	...	...	QSO	0.085	361.7	1	4.05×10 <sup>7</sup>	R	1
PG 1226+023 (3C 273)	E	...	QSO	0.158	705.1	1	5.5 ×10 <sup>8</sup>	R	1
PG 1229+204	S	...	QSO	0.064	268.4	1	7.5 ×10 <sup>7</sup>	R	1
PG 1307+085	E	...	QSO	0.155	690.4	1	2.8 ×10 <sup>8</sup>	R	1
PG 1351+640	...	...	QSO	0.087	370.7	1	4.6 ×10 <sup>7</sup>	R	1
PG 1411+442	...	...	QSO	0.089	379.8	1	8.0 ×10 <sup>7</sup>	R	1
PG 1426+015 (Mrk 1383)	...	...	QSO	0.086	366.2	1	4.7 ×10 <sup>8</sup>	R	1
PG 1613+658 (Mrk 876)	...	...	QSO	0.129	565.3	1	2.41×10 <sup>8</sup>	R	1
PG 1617+175 (Mrk 877)	...	...	QSO	0.114	494.7	1	2.73×10 <sup>8</sup>	R	1
PG 1700+518	...	...	QSO	0.292	1406	1	6 ×10 <sup>7</sup>	R	1
PG 1704+608 (3C 351)	E	...	QSO	0.371	1857	1	3.7 ×10 <sup>7</sup>	R	1
PG 2130+099	...	...	QSO	0.061	255.3	1	1.44×10 <sup>8</sup>	R	1

NOTE.— Col. (1) Galaxy name. Col. (2) Revised Hubble type from de Vaucouleurs et al. 1991 (RC3), except for QSOs, which is estimated by Hamilton, Casertano, & Turnshek 2001. Col. (3) Morphological type index from the RC3. Col. (4) Spectral class of the nucleus from Ho et al. 1997, and otherwise from Whittle 1992a and NED, where A = absorption-line nucleus, H = H II nucleus, L = LINER, S = Seyfert, T = “transition object” (LINER/H II), 1 = type 1, 2 = type 2, and a fractional number between 1 and 2 denotes various intermediate types; uncertain and highly uncertain classifications are followed by a single and double colon, respectively. Col. (5) Heliocentric radial velocity (redshift for QSOs) from NED. Col. (6) Adopted distance. Col. (7) Reference for  $D$ . Col. (8) Black hole mass, scaled to our adopted distances. Col. (9) Method for determining  $M_{\text{BH}}$ : G, gas kinematics; M, maser kinematics; R, reverberation mapping; S, stellar kinematics. Col. (10) Reference for  $M_{\text{BH}}$ .

REFERENCES.— *Distance*: (1) Luminosity distance derived from heliocentric redshift,  $H_0 = 75 \text{ km s}^{-1} \text{ Mpc}^{-1}$ ,  $\Omega_M = 0.3$ , and  $\Omega_\lambda = 0.7$ ; (2) Freeman et al. 1977; (3) McCall 1989; (4) Tonry et al. 2001; (5) Reid 1993; (6) Ferrarese et al. 2000; (7) Tully 1988, who also uses our value of  $H_0$ ; (8) Assumed to be at the distance of NGC 4486; (9) Assumed to be at the distance of NGC 5128, which is known from Tonry et al. 2001.

REFERENCES.— *Black hole mass*: (1) Kaspi et al. 2000; (2) Newman et al. 1997; (3) Greenhill et al. 2000; (4) Böker, van der Marel, & Vacca 1999; (5) Verdoes Kleijn et al. 2000; (6) Genzel et al. 2000; (7) Ho 1999a; (8) Jones et al. 1996; (9) van der Marel et al. 1998; (10) Kormendy & Bender 1999; (11) Gebhardt et al. 2001; (12) Gebhardt et al. 2000a; (13) Bower et al. 2001a; (14) Greenhill et al. 1996; (15) Sarzi et al. 2001; (16) Bower et al. 2001b; (17) Emsellem, Dejonghe, & Bacon 1999; (18) Barth et al. 2001; (19) Gebhardt et al. 2000b; (20) Miyoshi et al. 1995; (21) Ferrarese, Ford, & Jaffe 1996; (22) Cretton & van den Bosch 1999; (23) Bower et al. 1998; (24) Filippenko & Ho 2001; (25) Macchetto et al. 1997; (26) Kormendy et al. 1997a; (27) Kormendy et al. 1997b; (28) Greenhill, Moran, & Herrnstein 1997; (29) Ferrarese & Ford 1999; (30) van der Marel & van den Bosch 1998.

- Macho\_96\_5\_light\_curve
- Macho\_96\_6\_light\_curve
- Likelihood functions for BH microlenses
- Probable masses and distances for BH microlenses

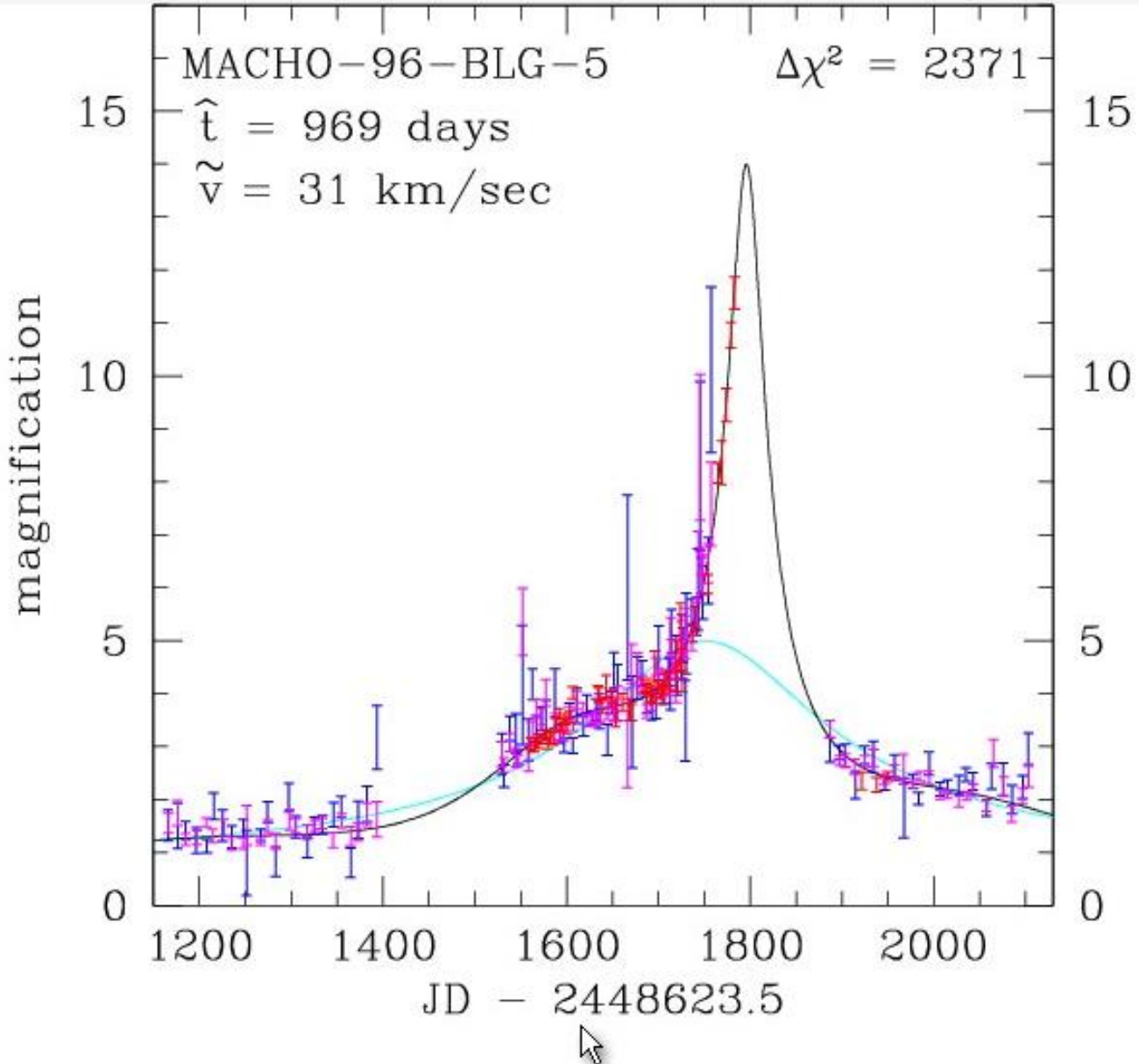


Fig. 7.— MACHO-96-BLG-5 lightcurves normalized to the unlensed flux of the lensed star. The MACHO red and blue data are plotted in magenta and blue, respectively, and the CTIO data are shown in red. The black curve is the parallax fit while the cyan curve is the best fit standard microlensing lightcurve. An additional 4 years of data showing very little photometric variation are not shown.

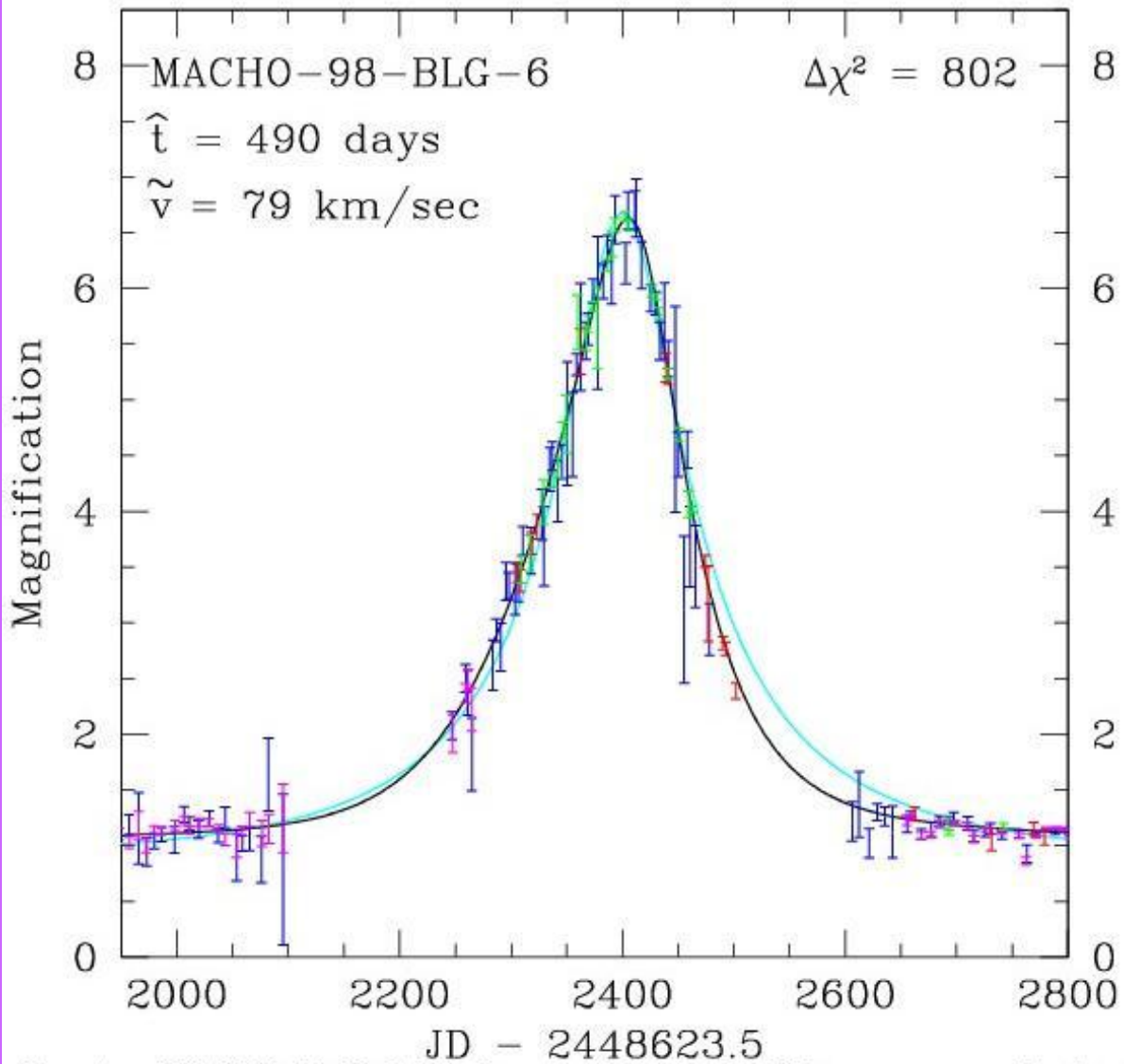


Fig. 4.— MACHO-98-BLG-6 lightcurve closeup with lightcurves normalized to the unlensed flux of the lensed star. The MACHO red and blue data are plotted in magenta and blue, respectively, the CTIO data are shown in red, and the MPS data are shown in green. The black curve is the parallax fit while the cyan curve is the best fit standard microlensing lightcurve. The gap in the MACHO red data during the day 2280-2650 interval is due to a CCD failure. An additional year of data showing no photometric variation is not shown.

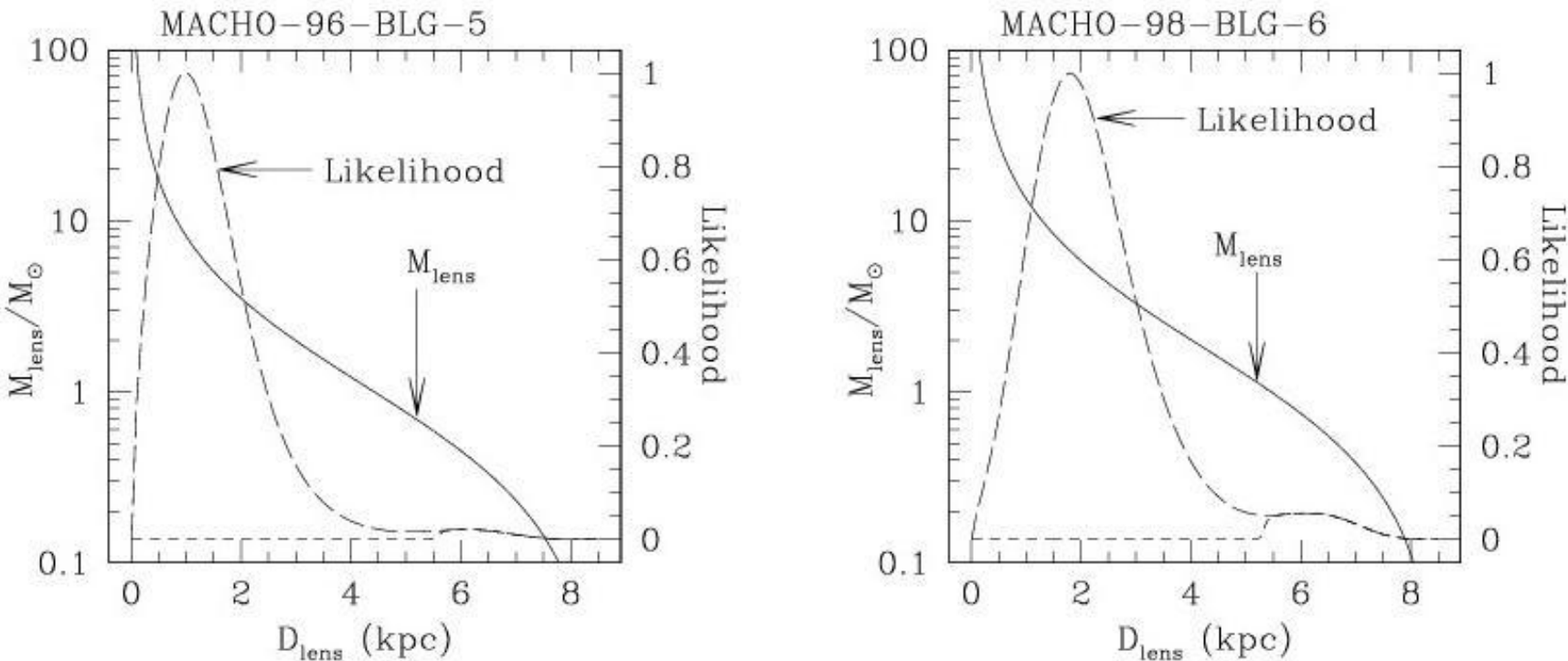


Fig. 11.— The mass vs. distance relations (solid curves) for our candidate black hole lenses are shown along with the likelihood functions (long dashed curves) computed assuming a standard model for the Galactic phase space distribution. The source star is assumed to reside in the bulge for both events. The implied best fit masses are  $M = 6^{+10}_{-3} M_{\odot}$  for the MACHO-96-BLG-5 lens and  $M = 6^{+7}_{-3} M_{\odot}$  for the MACHO-98-BLG-6. The 95% confidence level lower limits on the masses are  $1.6 M_{\odot}$  and  $0.94 M_{\odot}$  respectively. The short dashed curves delineate the portion of the likelihood functions that is allowed when the lens is assumed to be a main sequence star. The ratio of the area below this portion to the entire area below the likelihood curve gives a probability that a lens is a main sequence star. For MACHO-96-BLG-5, the upper limit on the lens brightness is very stringent because of the HST images, and a main sequence lens is ruled out.

**Table 7. Mass & Magnitude Estimates for the MACHO Microlensing Parallax Events**

Event	$M/M_{\odot}$	$M_{\text{MS}}/M_{\odot}$	$D_{\ell-\text{MS}}$	sep-MS	$V_s$	$\Delta I_{\ell s}$	$\Delta V_{\ell s}$	$\Delta B_{\ell s}$	$\Delta U_{\ell s}$
104-C	$1.1^{+1.1}_{-0.5}$	0.74	2.7 kpc	40 mas	17.3	3.5	3.5	3.5	3.2
96-BLG-5	$6^{+10}_{-3}$	-	-	-	-	-	-	-	-
96-BLG-12	$1.3^{+1.8}_{-0.7}$	0.75	2.0 kpc	28 mas	18.0	2.1	2.2	2.2	2.3
98-BLG-6	$2.5^{+1.7}_{-0.9}$	0.88	5.7 kpc	5 mas	20.1	2.2	1.9	1.6	1.1
99-BLG-1	$0.7^{+1.2}_{-0.4}$	0.40	1.7 kpc	17 mas	18.9	1.8	3.2	3.6	3.9
99-BLG-8	$1.2^{+1.6}_{-0.6}$	1.2	1.6 kpc	25 mas	16.3	1.3	0.7	-0.3	-1.1

Note. — These are the parameters of the “most likely” main sequence star lenses for our best microlensing parallax events. For MACHO-96-BLG-5, a main sequence lens is ruled out.

## SYSTEMATIC ANALYSIS OF 22 MICROLENSING PARALLAX CANDIDATES

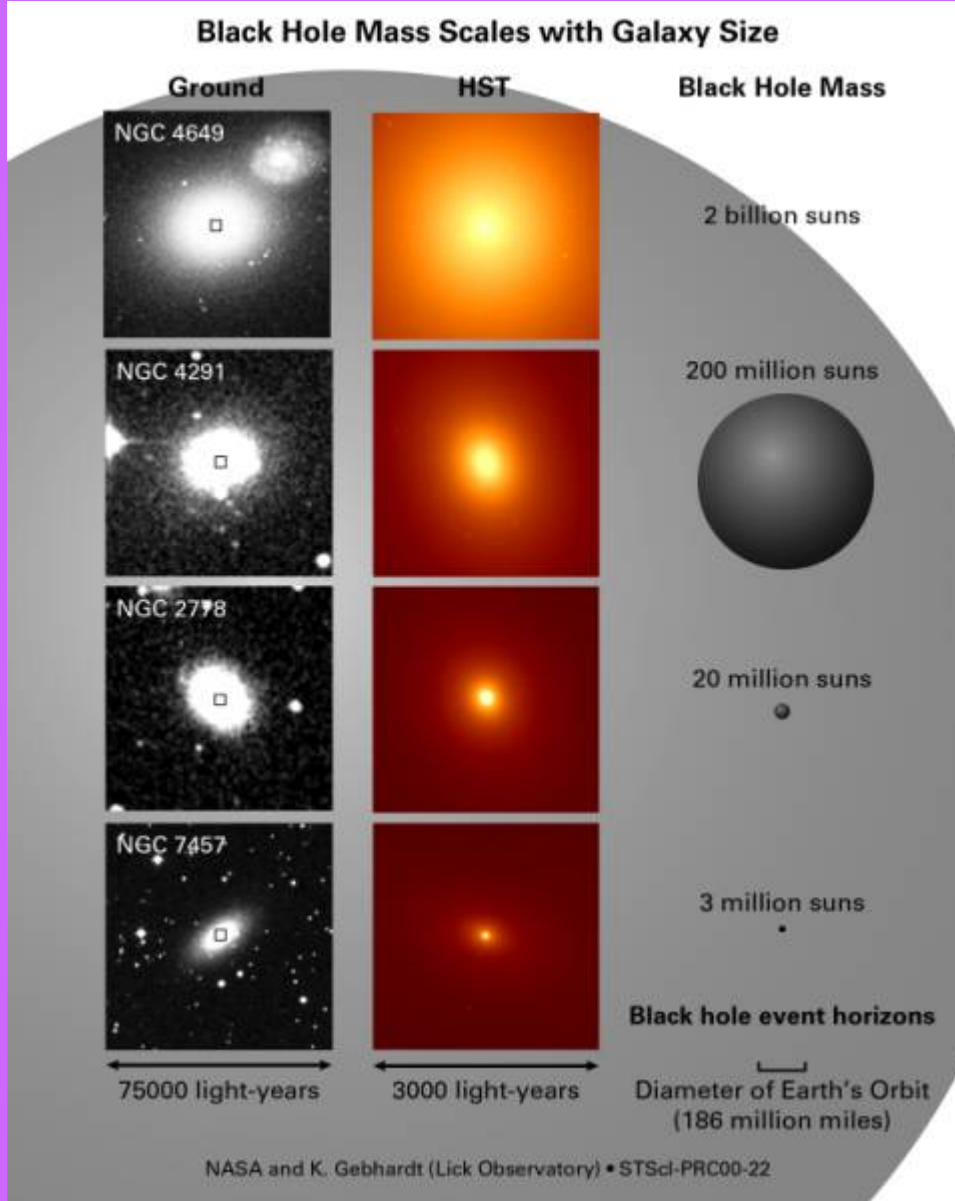
SHAWN POINDEXTER,<sup>1</sup> CRISTINA AFONSO,<sup>2</sup> DAVID P. BENNETT,<sup>3</sup> JEAN-FRANCOIS GLICENSTEIN,<sup>4</sup>  
ANDREW GOULD,<sup>1</sup> MICHAŁ K. SZYMAŃSKI,<sup>5</sup> AND ANDRZEJ UDALSKI<sup>5</sup>

*Received 2005 June 10; accepted 2005 July 15*

### ABSTRACT

We attempt to identify all microlensing parallax events for which the parallax fit improves  $\Delta\chi^2 > 100$  relative to a standard microlensing model. We outline a procedure to identify three types of discrete degeneracies (including a new one that we dub the “ecliptic degeneracy”) and find many new degenerate solutions in 16 previously published and six unpublished events. Only four events have one unique solution, and the other 18 events have a total of 44 solutions. Our sample includes three previously identified black hole (BH) candidates. We consider the newly discovered degenerate solutions and determine the relative likelihood that each of these is a BH. We find that the lens of event MACHO-99-BLG-22 is a strong BH candidate (78%), event MACHO-96-BLG-5 is a marginal BH candidate (37%), and MACHO-98-BLG-6 is a weak BH candidate (2.2%). The lens of event OGLE-2003-BLG-84 may be a Jupiter-mass free-floating planet candidate based on a weak  $3\sigma$  detection of finite-source effects. We find that event MACHO-179-A is a brown dwarf candidate within  $\sim 100$  pc of the Sun, mostly due to its very small projected Einstein radius,  $\tilde{r}_E = 0.23 \pm 0.05$  AU. As expected, these microlensing parallax events are biased toward lenses that are heavier and closer than average. These events were examined for xallarap (or binary-source motion), which can mimic parallax. We find that 23% of these events are strongly affected by xallarap.

# Black holes in galaxy centers

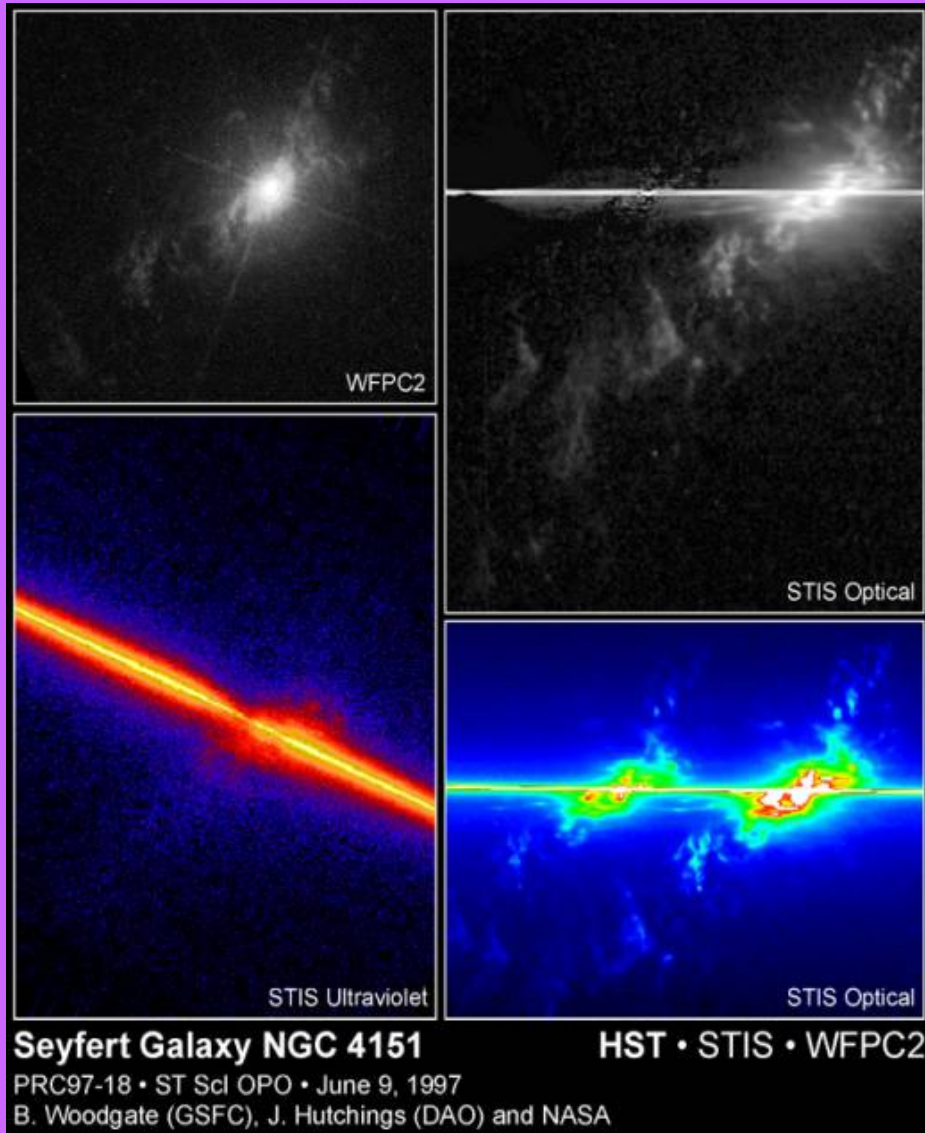


Many galaxies are assumed to have the black holes in their centers.

The black hole masses vary from million to dozens of billion Solar mass.

Because of the small size we cannot observe the black hole itself, but can register the emission of the accretion disk, rotating around the black hole.

# Seyfert galaxies and K $\alpha$ line

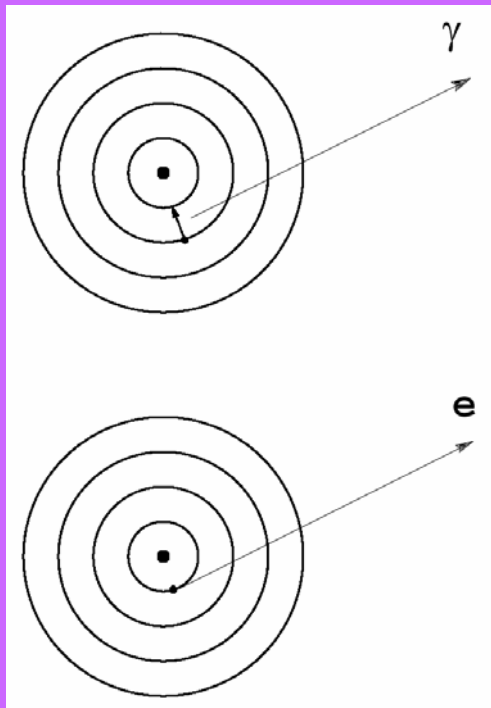


Seyfert galaxies give us a wonderful possibility of direct observations of black holes in their centers.

They often have a wide iron K $\alpha$  line in their spectra, which seems to arise in the innermost part of the accretion disk close to the event horizon.

Hubble image of Seyfert galaxy NGC 4151 shown at the left.

## Fe K $\alpha$ line origin



K $\alpha$  (6.4 keV) analogous to L $\alpha$  in hydrogen,  
electron transition to the lowest level

excitation by electronic shock

$h\nu > 7.1$  keV neutral iron  
photoionization and recombination

Fe XXV, XXVI – 6.9 keV hydrogen-like Fe

# Emission lines in Seyfert galaxies

O VIII	0.653 keV	Fe L	0.7– 0.8 keV
Ne IX	0.915 keV	Ne X	1.02 keV
Fe L	1.03 – 1.25 keV	Mg XI	1.34 keV
Mg XII	1.47 keV	Si XIII	1.85 keV
Si XIV	2.0 keV	S XIV	2.35 keV
S XV	2.45 keV	S XVI	2.62 keV
Ar XVII	3.10 keV	Ar XVIII	3.30 keV
Fe I – Fe XVI	6.4 keV		
Fe XVII – Fe XXIII	6.5 keV		
Fe XXV	6.68 keV		
Fe XXVI	6.96 keV		

K  $\alpha$

Turner, George, Nandra, Mushotzky

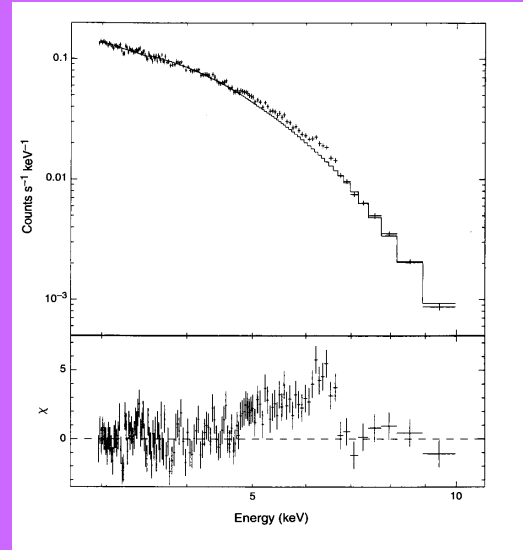
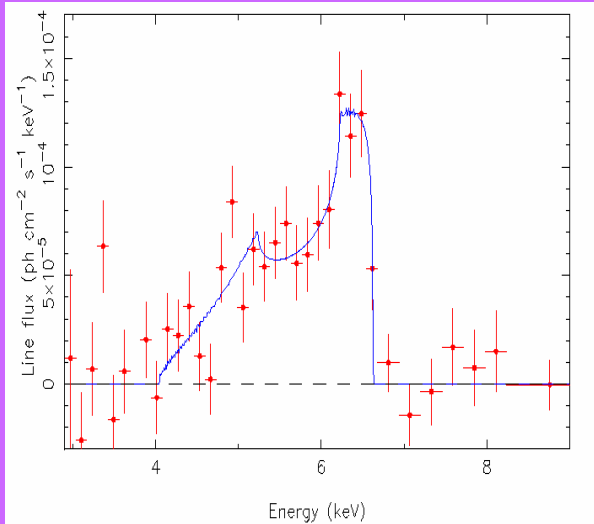
ApJSS, 113, 23, 1997, November

We find a 6.4 keV emission line in 72% of the sample (18 of 25 sources) at the 99% confidence level.  
The 5 – 7 keV regime is dominated by emission from neutral iron (< Fe XVI).

# Observations

Tanaka, Nandra, Fabian. Nature, 1995, **375**, 659.  
Galaxy MCG-6-30-15, ASCA satellite, SIS detectors

Sy 1 type



The line profile of iron K $\alpha$  line in X-ray emission from MCG-6-30-15.

Width corresponds to 80000 – 100000 km/s.

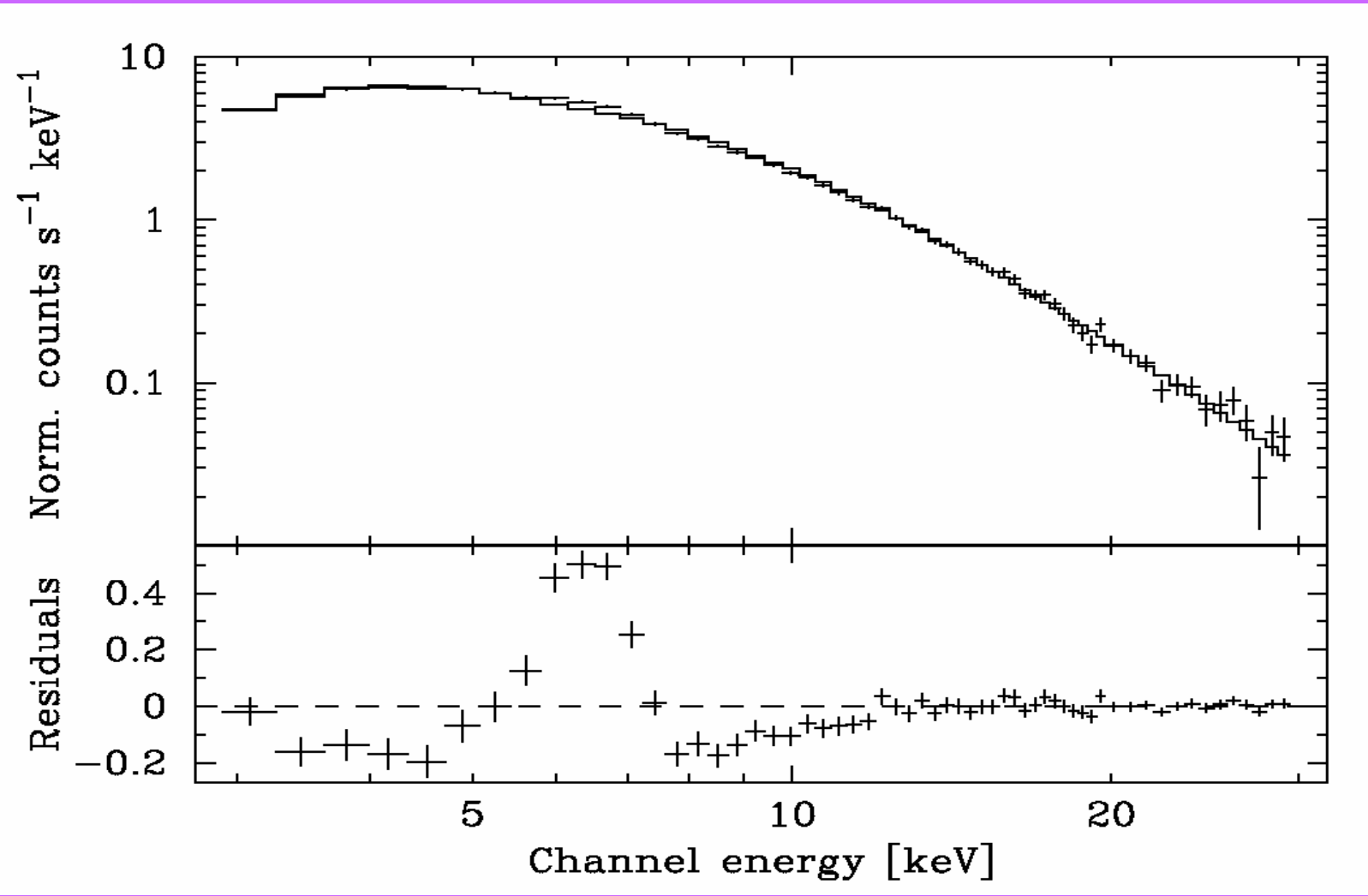
- **Variability**

Sulentic, Marziani, Calvani. ApJL, 1998, **497**, L65.

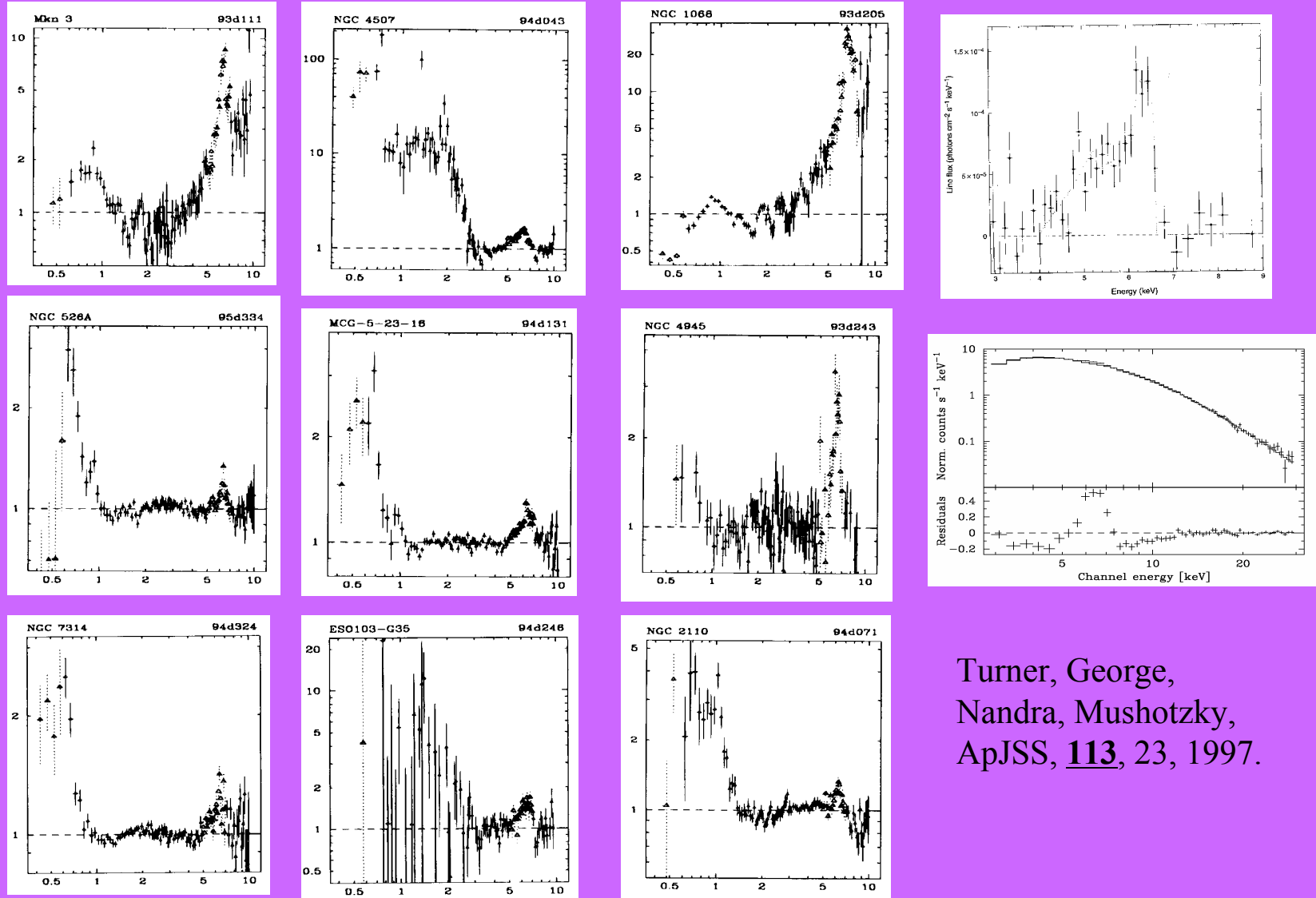
## Observations

Weaver, Krolik, Pier. ApJ, 1998, **498**, 213. (astro-ph / 9712035).

MCG-5-23-16 K $\alpha$  FWHM = 48000 km/s RXTE observations (launched Dec.95)



# ASCA observations. Seyfert 2 galaxies.



Turner, George,  
Nandra, Mushotzky,  
ApJSS, **113**, 23, 1997.

## Properties of wide lines at 6.4 keV

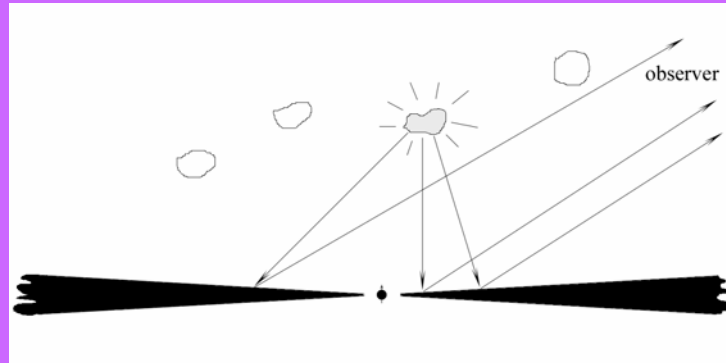
- Line width corresponds to velocity
  - $v \sim 80000 - 100000$  km/s MCG-6-30-15
  - $v \sim 48000$  km/s MCG-5-23-16
  - $v \sim 20000 - 30000$  km/s many other galaxies
- Asymmetric structure (profile)
  - two-peak shape
  - narrow bright **blue** wing
  - wide faint **red** wing
- Variability of both
  - line shape
  - intensity

## Possible interpretation

- • iron K $\alpha$  emission line
  - 6.4 – 6.9 – 7.1 keV
  
- • radiation of inner part of accretion disk around a supermassive **black hole** in the center of the galaxy

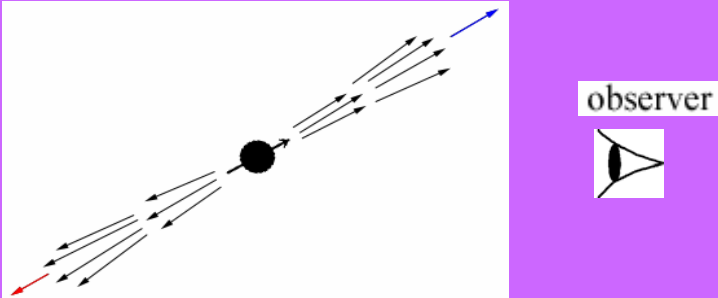
$$r_{\text{emission}} \sim 1 - 4 r_g$$

$$r_g = \frac{2km}{c^2}$$



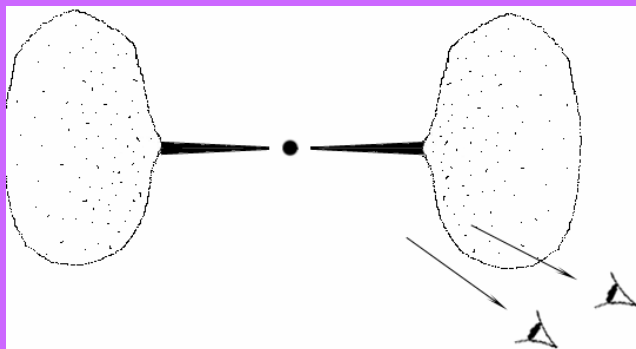
# Interpretation

## 1. Jets



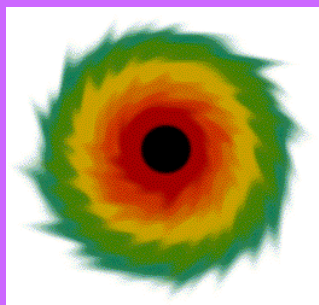
- ? Blue shift has never been seen
- ? Broad red wing

## 2. Multiple Compton scattering



- ? Line profile
- ? High frequency variability

## 3. Accretion disk



!!! Line profile !!!  
Variability !

## Equations of motion

Kerr metric

$$ds^2 = -\frac{\Delta}{\rho^2} (dt - a \sin^2 \theta d\phi)^2 + \frac{\rho^2}{\Delta} dr^2 + \rho^2 d\theta^2 + \\ + \frac{\sin^2 \theta}{\rho^2} [(r^2 + a^2) d\phi - a dt]^2$$

or

$$ds^2 = - \left( 1 - \frac{2Mr}{\rho^2} \right) dt^2 + \frac{\rho^2}{\Delta} dr^2 + \rho^2 d\theta^2 + \\ + \left( r^2 + a^2 + \frac{2Mra^2}{\rho^2} \sin^2 \theta \right) \sin^2 \theta d\phi^2 - \frac{4Mra}{\rho^2} \sin^2 \theta d\phi dt,$$

## Equations of motion

Equations of photon motion:

$$\begin{aligned}\frac{dt}{d\lambda} &= -\frac{r_g r a}{\rho^2 \Delta} L + \frac{\omega_0}{\Delta} \left( r^2 + a^2 + \frac{r_r r a^2}{\rho^2} \sin^2 \theta \right) \\ \frac{d\phi}{d\lambda} &= \frac{L}{\Delta \sin^2 \theta} \left( 1 - \frac{r_g r}{\rho^2} \right) + \frac{r_g r a}{\rho^2 \Delta} \omega_0 \\ \left( \frac{dr}{d\lambda} \right)^2 &= \frac{1}{\rho^4} \left[ (r^2 + a^2) \omega_0 - a L \right] - \frac{K \Delta}{\rho^4} \\ \left( \frac{d\theta}{d\lambda} \right)^2 &= \frac{K}{\rho^4} - \frac{1}{\rho^4} \left[ a \omega_0 \sin \theta - \frac{L}{\sin \theta} \right]^2\end{aligned}$$

where

$$\Delta = r^2 - r_g r + a^2, \quad \rho^2 = r^2 + a^2 \cos^2 \theta,$$

$$r_g = 2km, \quad a = M/m$$

## Equations of motion

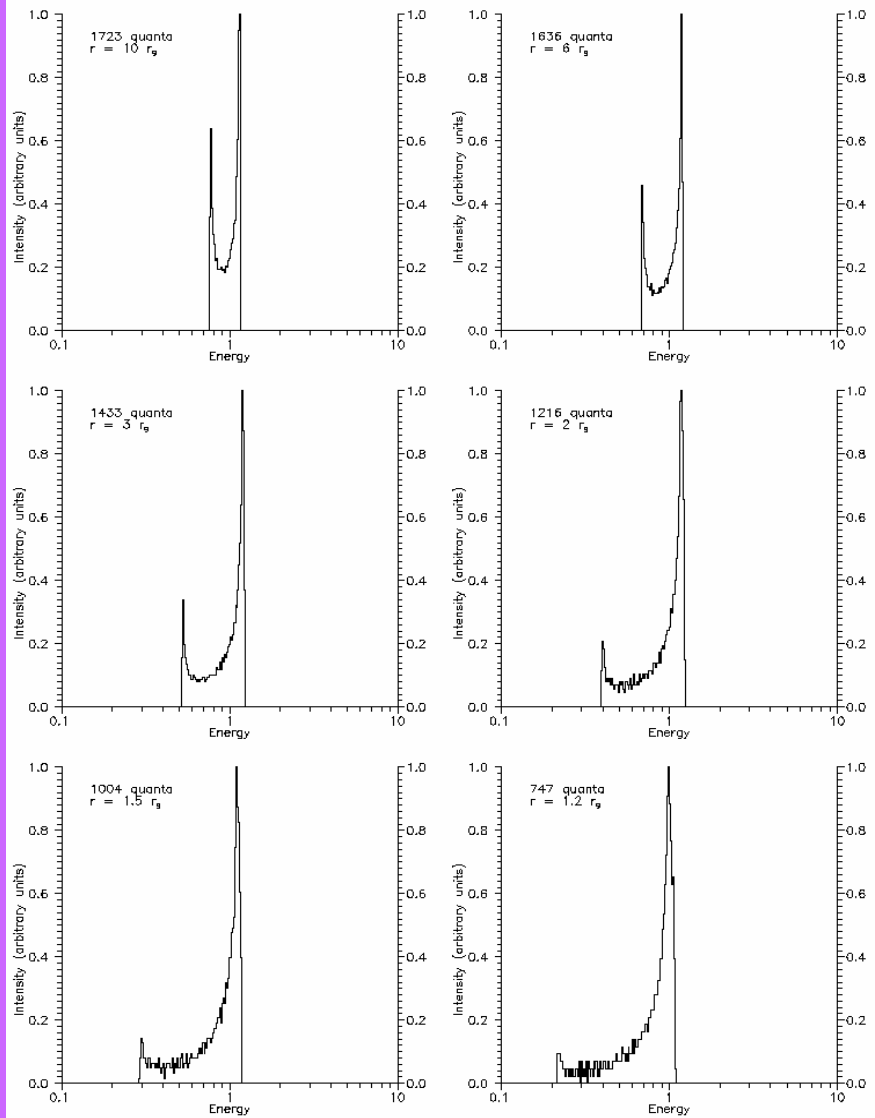
For numerical solution the system should be replaced with

$$\begin{aligned}\frac{dt'}{d\sigma} &= -\hat{a}(\hat{a} \sin^2 \theta - \xi) + \frac{\hat{r}^2 + \hat{a}^2}{\hat{\Delta}} (\hat{r}^2 + \hat{a}^2 - \xi \hat{a}), \\ \frac{d\hat{r}}{d\sigma} &= r_1, \\ \frac{dr_1}{d\sigma} &= 2\hat{r}^3 + (\hat{a}^2 - \xi^2 - \eta)\hat{r} + (\hat{a} - \xi) + \eta, \\ \frac{d\theta}{d\sigma} &= \theta_1, \\ \frac{d\theta_1}{d\sigma} &= \cos \theta \left( \frac{\xi^2}{\sin^3 \theta} - \hat{a}^2 \sin \theta \right), \\ \frac{d\phi}{d\sigma} &= -\left( \hat{a} - \frac{\xi}{\sin^2 \theta} \right) + \frac{\hat{a}}{\hat{\Delta}} (\hat{r}^2 + \hat{a}^2 - \xi \hat{a}).\end{aligned}$$

The system has two integrals:

$$\begin{aligned}\epsilon_1 &\equiv r_1^2 - \hat{r}^4 - (\hat{a}^2 - \xi^2 - \eta)\hat{r}^2 - 2[(\hat{a} - \xi)^2 + \eta]\hat{r} + \hat{a}^2\eta = 0, \\ \epsilon_2 &\equiv \theta_1^2 - \eta - \cos^2 \theta \left( \hat{a}^2 - \frac{\xi^2}{\sin^2 \theta} \right) = 0,\end{aligned}$$

# Simulation result



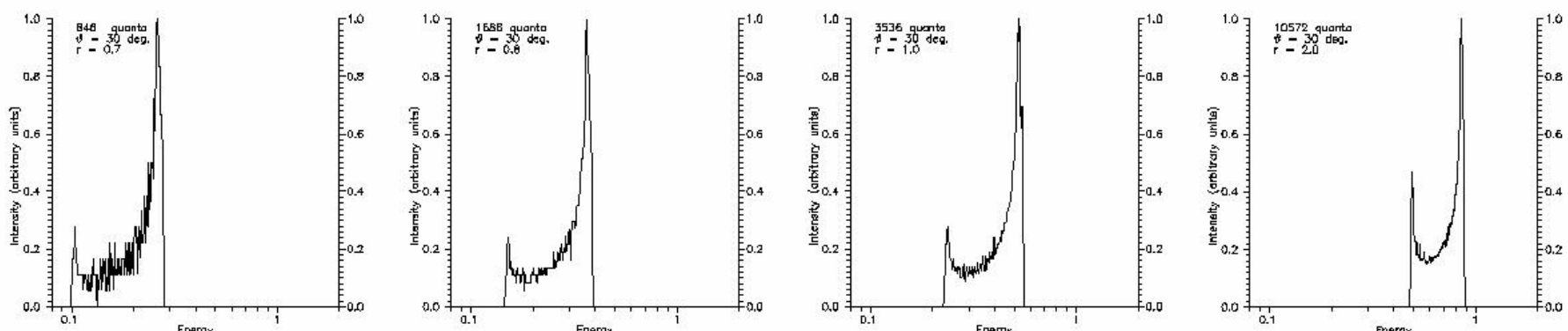
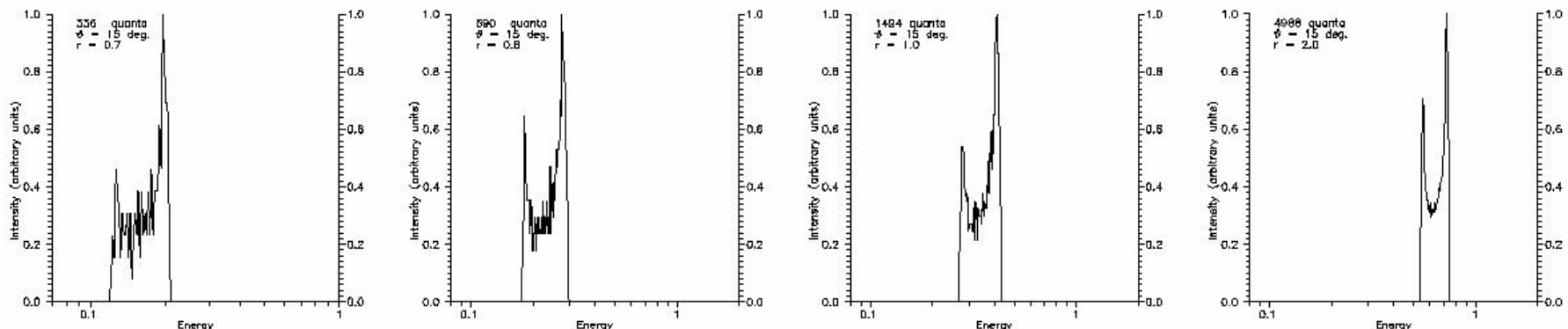
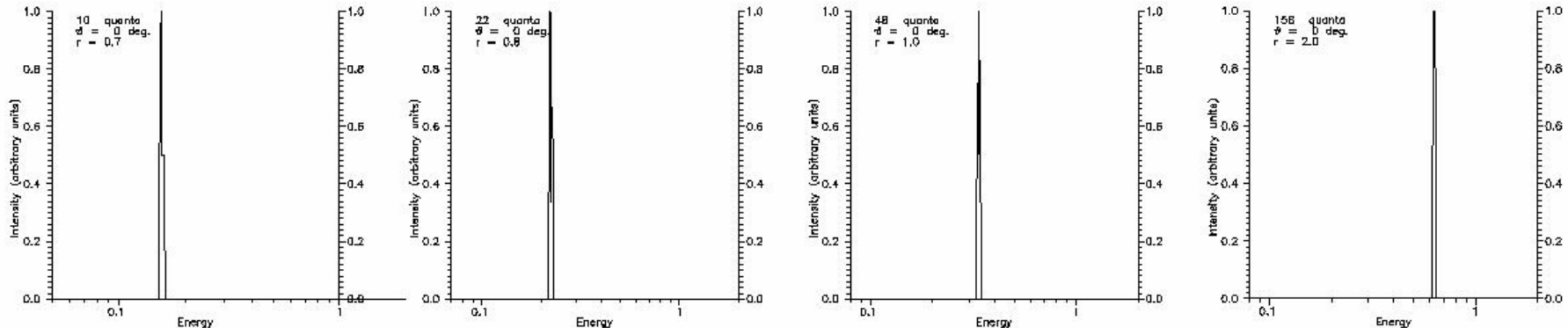
Spectrum of a hot spot for  $a=0.9$ ,  $\theta=60$  deg. and different values of radial coordinate.

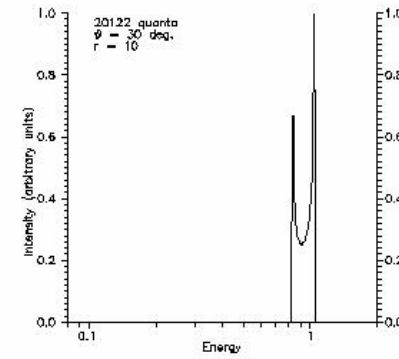
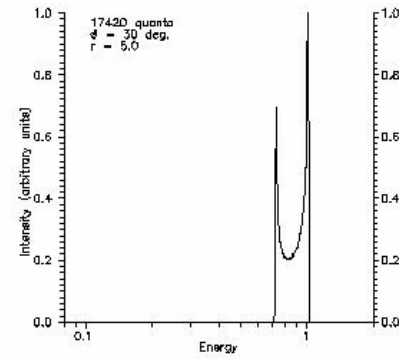
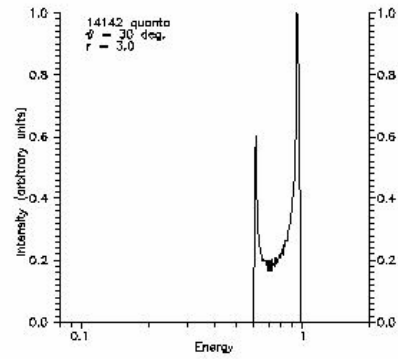
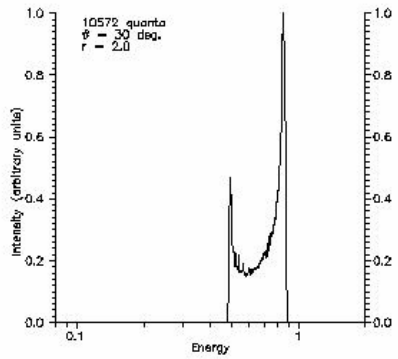
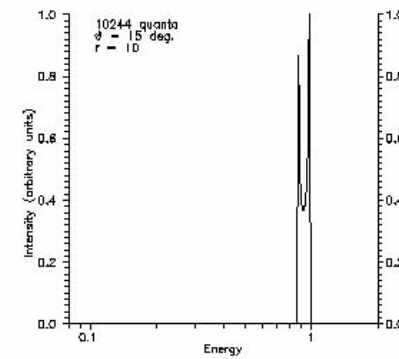
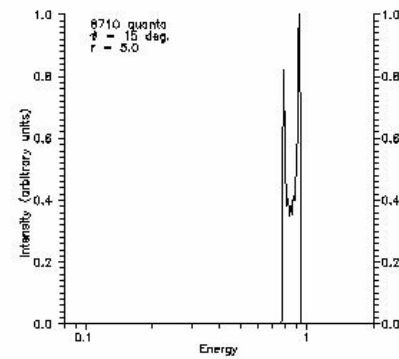
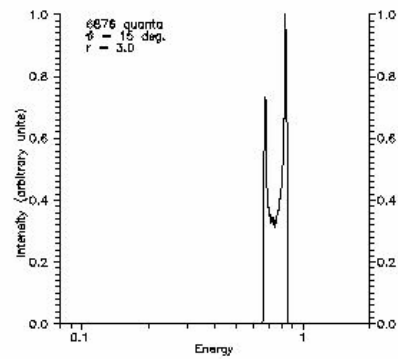
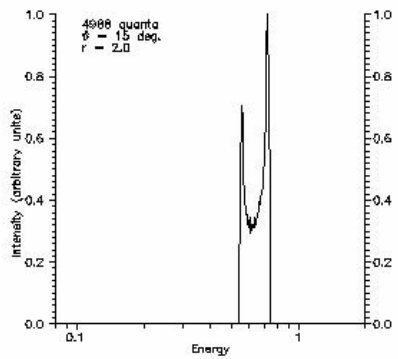
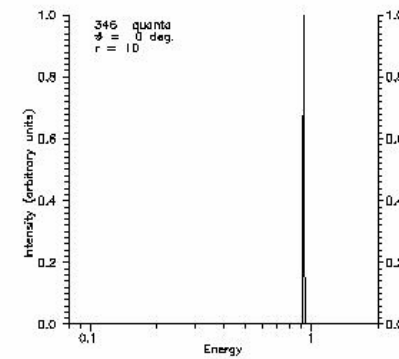
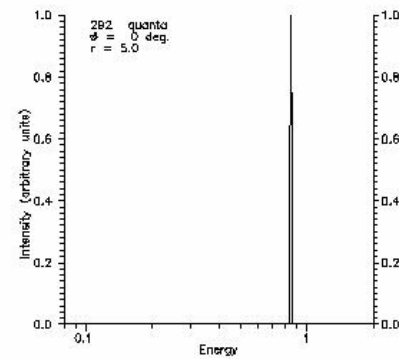
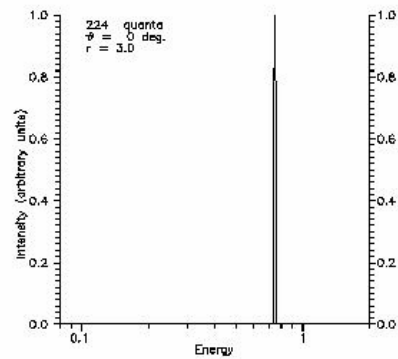
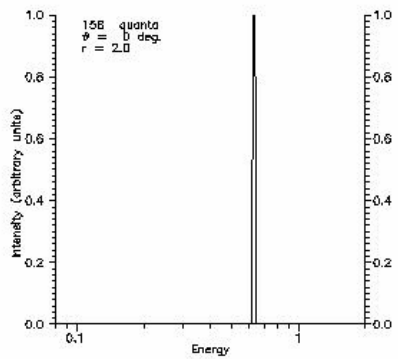
Marginally stable orbit lays at  $r = 1.16 r_g$ .

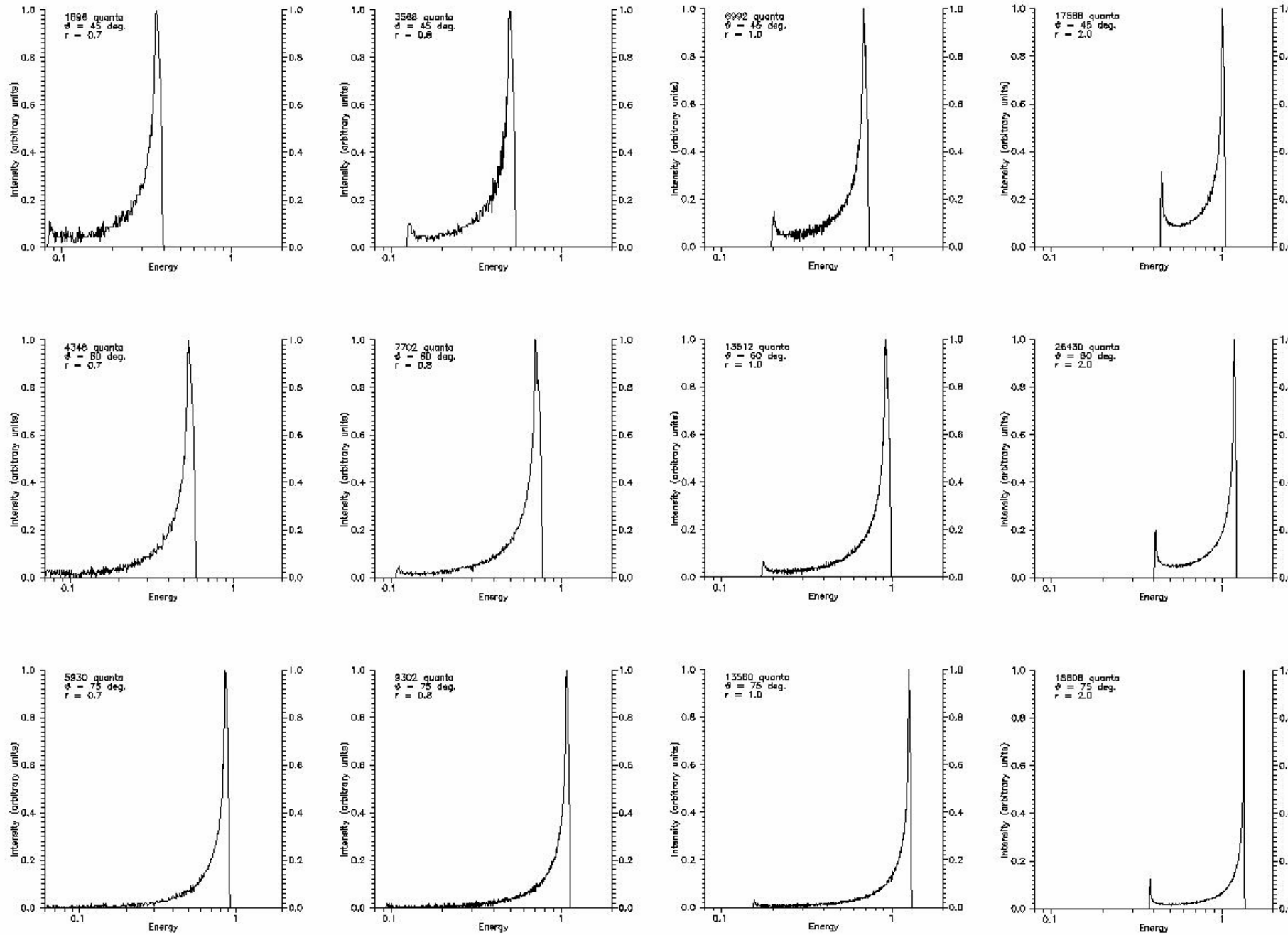
# Gallery of profiles

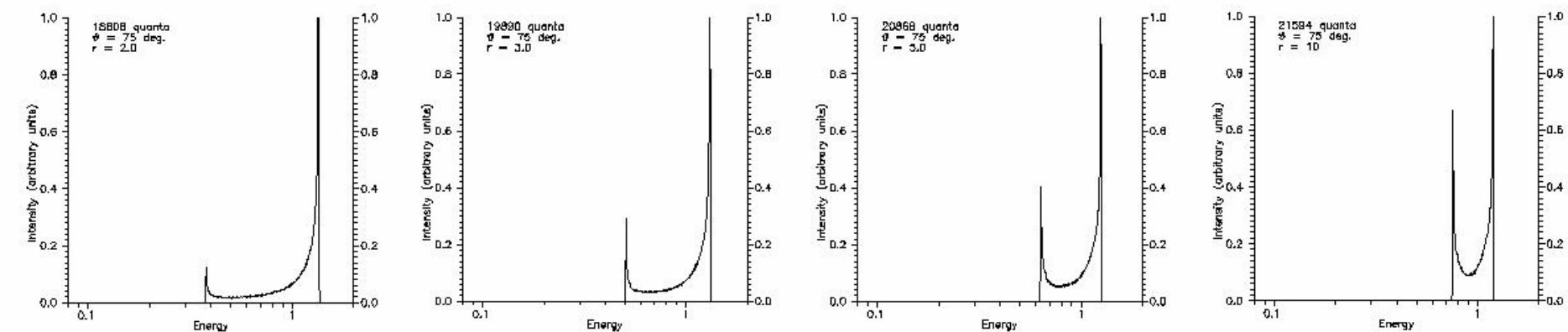
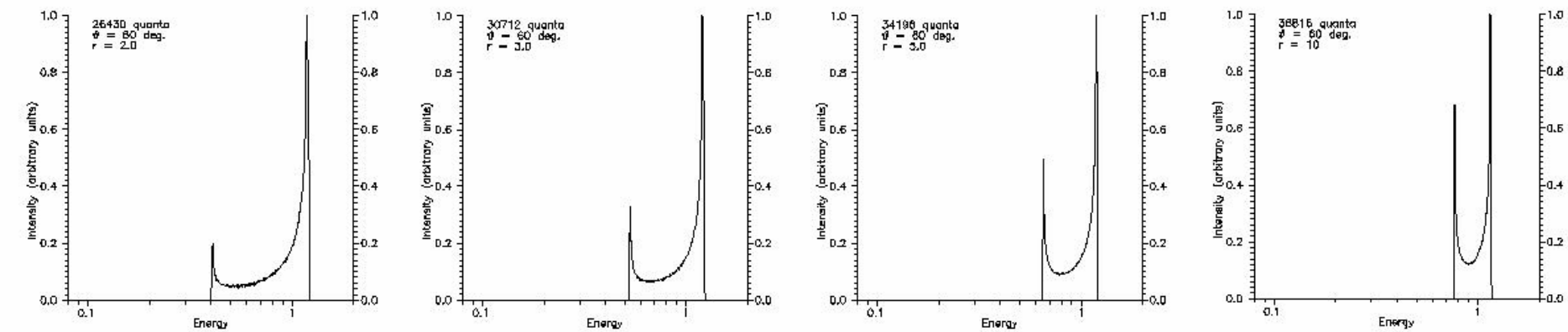
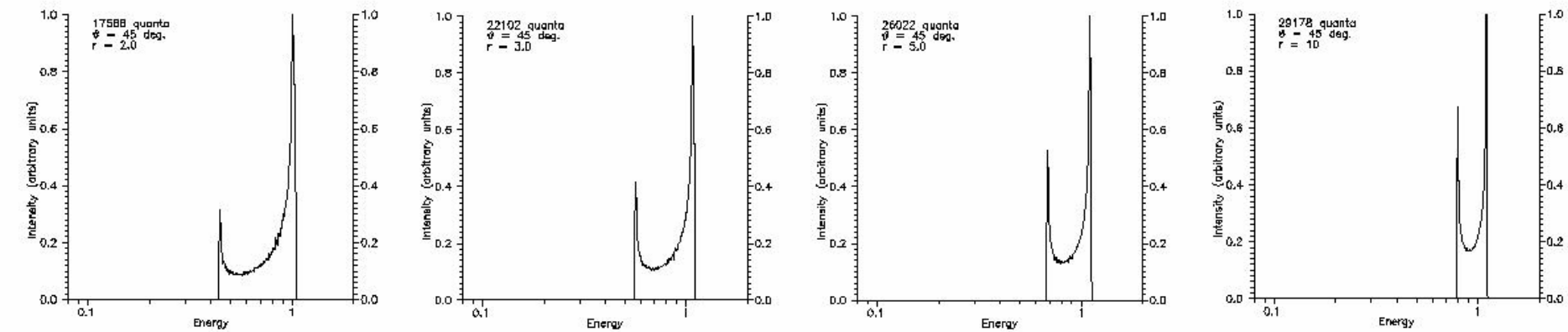
A.F. Zakharov & S.V. Repin, **Mem. SAIt, 7, 60 (2005)** ; **New Astronomy, 11, 405 (2006)**; astro-

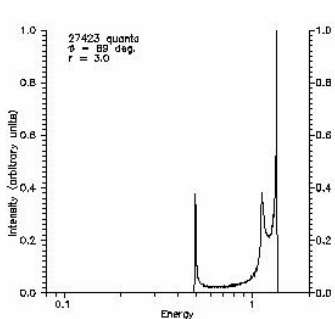
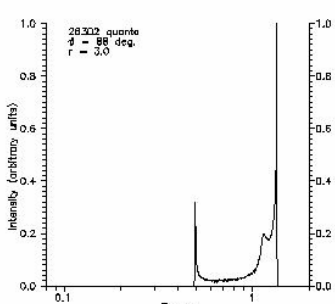
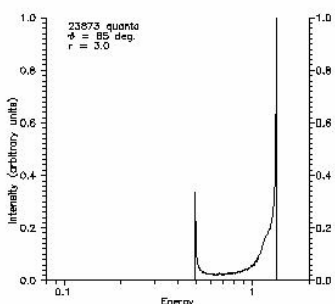
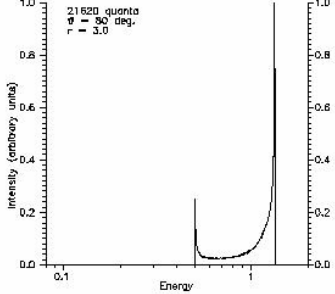
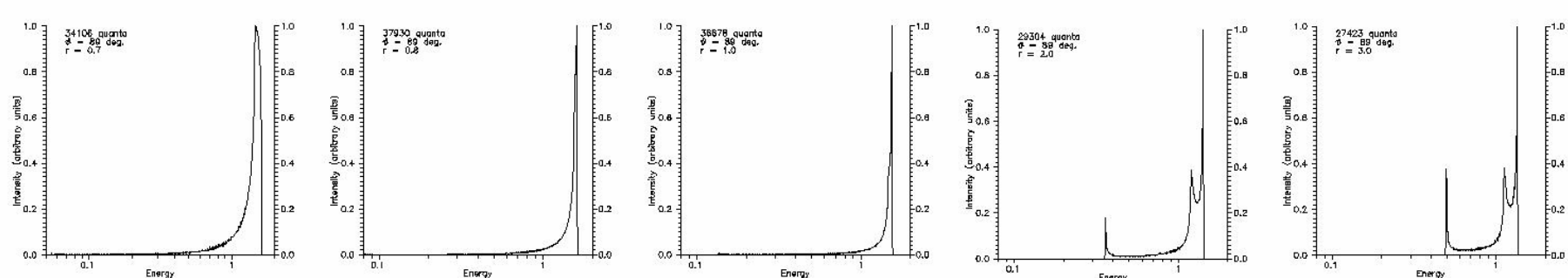
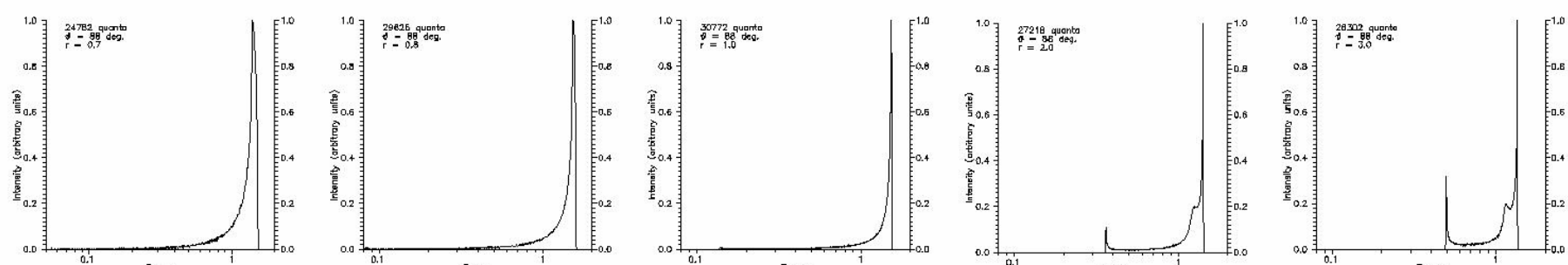
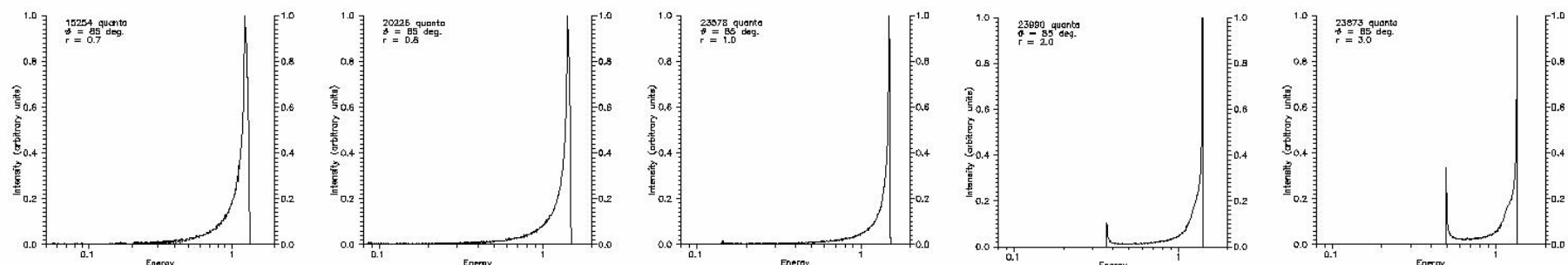
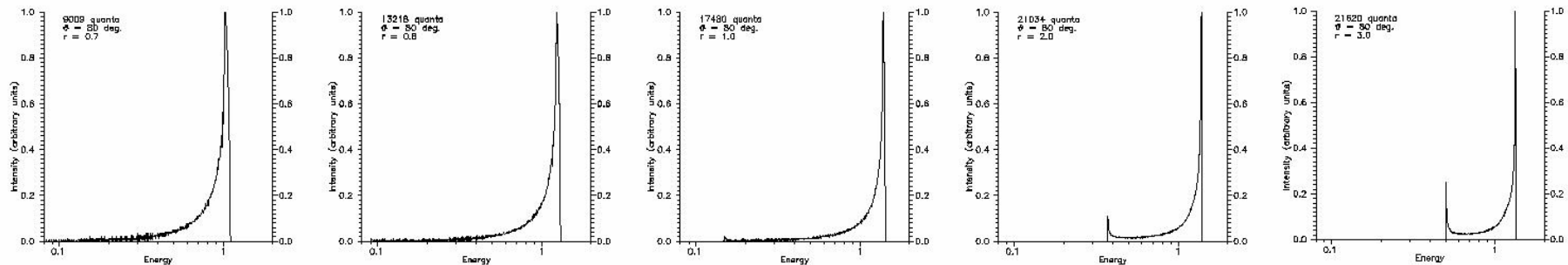
ph/0510548

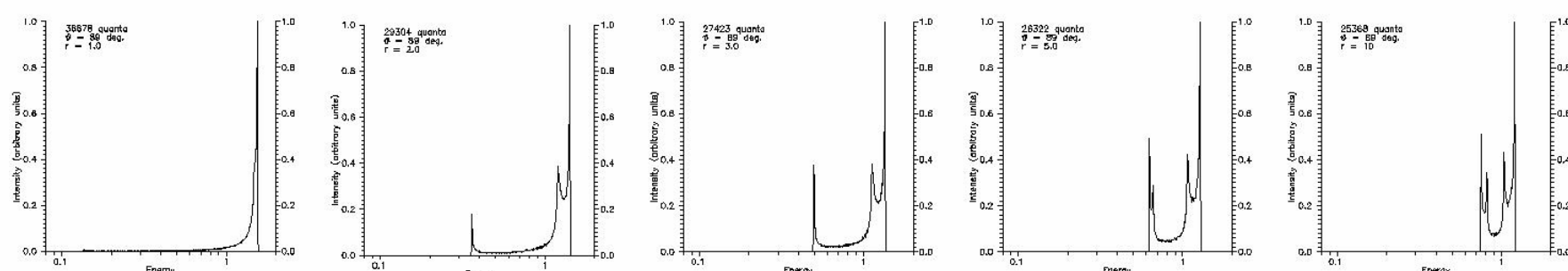
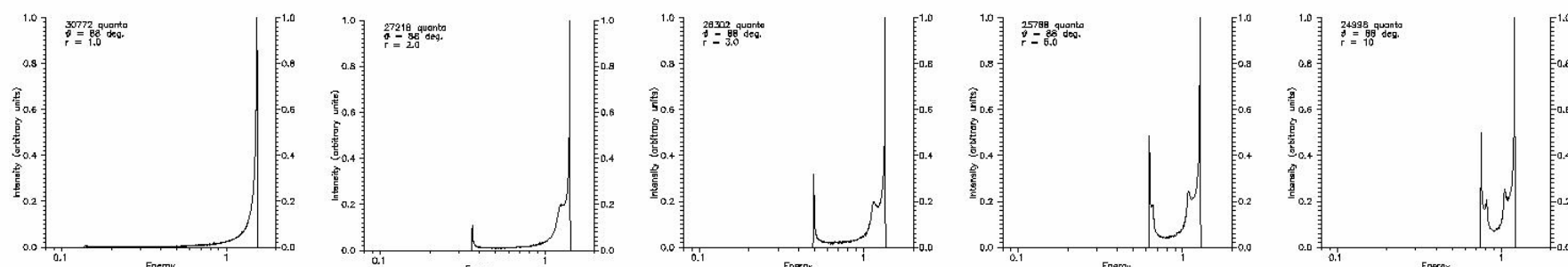
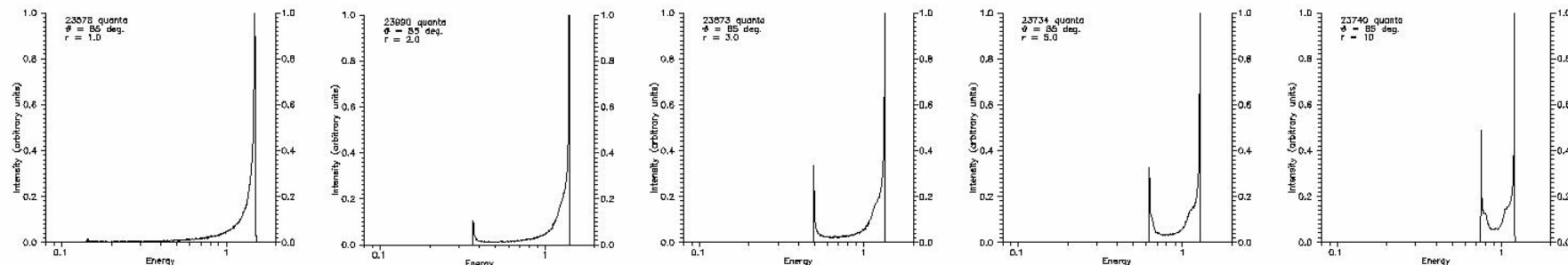
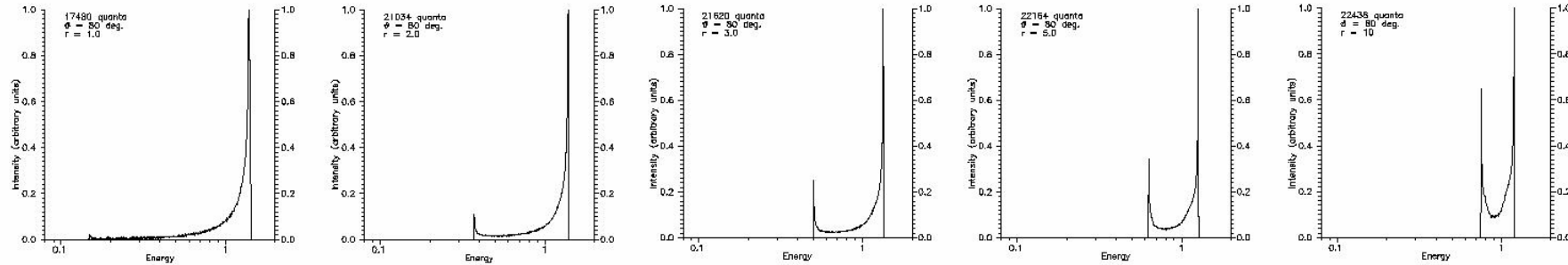












## Rings summation

Classical expression for the ring area

$$dS = 2\pi r dr$$

should be replaced in General Relativity with

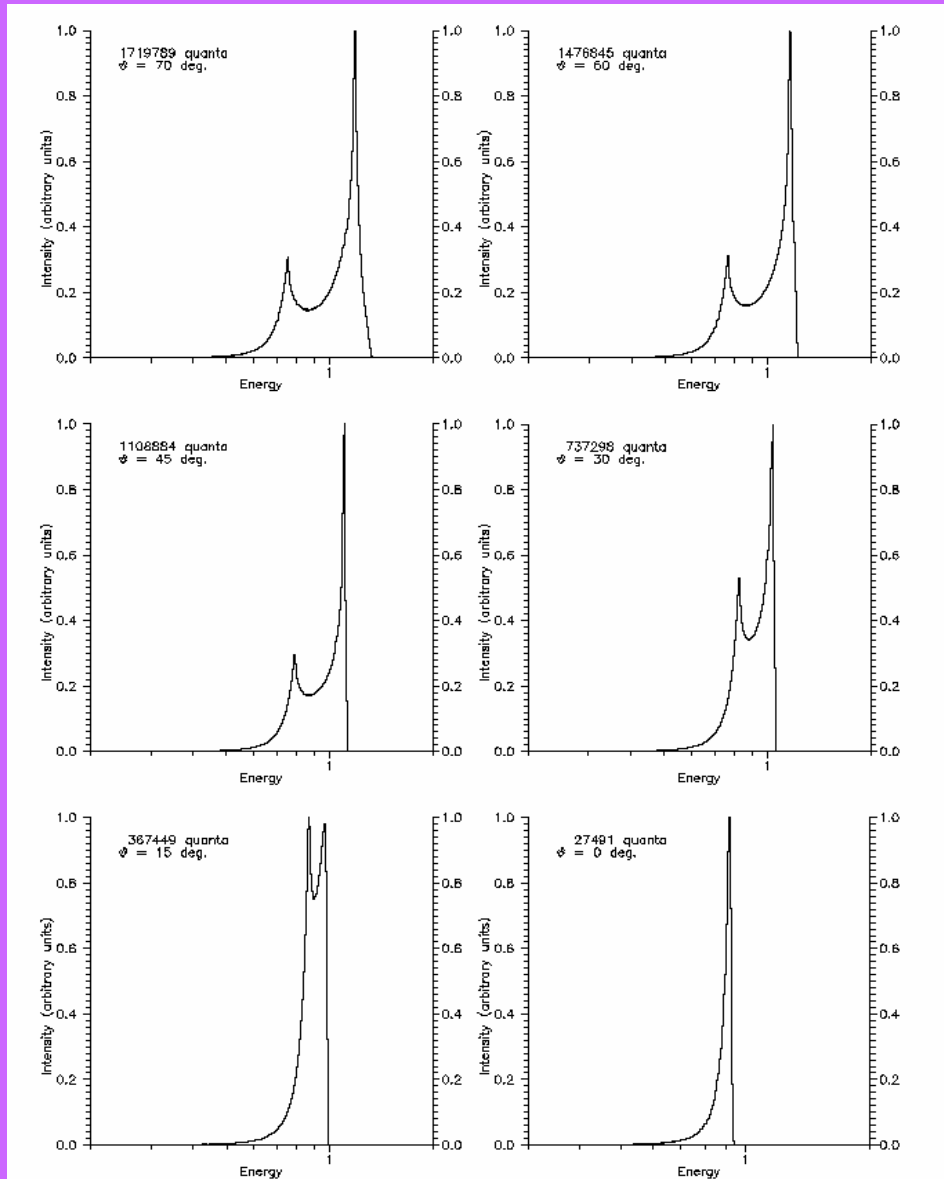
$$dS = \frac{2\pi (r^2 + a^2)}{\sqrt{r^2 - rr_g + a^2}} dr$$

where

$$f_{GR} = \frac{r^2 + a^2}{r \sqrt{r^2 - rr_g + a^2}}$$

is the additional relativistic factor, appearing due to the frame dragging.

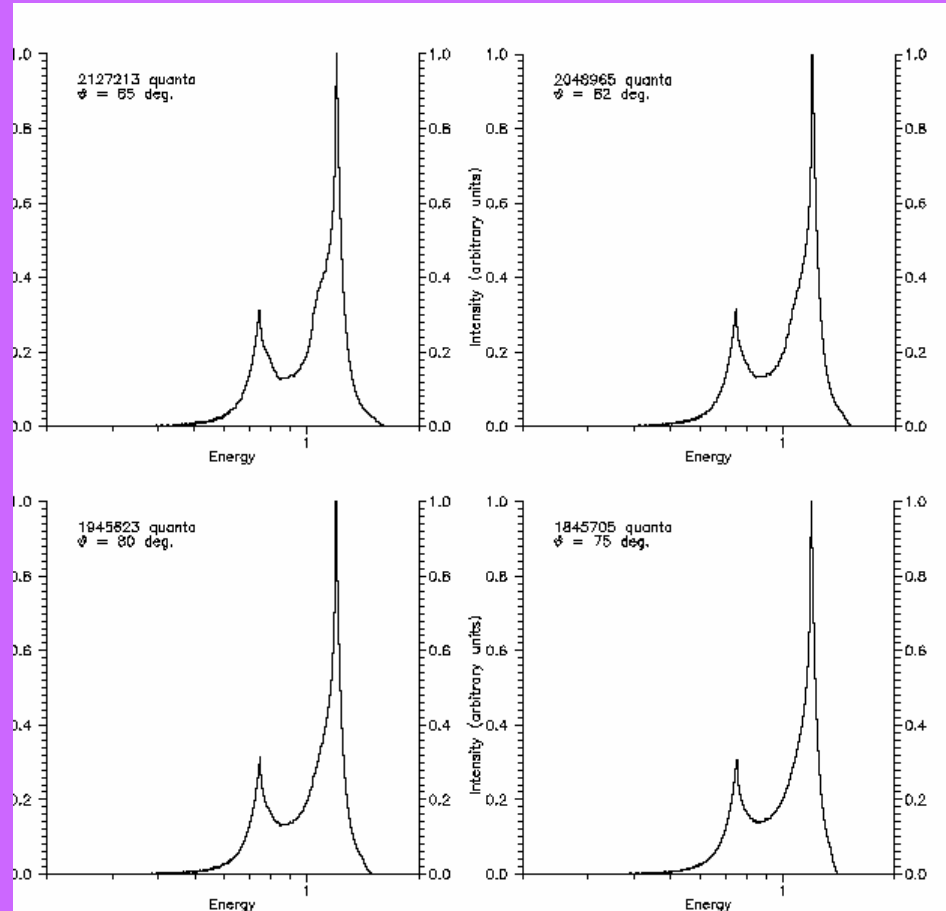
# Simulation result



Spectrum of Fe K $\alpha$  line in isothermal disk with  $a = 0.9$  and emission region between  $10 r_g$  and marginally stable orbit at  $1.16 r_g$ .

The figure presents the dependence on  $\theta$  angle.

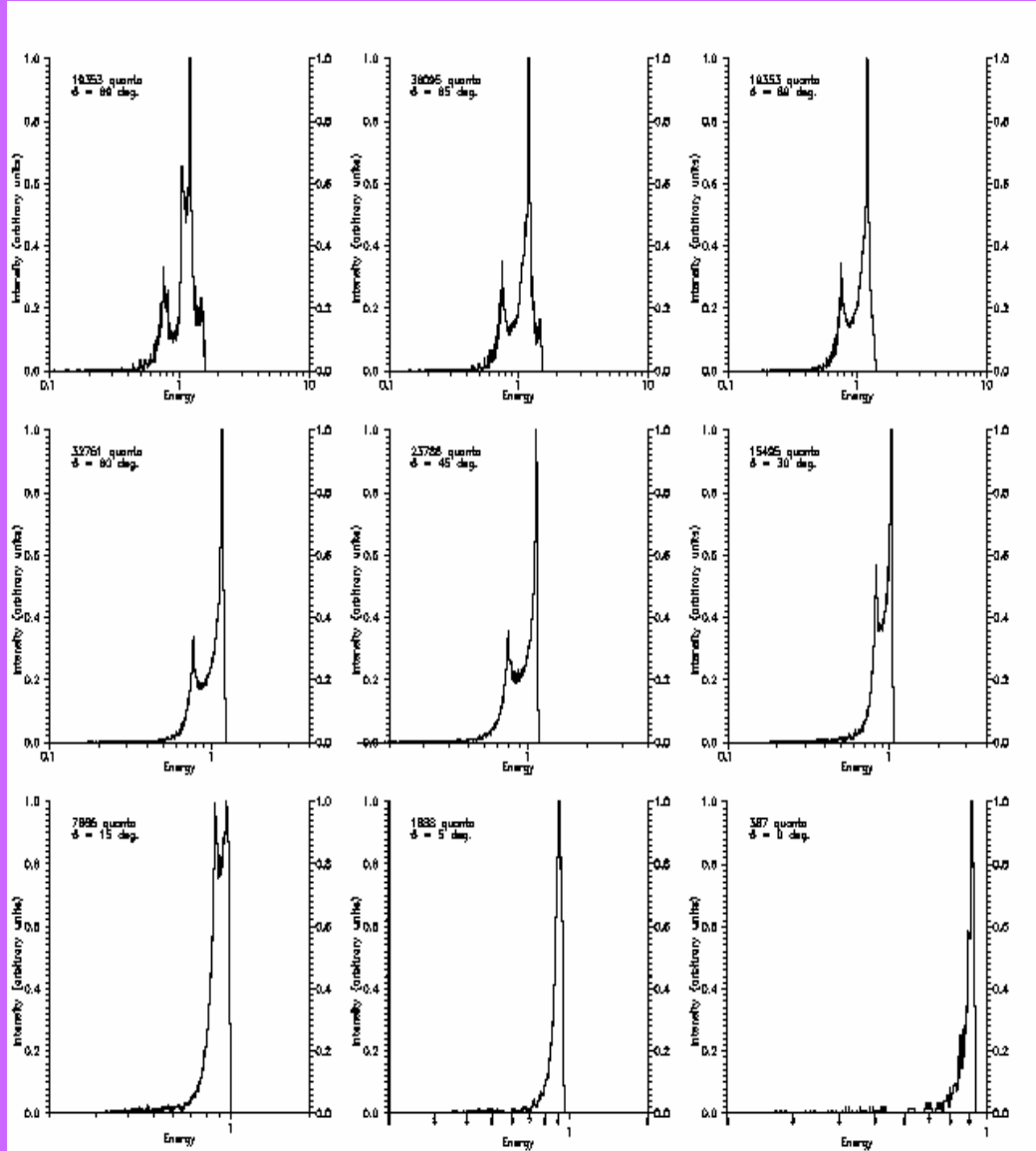
# Simulation result



Spectrum of Fe K $\alpha$  line in isothermal disk with  $a = 0.9$  and emission region between  $10 r_g$  and marginally stable orbit at  $1.16 r_g$ .

The figure presents the dependence on  $\theta$  angle (large  $\theta$  values).

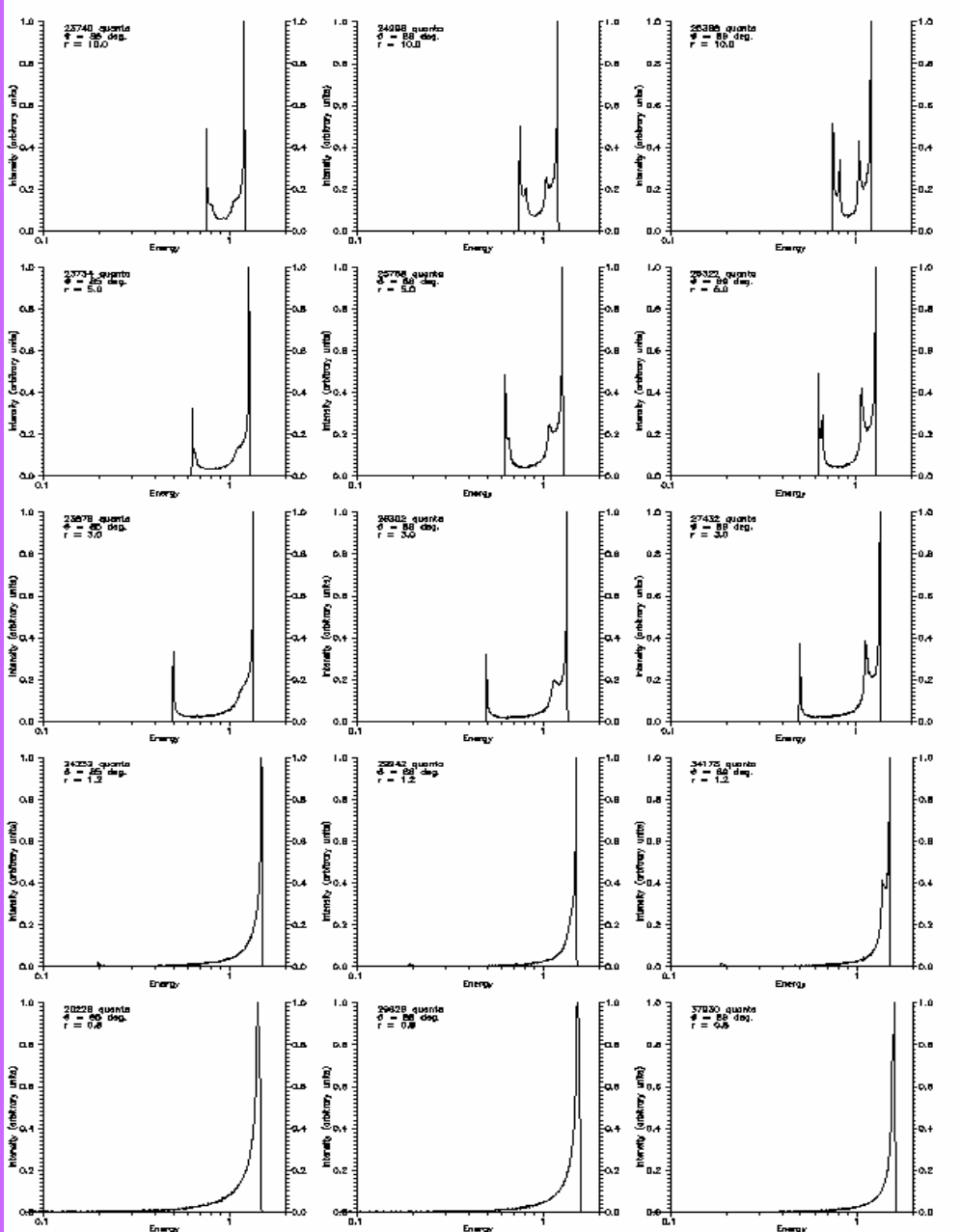
# Simulation result



Spectrum of Fe K $\alpha$  line in isothermal disk with  $a = 0.99$  and emission region between  $10 r_g$  and marginally stable orbit at  $0.727 r_g$ .

At large  $\theta$  one can see the lensing effect.

# Simulation result

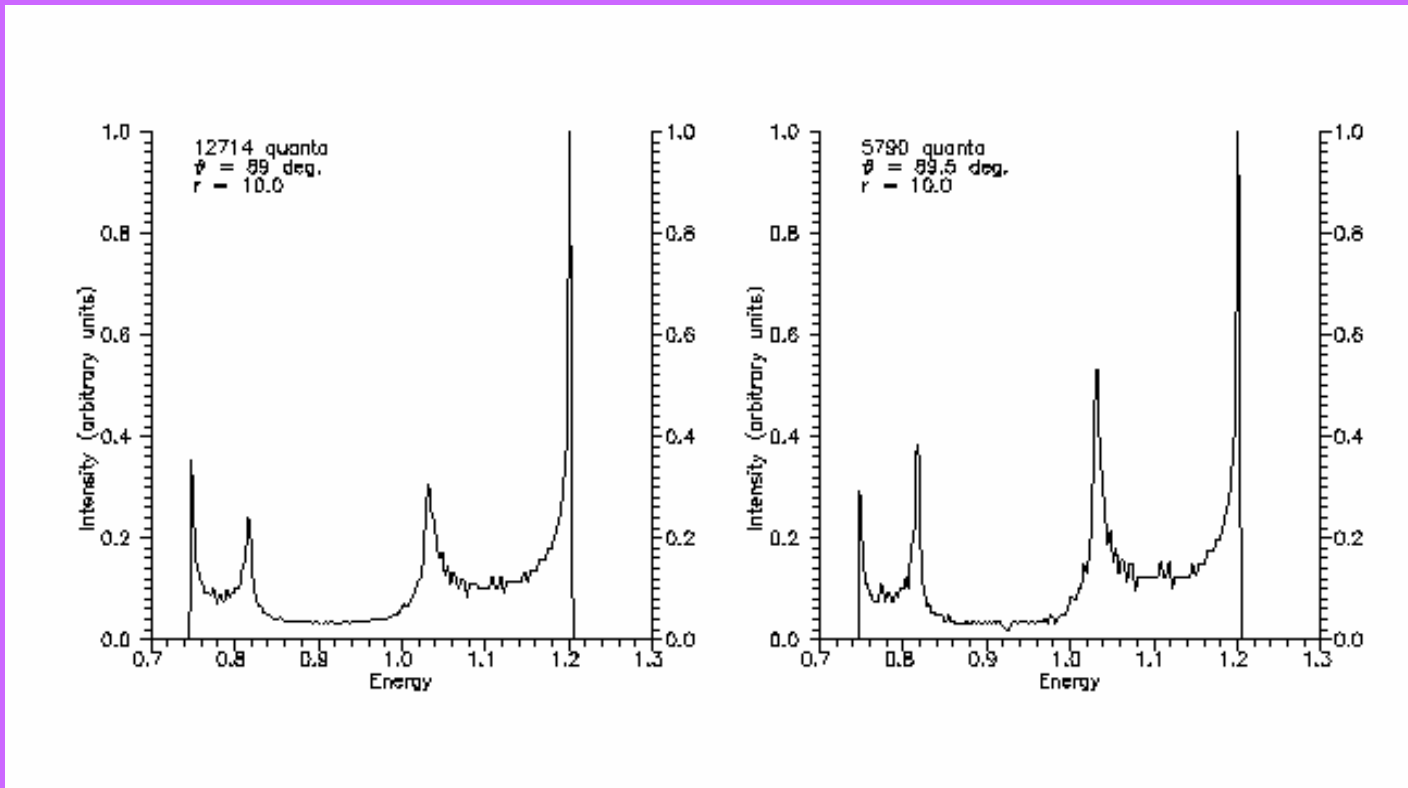


Overview of possible line profiles of a hot spot for different values of radial coordinate and inclination angle.

The radial coordinate decreases from  $10 r_g$  on the top to  $0.8 r_g$  on the bottom. The inclination angle increases from 85 degrees in the left column to 89 degrees in the right.

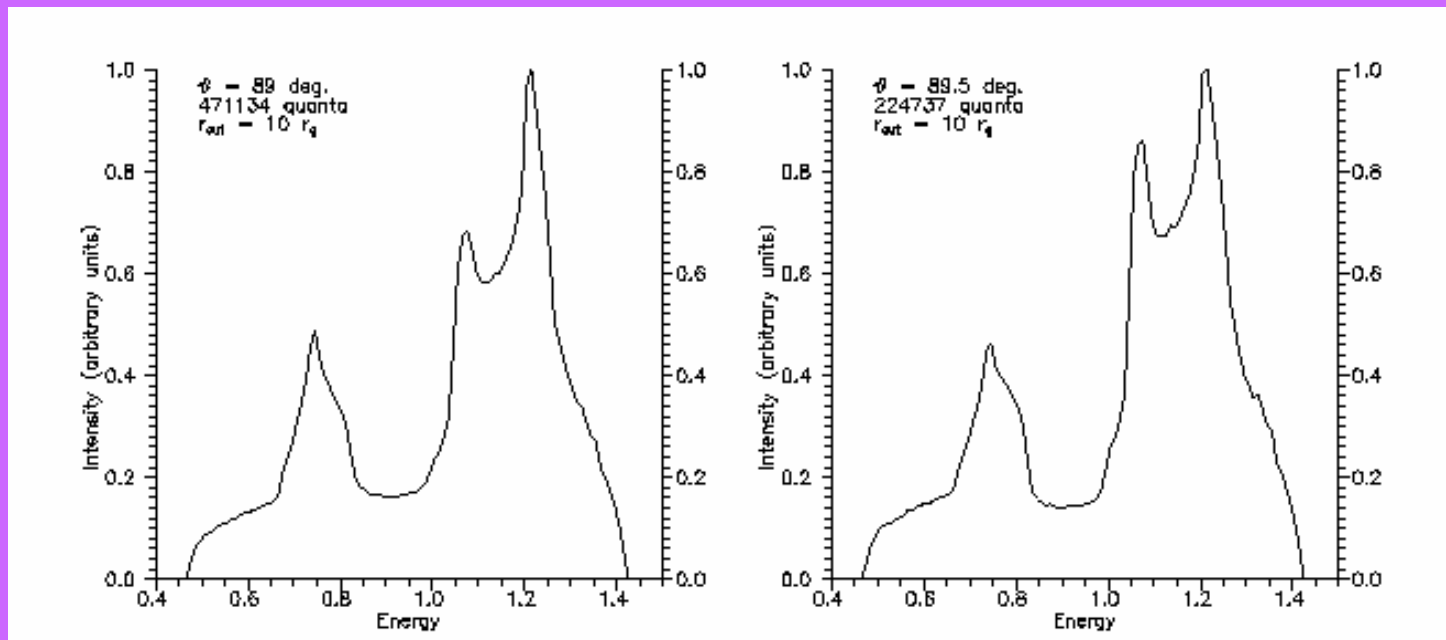
Zakharov A.F, Repin S.V. A&A, 2003,  
406, 7.

## Simulation result



Spectrum of a hot spot rotating at the distance  $10 r_g$  and observed at large inclination angles. Left panel includes all the quanta with  $\theta > 89$  degrees. The right one includes the quanta with  $\theta > 89.5$  degrees.

## Simulation result

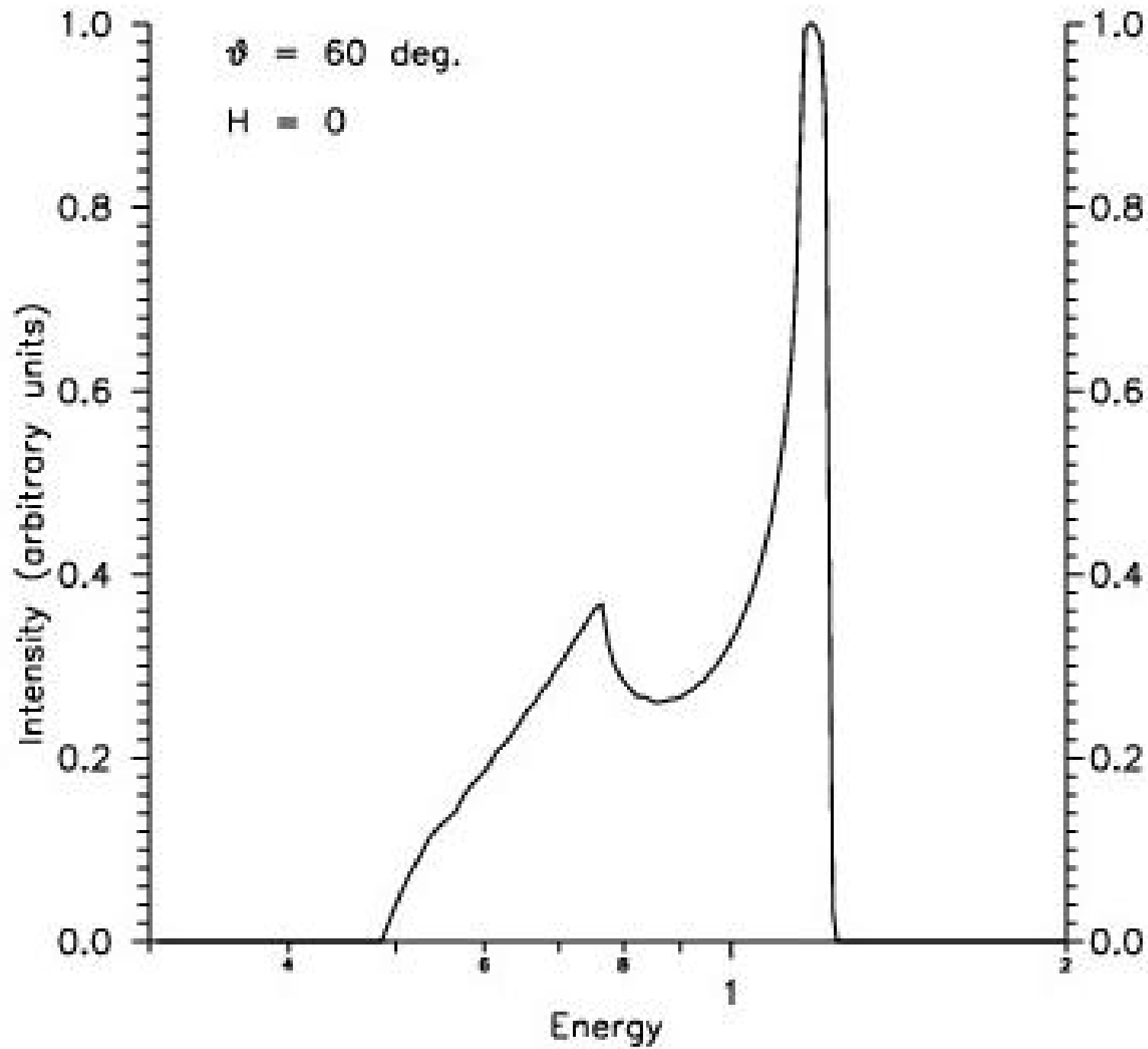


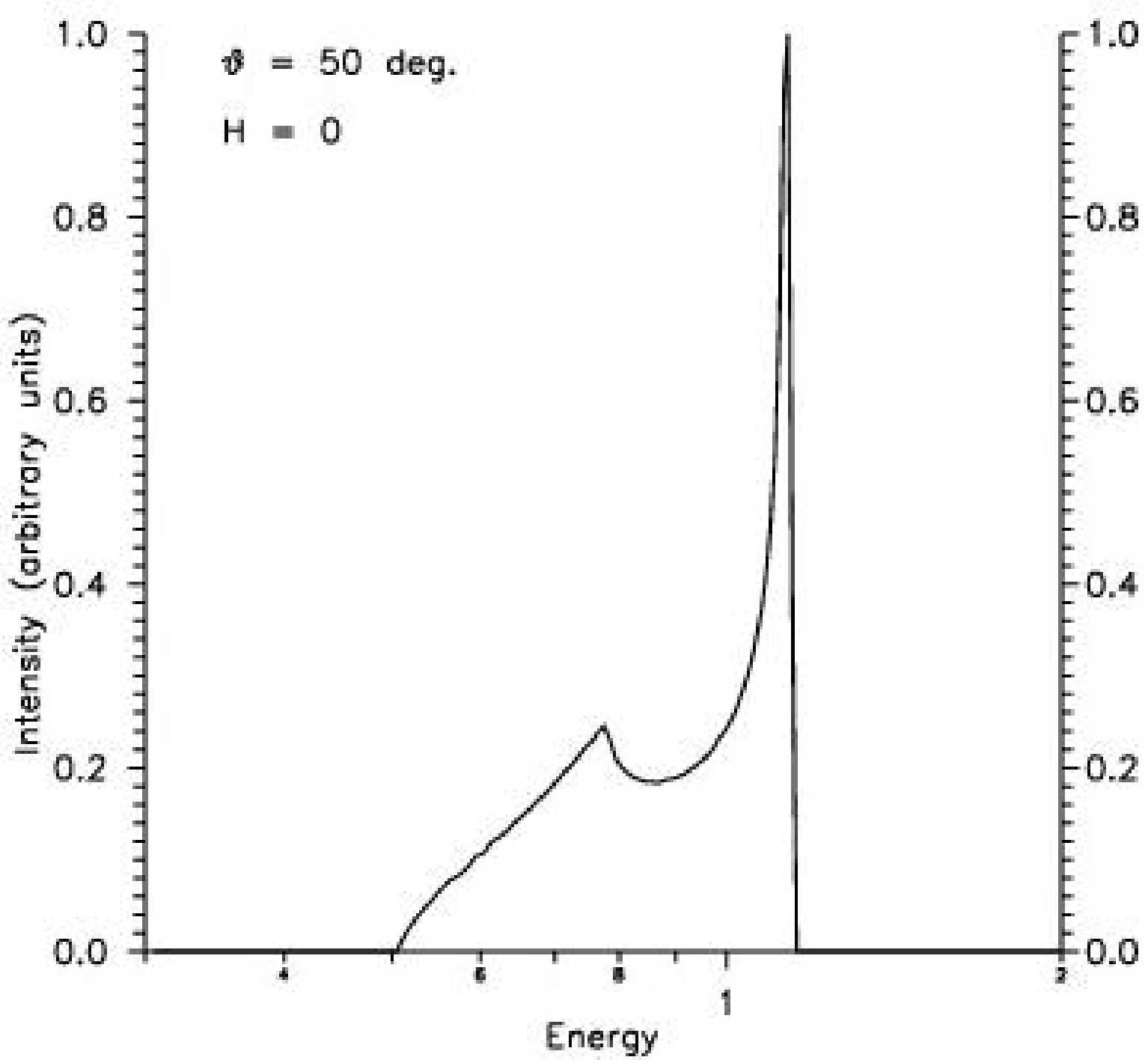
Spectrum of an entire  $\alpha$ -disk observed at large inclination angles. Emitting region lies between  $3 r_g$  and  $10 r_g$ . Left panel includes all the quanta with  $\theta > 89$  degrees. The right one includes the quanta with  $\theta > 89.5$  degrees.

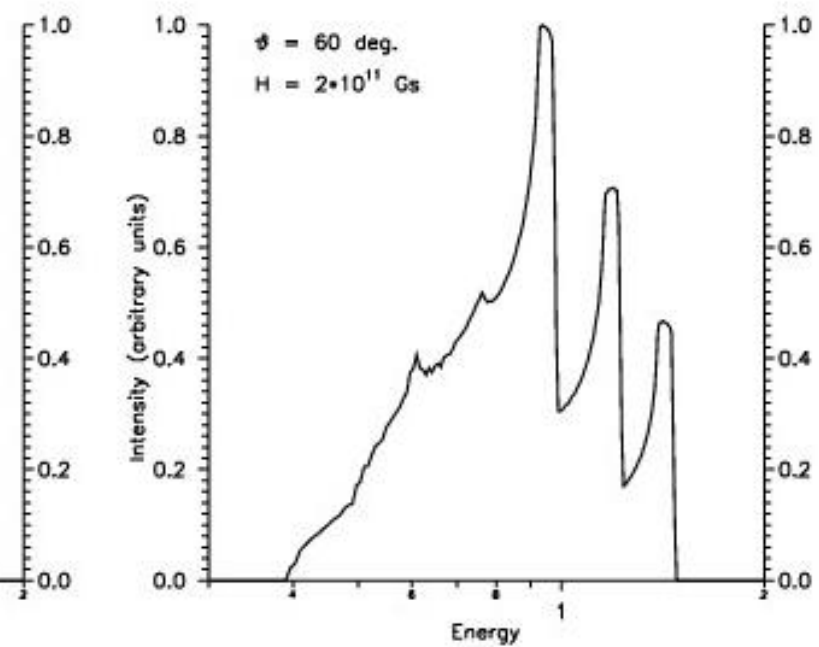
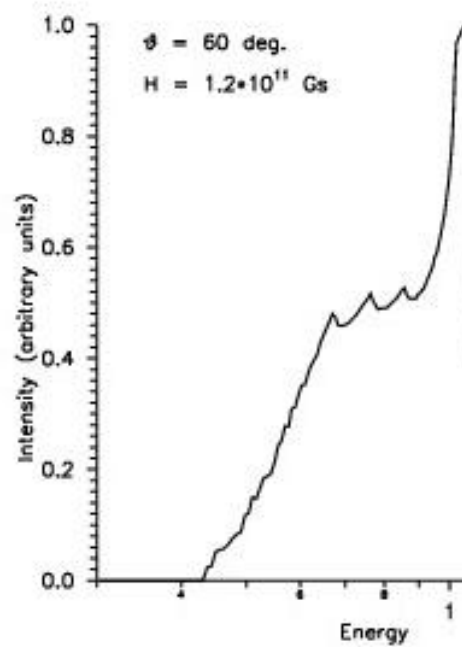
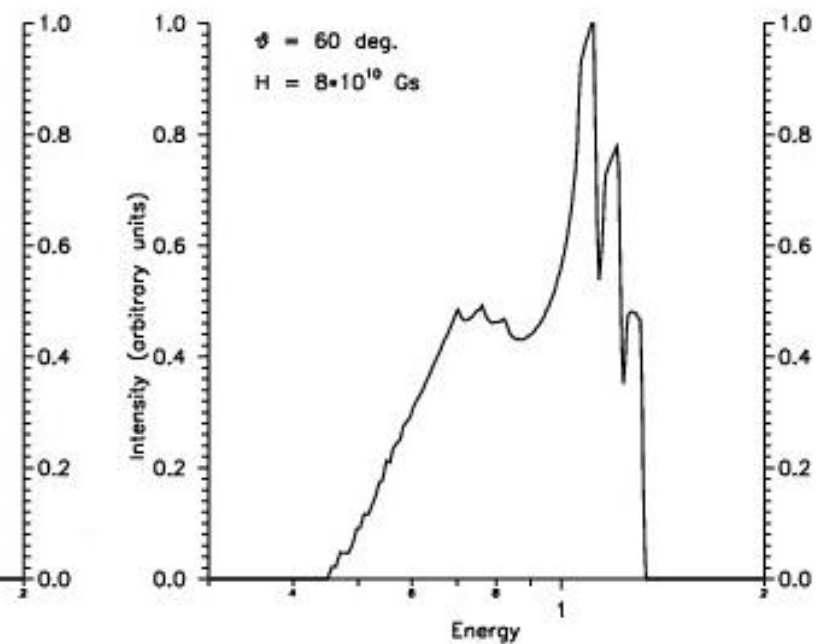
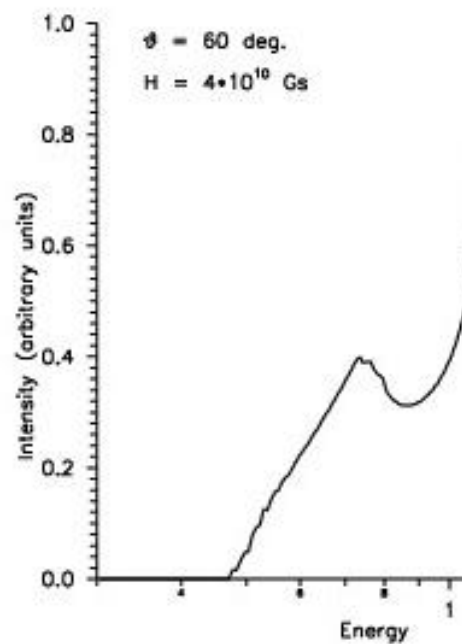
# Magnetic field estimations near BH horizon in AGNs and GBHCs

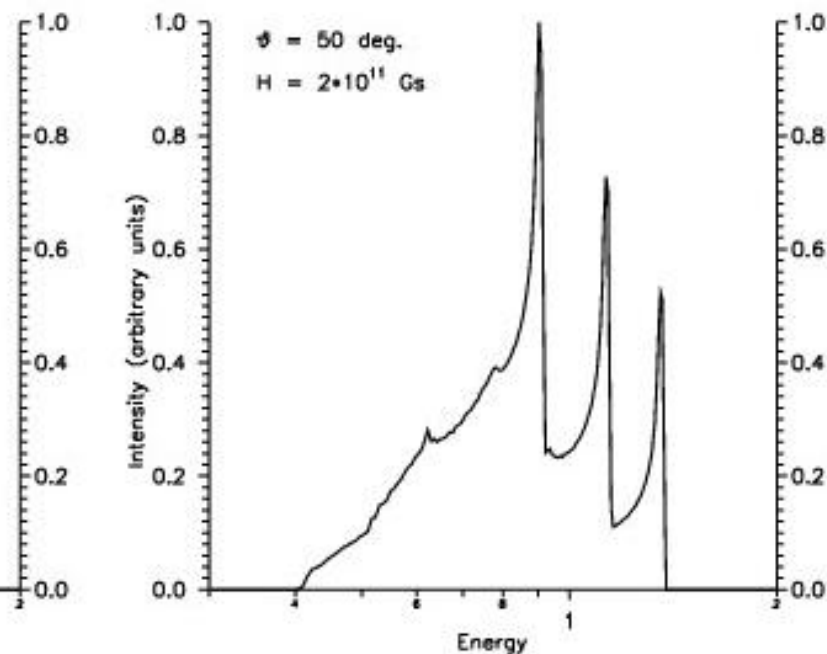
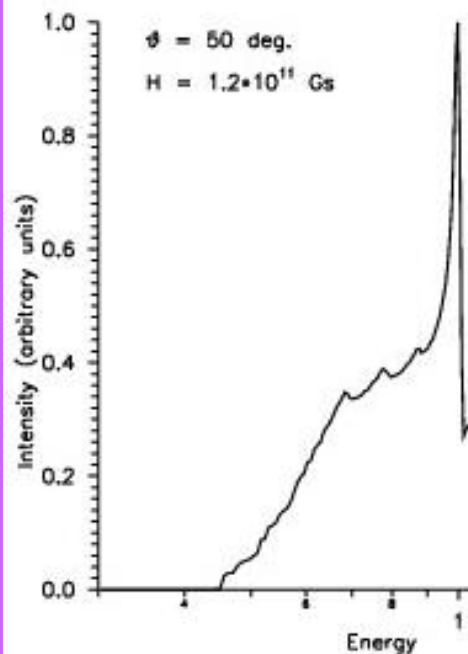
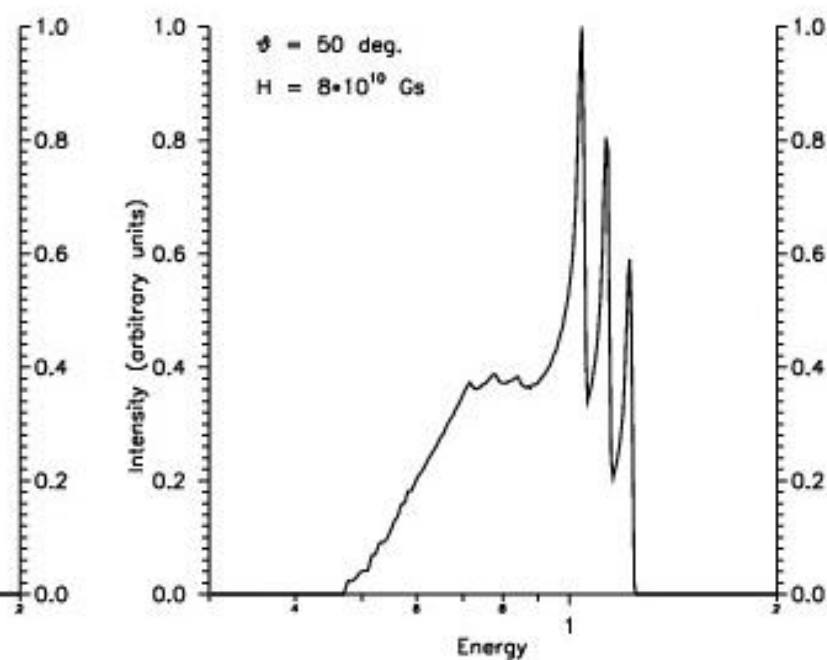
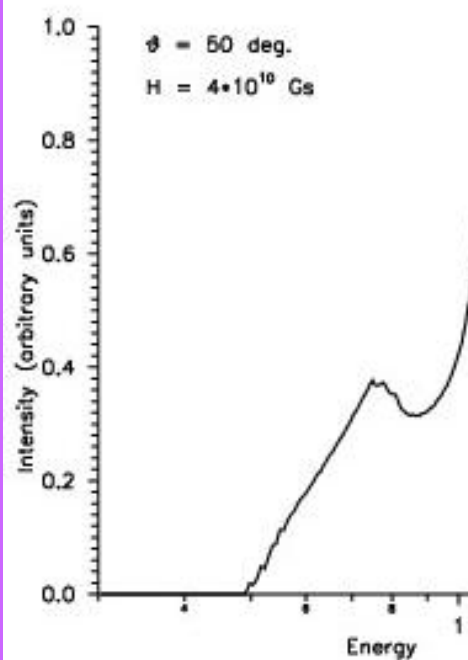
(Zakharov, Kardashev, Lukash, Repin, MNRAS, 342,1325,  
(2003))

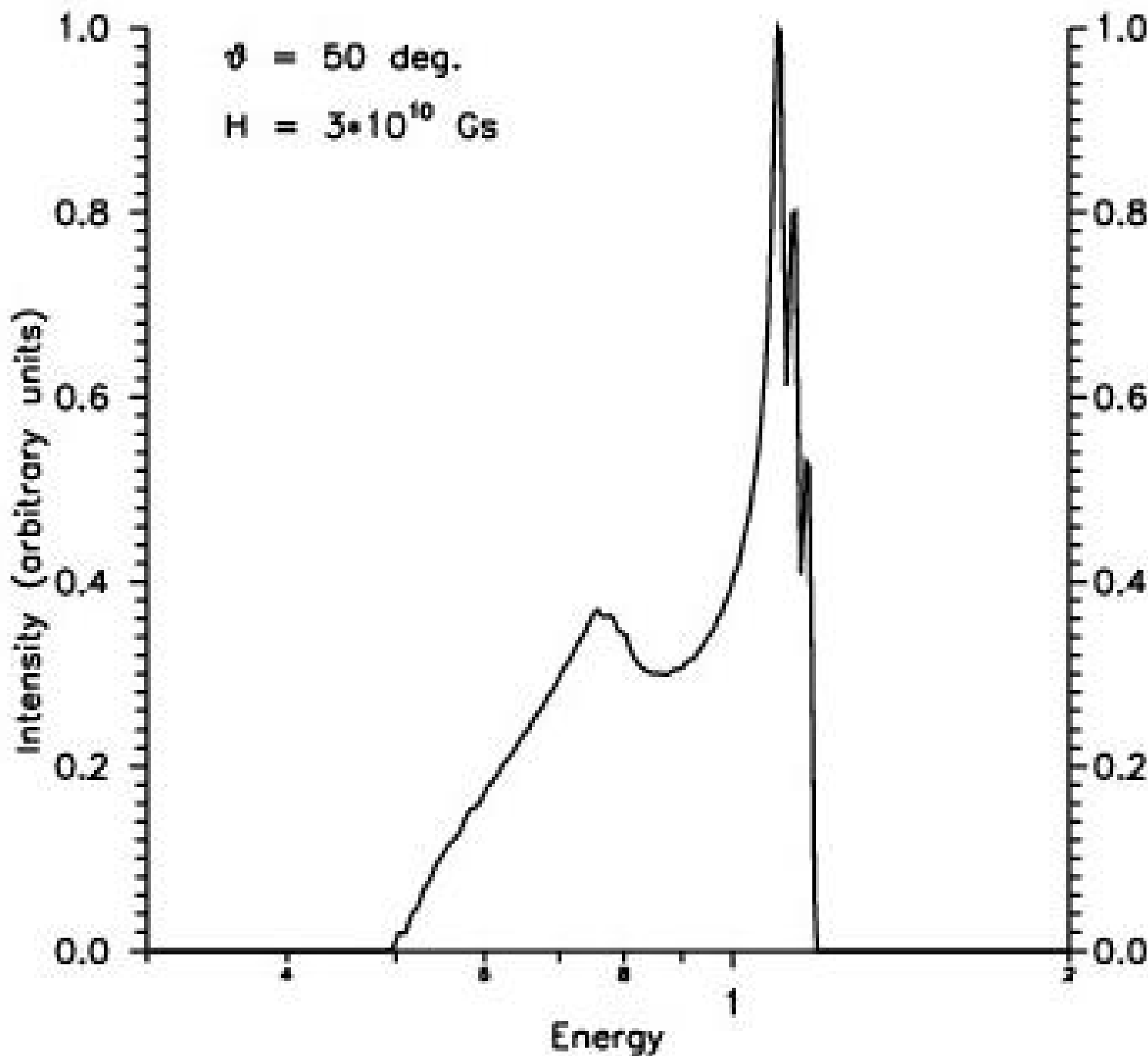
- Zeeman splitting  $E_1 = E_0 - \mu_B H$ ,  $E_2 = E_0 + \mu_B H$ ,  
 $\mu_B = e\hbar/(2m_e c)$ ,  $\mu_B = 9.3 \times 10^{-21}$  erg/G
- [Figure1](#)
- [Figure2](#)
- [Figure3](#)
- [Figure4](#)
- [Figure5](#)
- [Figure6](#)
- [ASCAdata](#)

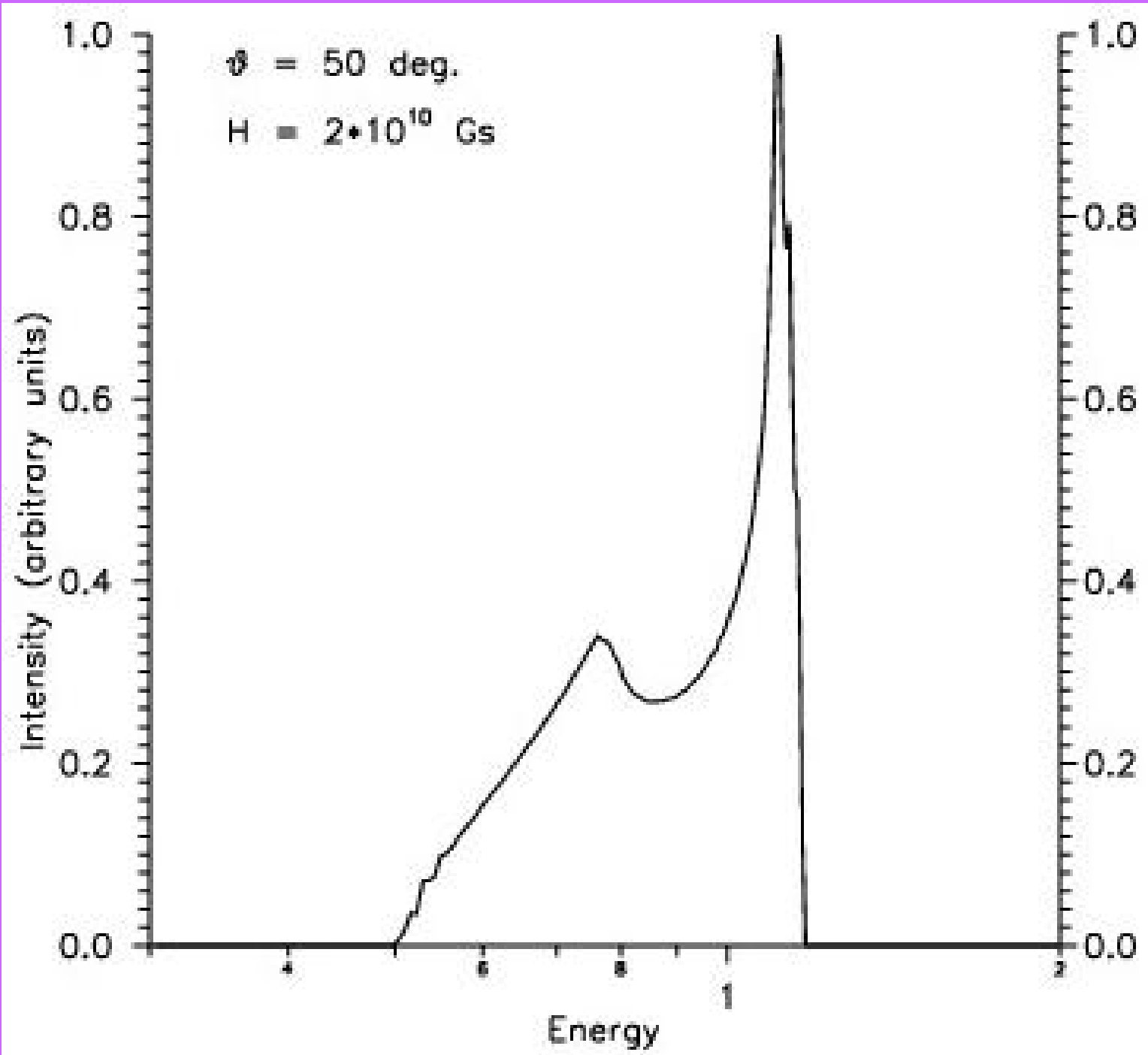


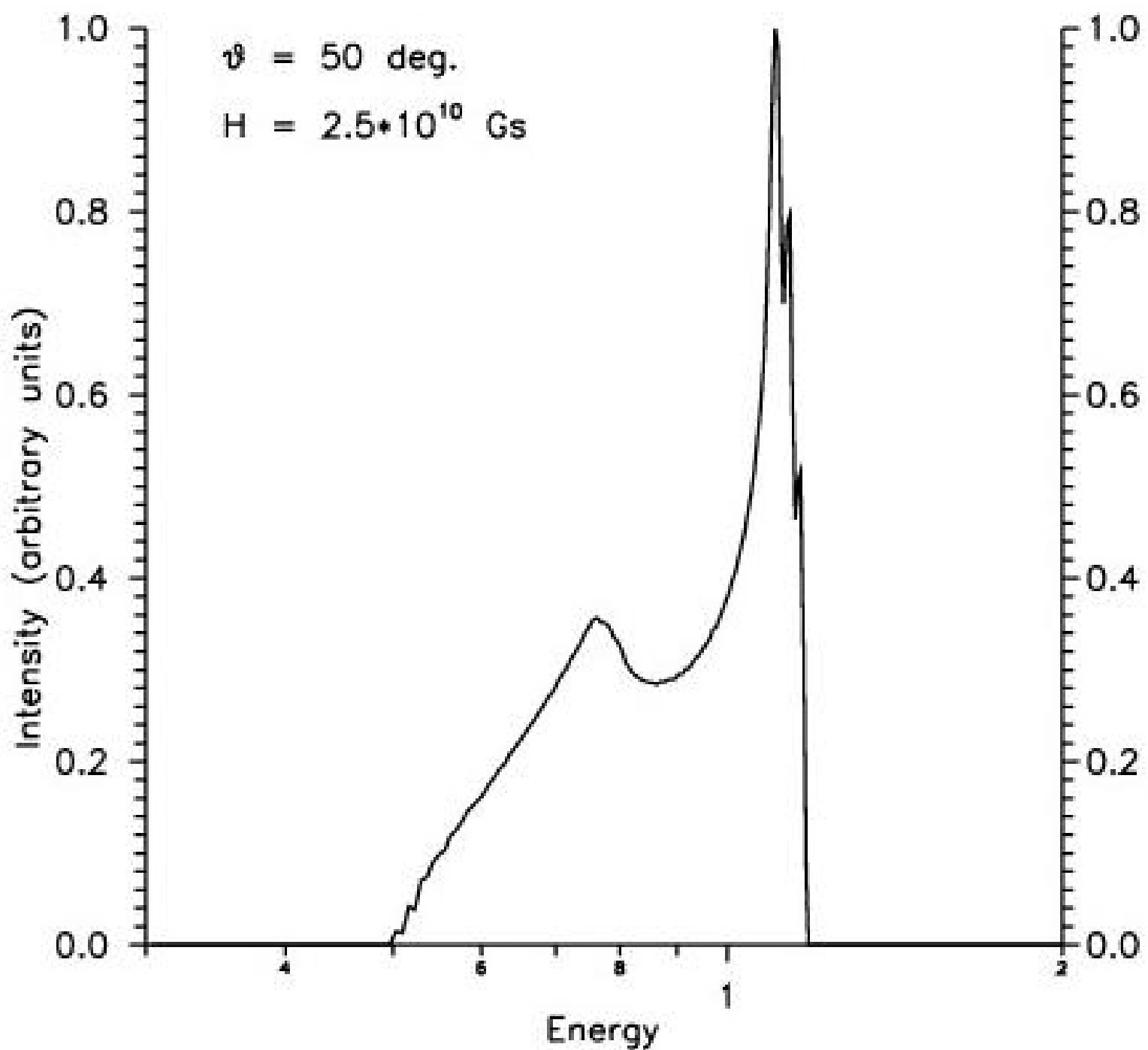


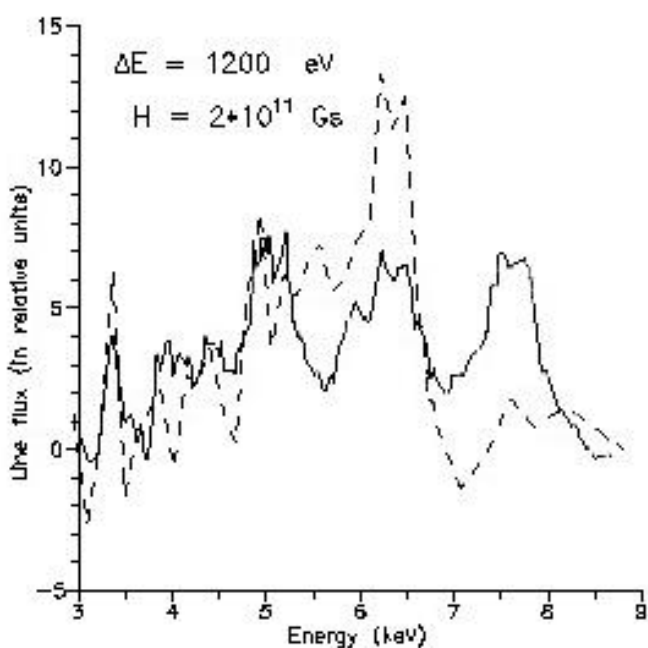
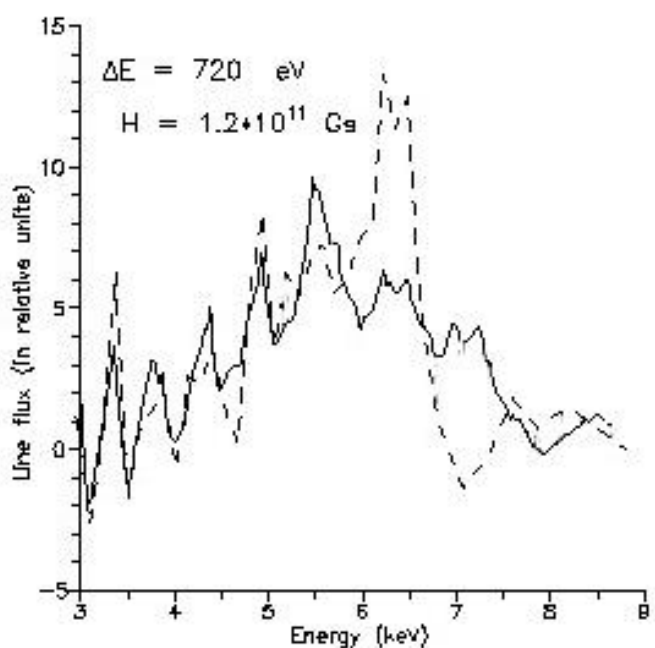
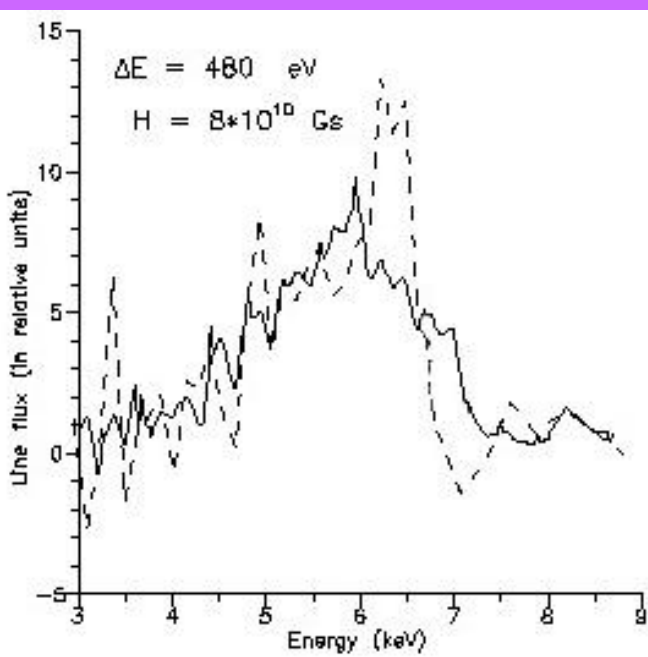
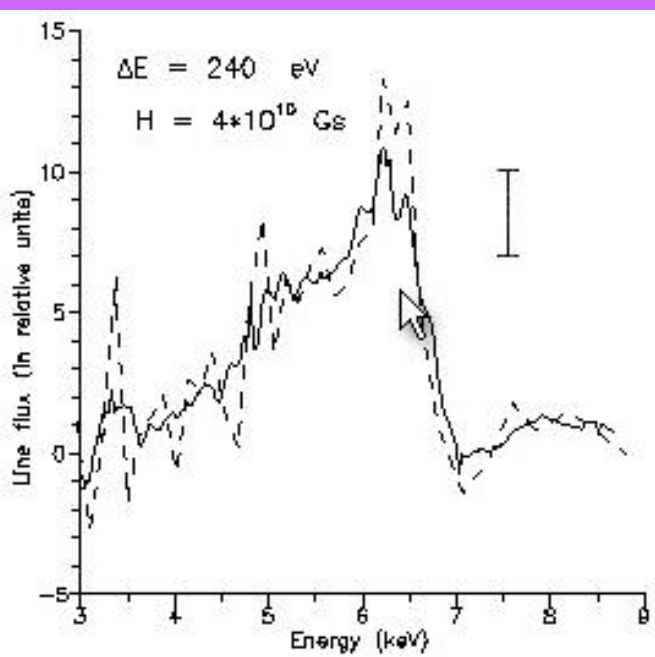






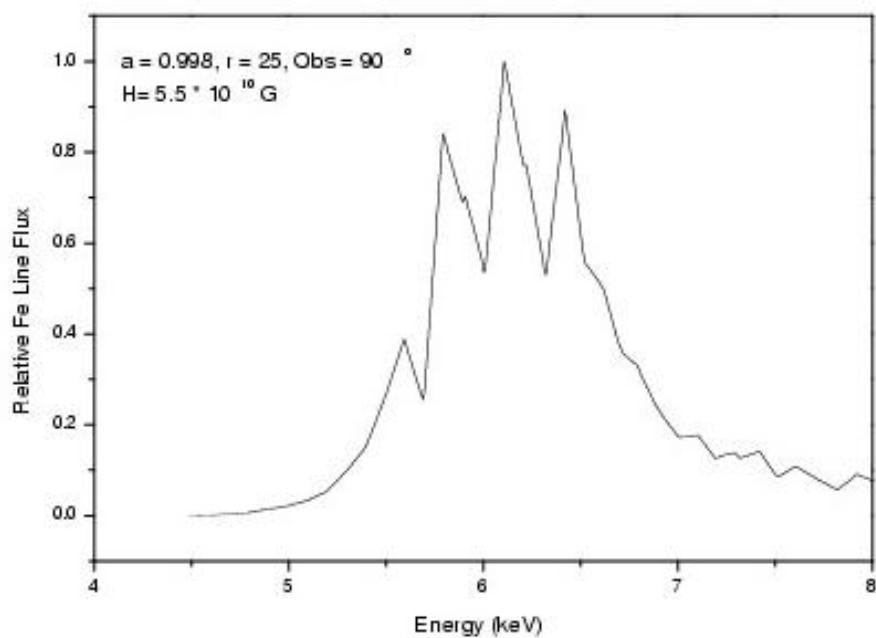
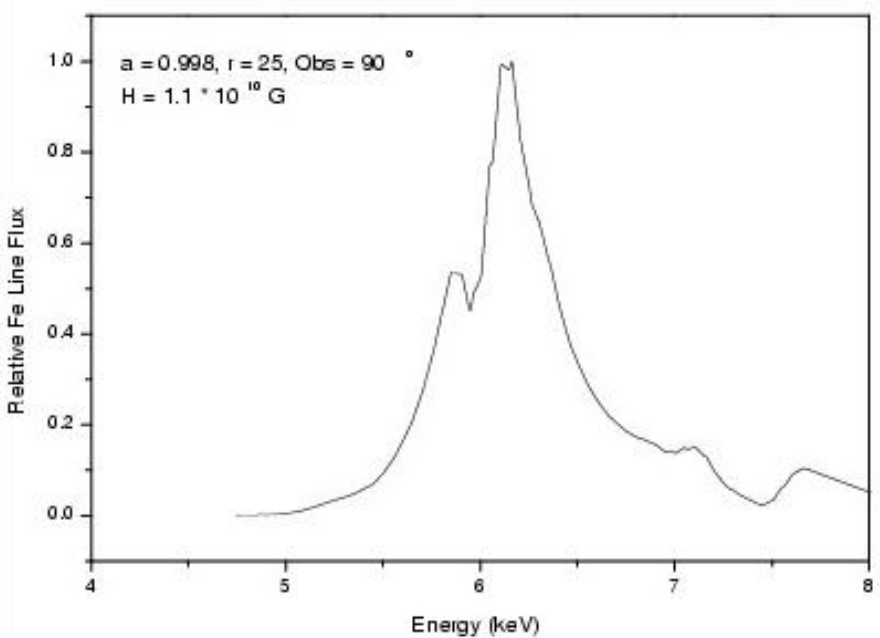
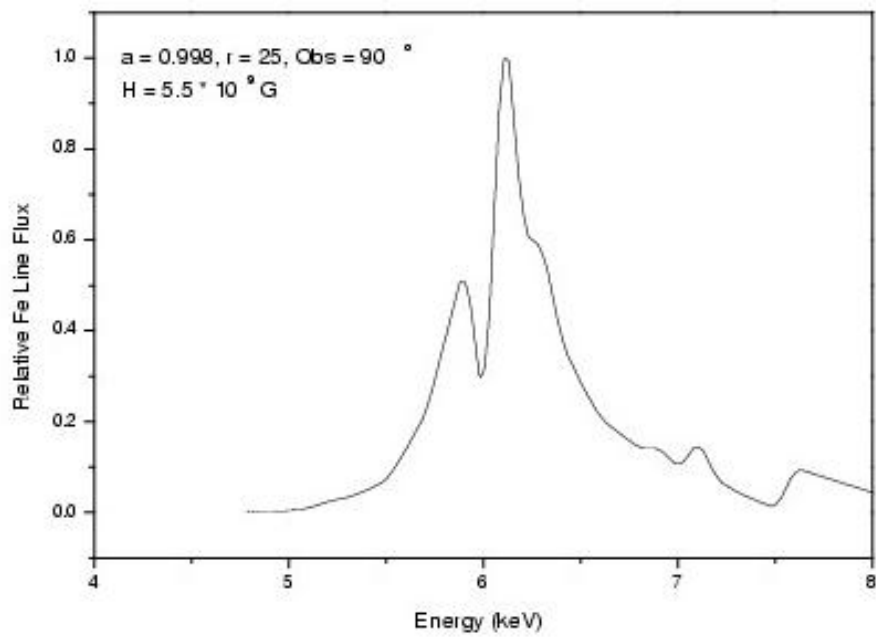
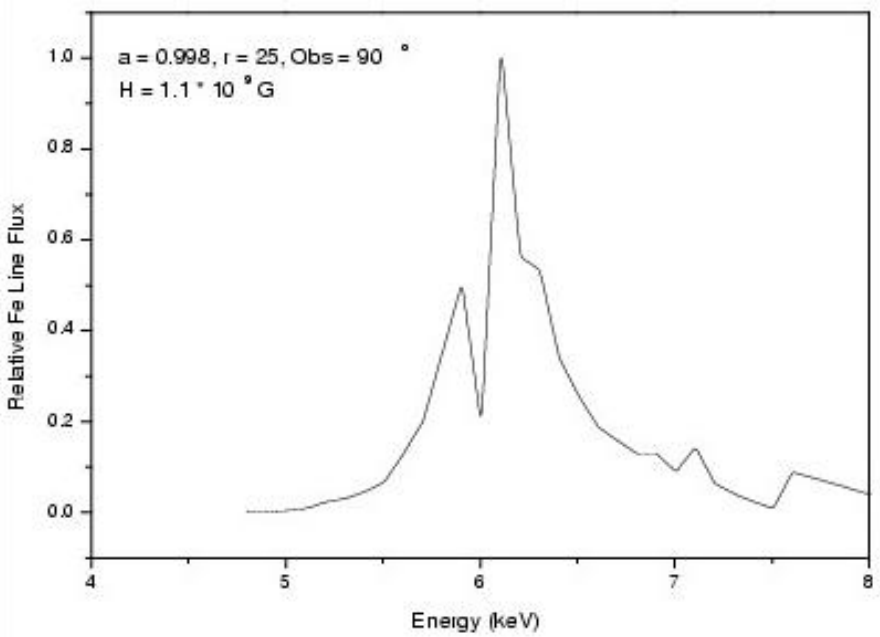


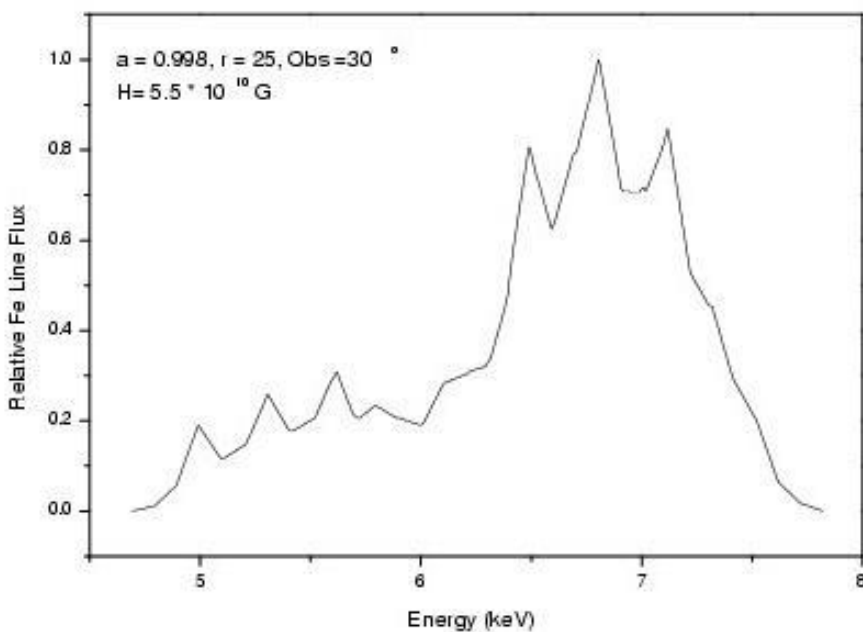
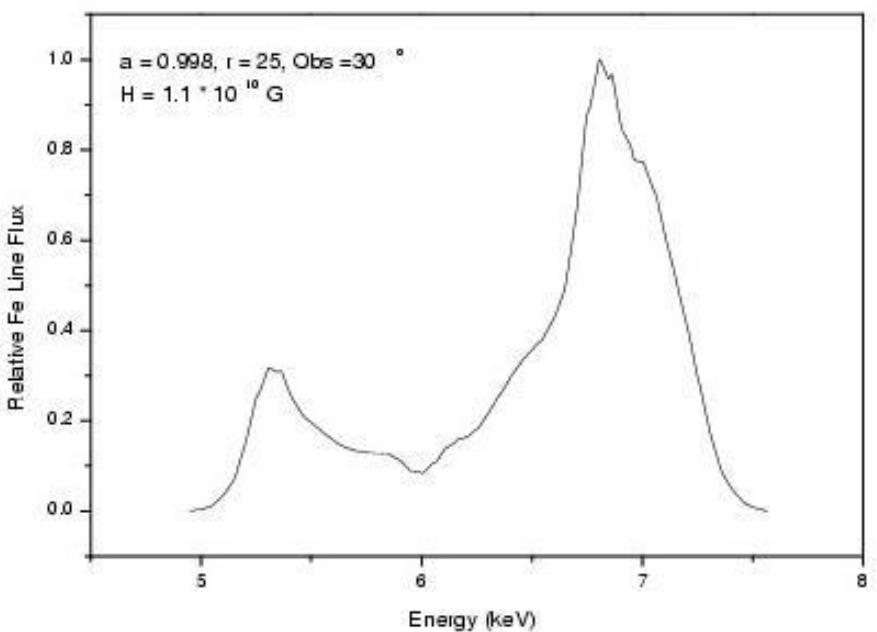
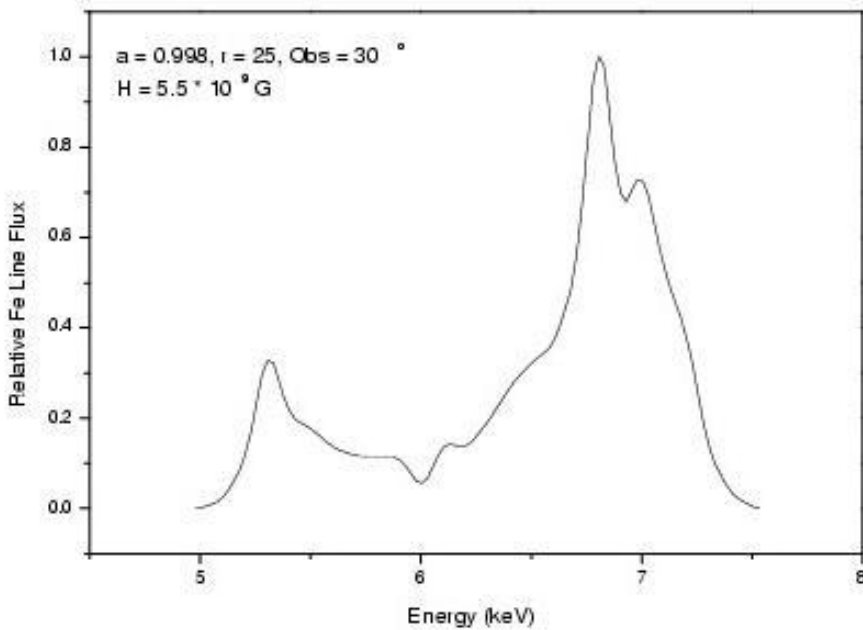
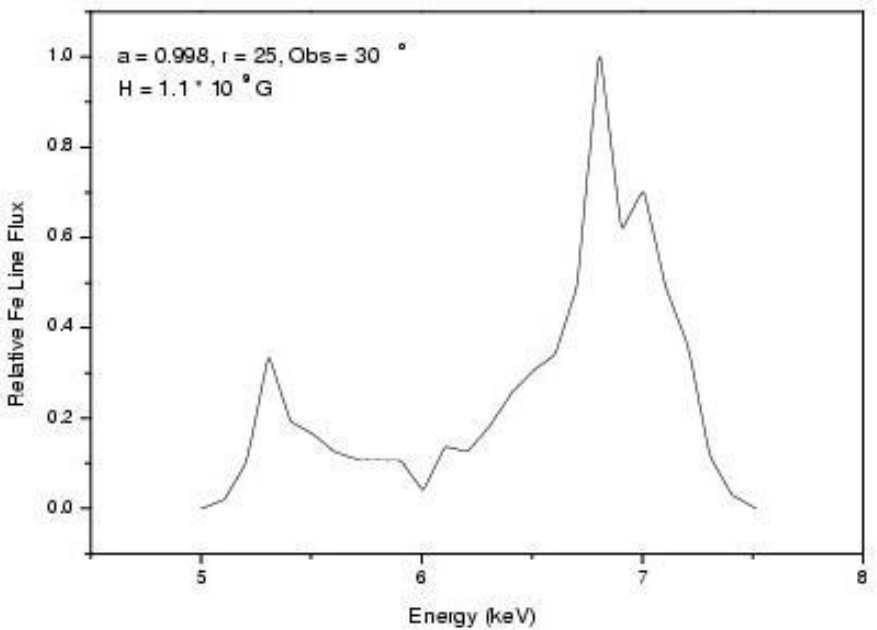


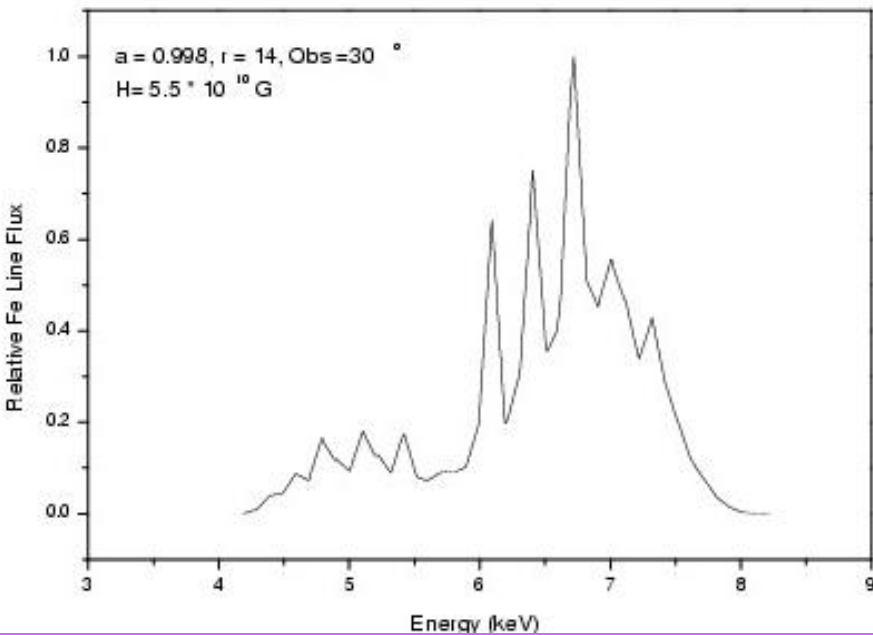
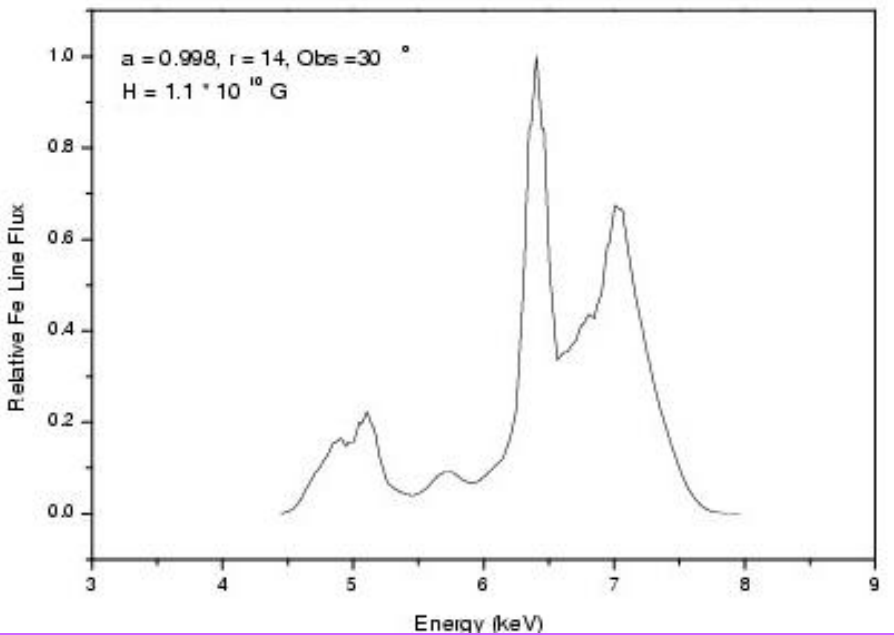
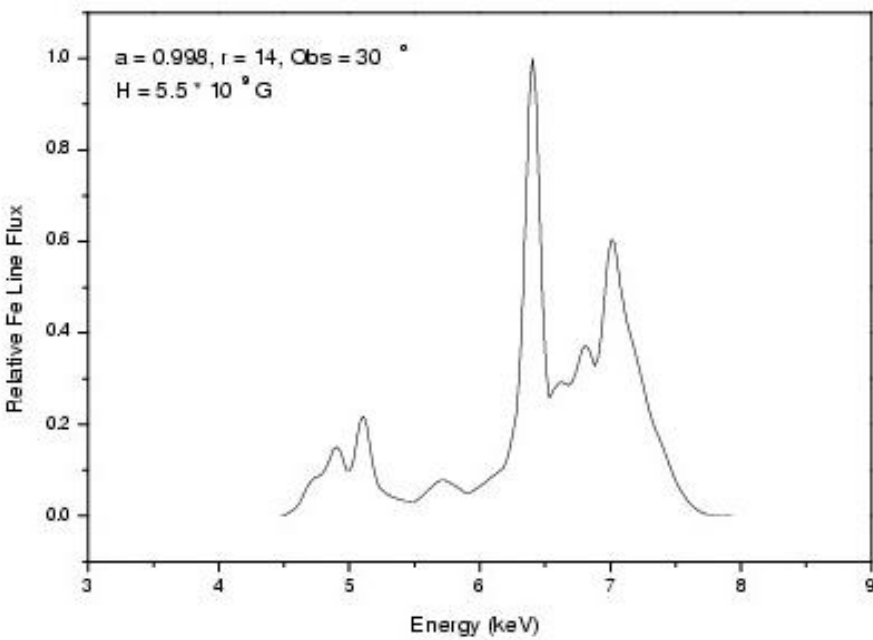
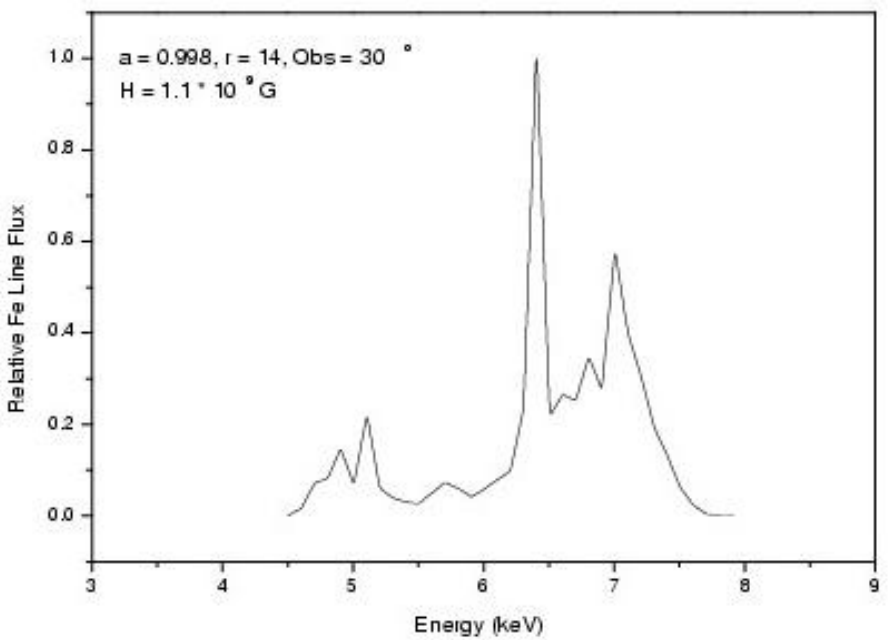


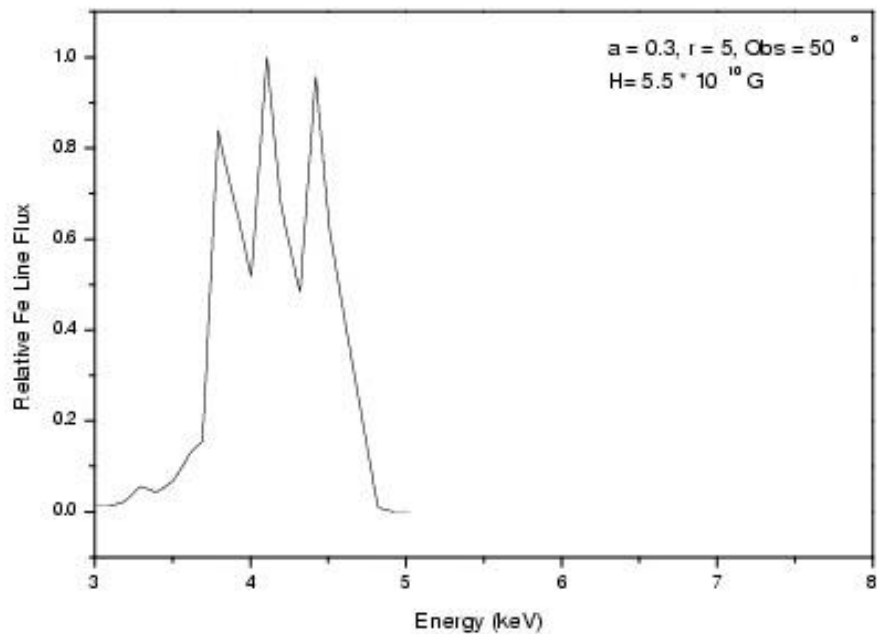
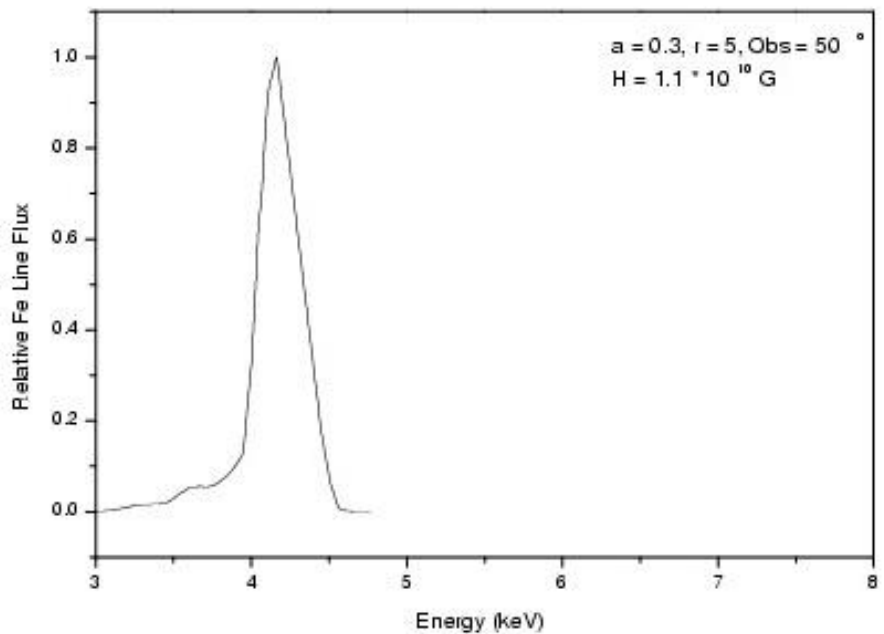
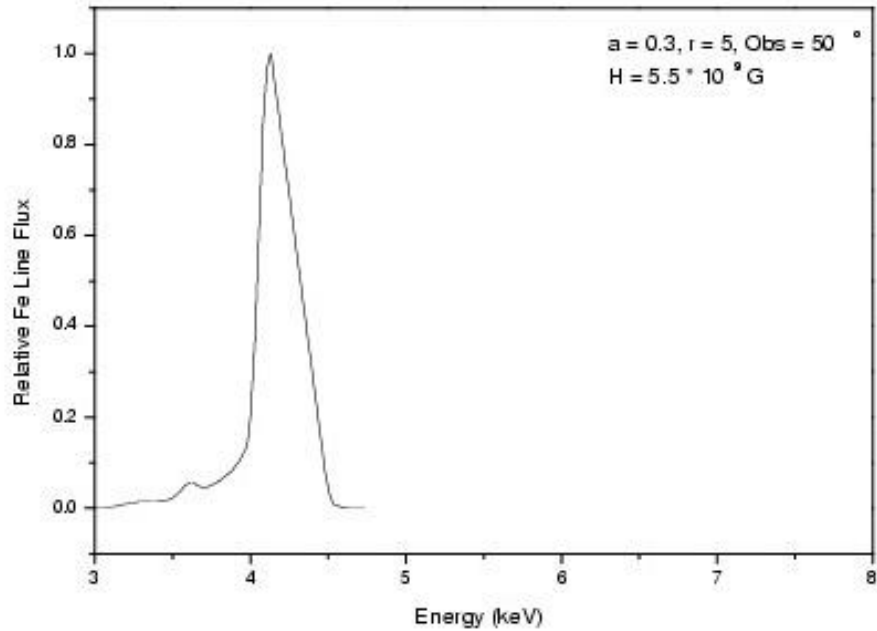
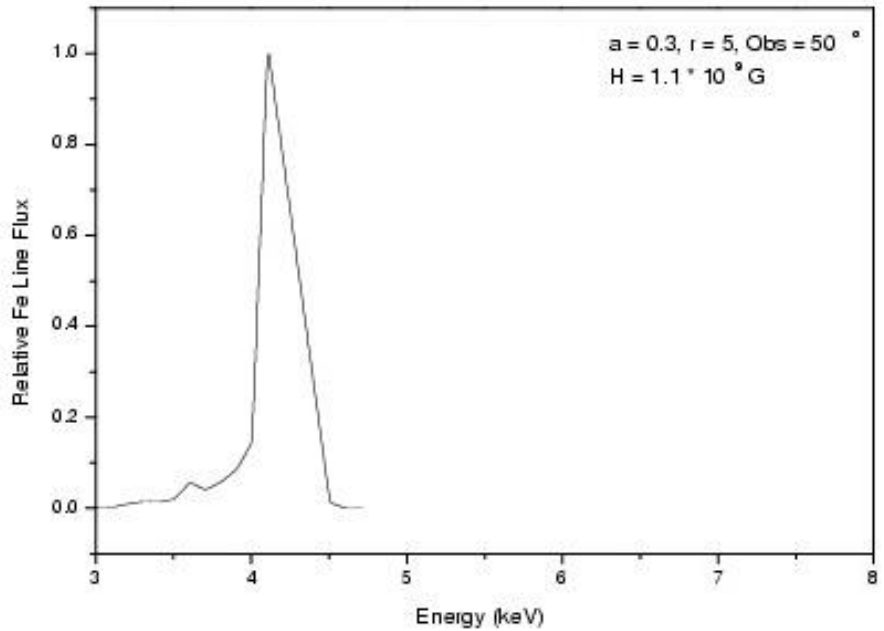
Magnetic field estimations near BH horizon in AGNs and  
GBHCs for non-flat accretion flows  
(Zakharov, Ma, Bao, New Astronomy, **9**, 663 (2004))

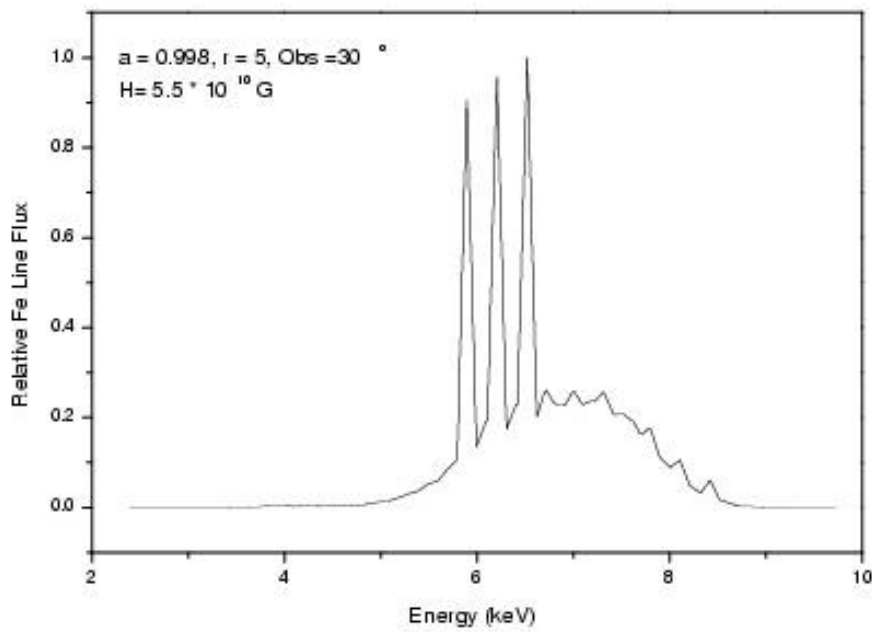
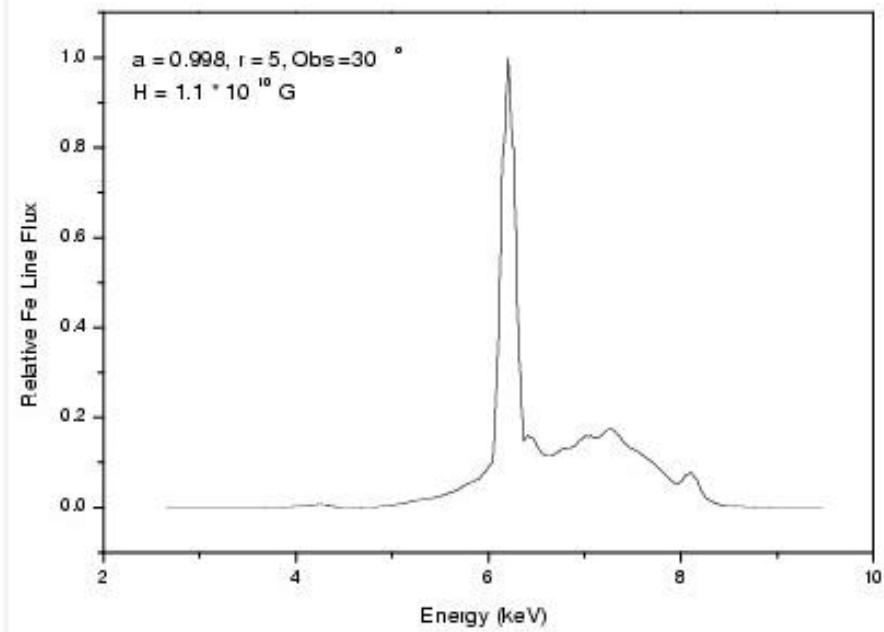
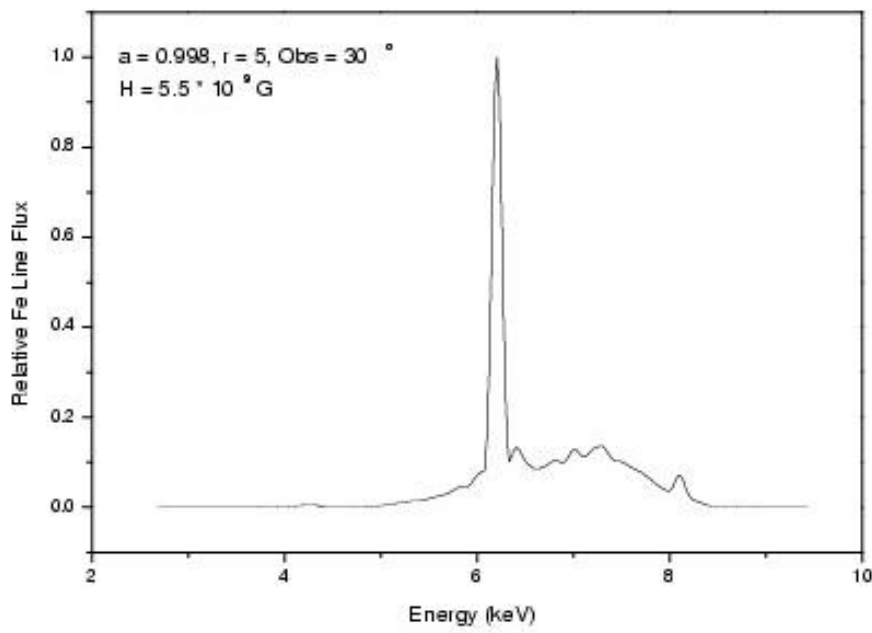
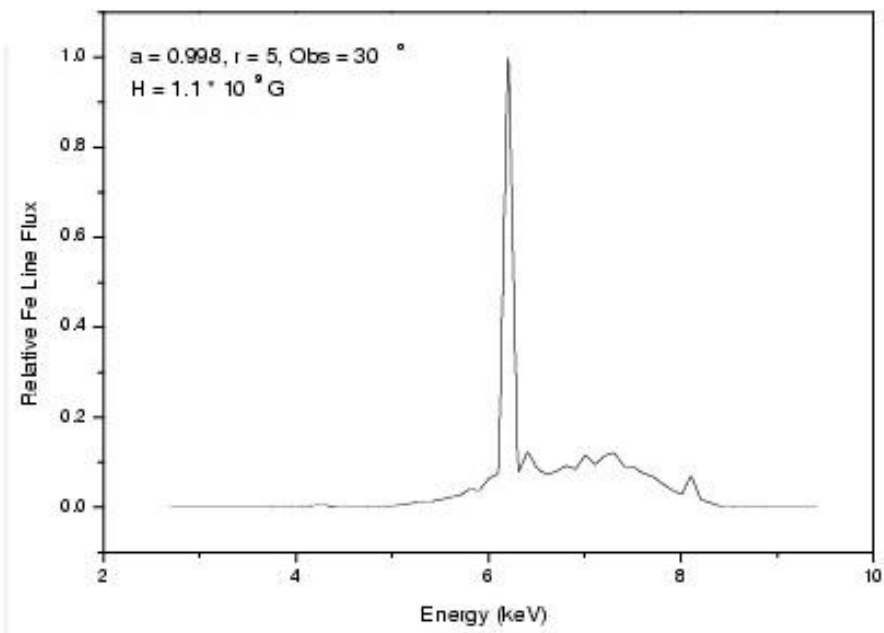
- Figure1
- Figure2
- Figure3
- Figure4
- Figure5
- Figure6

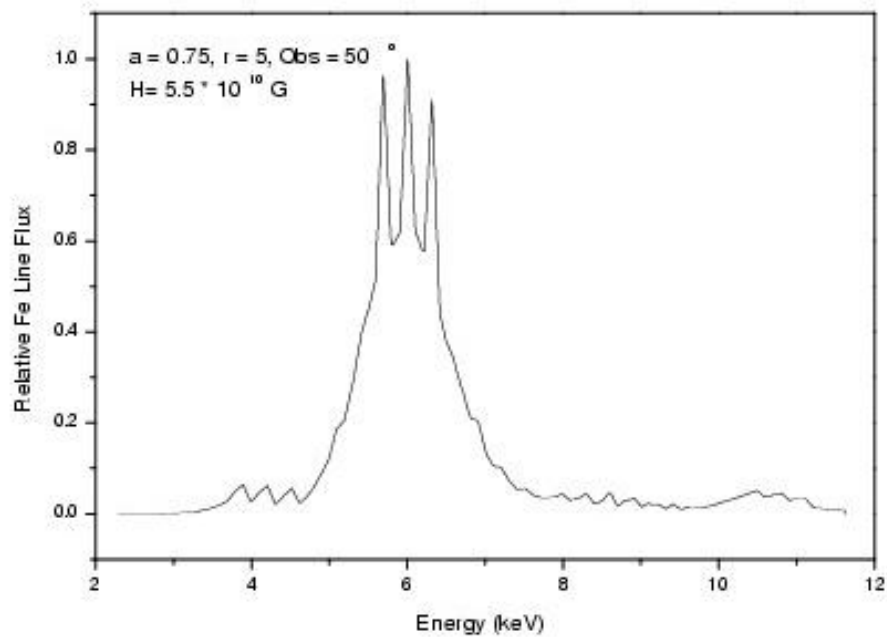
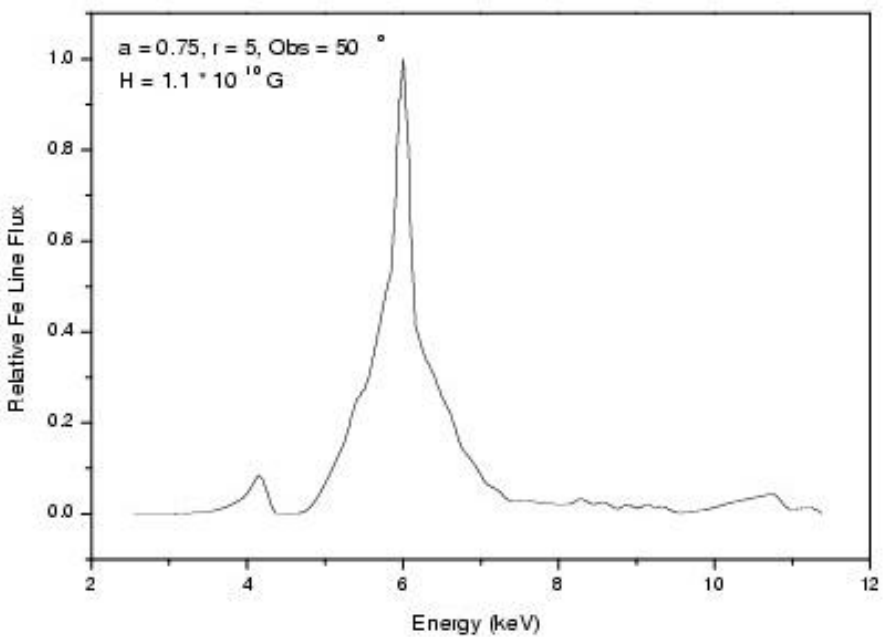
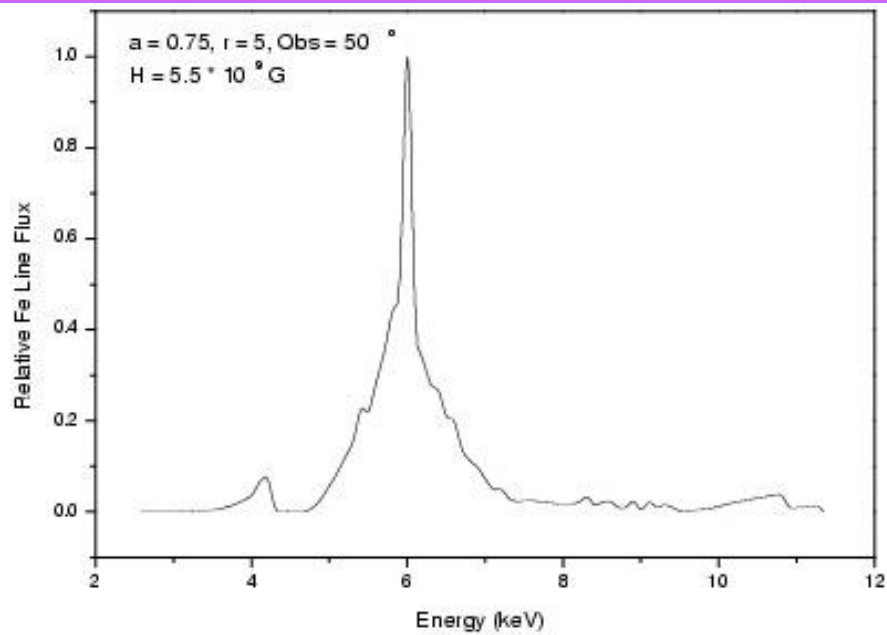
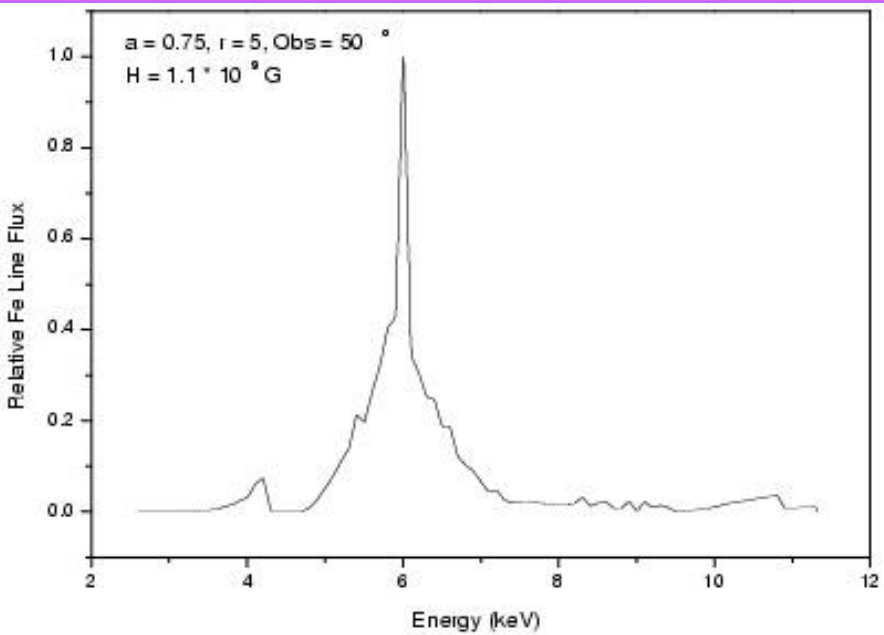












# XMM-EPIC observation of MCG–6–30–15: direct evidence for the extraction of energy from a spinning black hole?

Jörn Wilms,<sup>1</sup>★ Christopher S. Reynolds,<sup>2,3</sup>† Mitchell C. Begelman,<sup>3,4</sup> James Reeves,<sup>5</sup> Silvano Molendi,<sup>6</sup> Rüdiger Staubert<sup>1</sup> and Eckhard Kendziorra<sup>1</sup>

<sup>1</sup>Institut für Astronomie und Astrophysik, Abt. Astronomie, Universität Tübingen, Sand 1, D-72076 Tübingen, Germany

<sup>2</sup>Department of Astronomy, University of Maryland, College Park, MD 20742, USA

<sup>3</sup>JILA, Campus Box 440, University of Colorado, Boulder, CO 80309, USA

<sup>4</sup>Department of Astrophysical and Planetary Sciences, University of Colorado, Boulder, CO 80309, USA

<sup>5</sup>X-Ray Astronomy Group, Department of Physics and Astronomy, Leicester University, Leicester LE1 7RH

<sup>6</sup>Istituto di Fisica Cosmica, CNR, via Bassini 15, I-20133 Milano, Italy

Accepted 2001 October 22. Received 2001 October 22; in original form 2001 August 24

## ABSTRACT

We present *XMM-Newton* European Photon Imaging Camera (EPIC) observations of the bright Seyfert 1 galaxy MCG–6–30–15, focusing on the broad Fe K $\alpha$  line at  $\sim 6$  keV and the associated reflection continuum, which is believed to originate from the inner accretion disc. We find these reflection features to be *extremely* broad and redshifted, indicating an origin in the very central regions of the accretion disc. It seems likely that we have caught this source in the ‘deep minimum’ state first observed by Iwasawa et al. The implied central concentration of X-ray illumination is difficult to understand in any pure accretion disc model. We suggest that we are witnessing the extraction and dissipation of rotational energy from a spinning black hole by magnetic fields connecting the black hole or plunging region to the disc.

**Key words:** accretion, accretion discs – black hole physics – galaxies: individual: MCG–6–30–15 – galaxies: Seyfert – X-rays: galaxies.

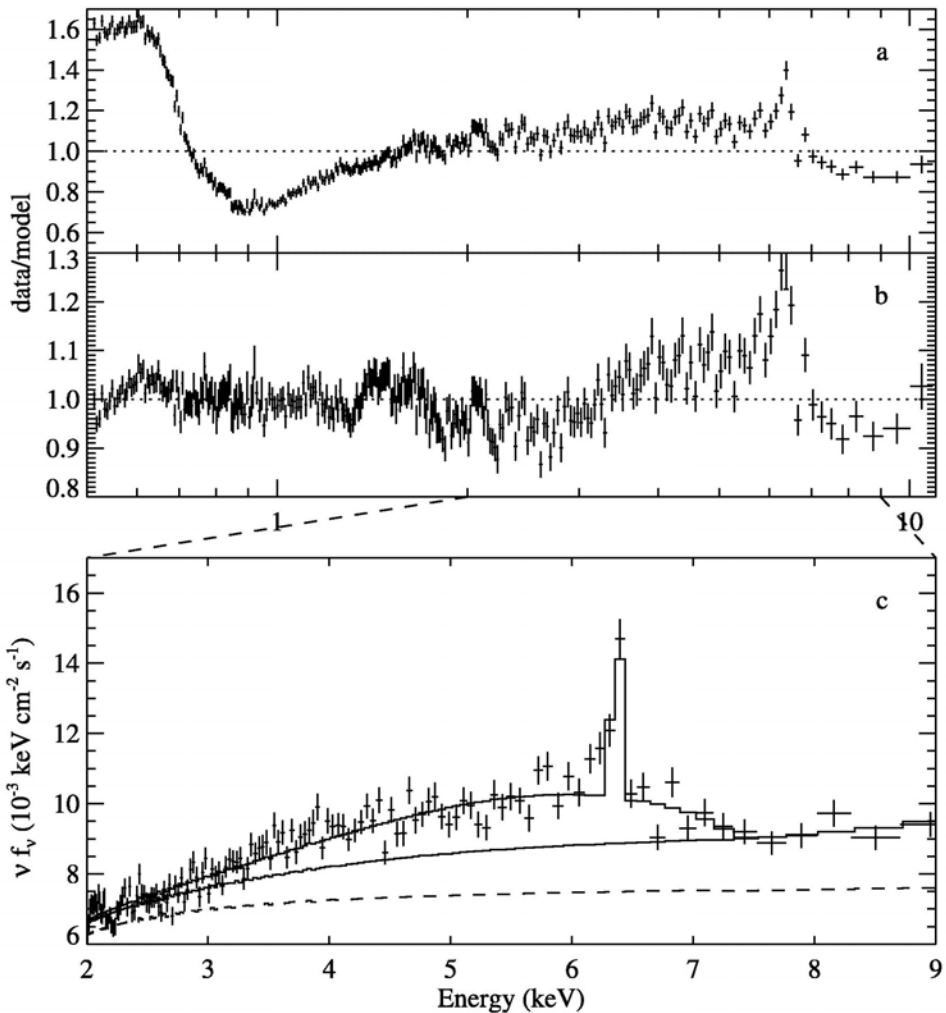
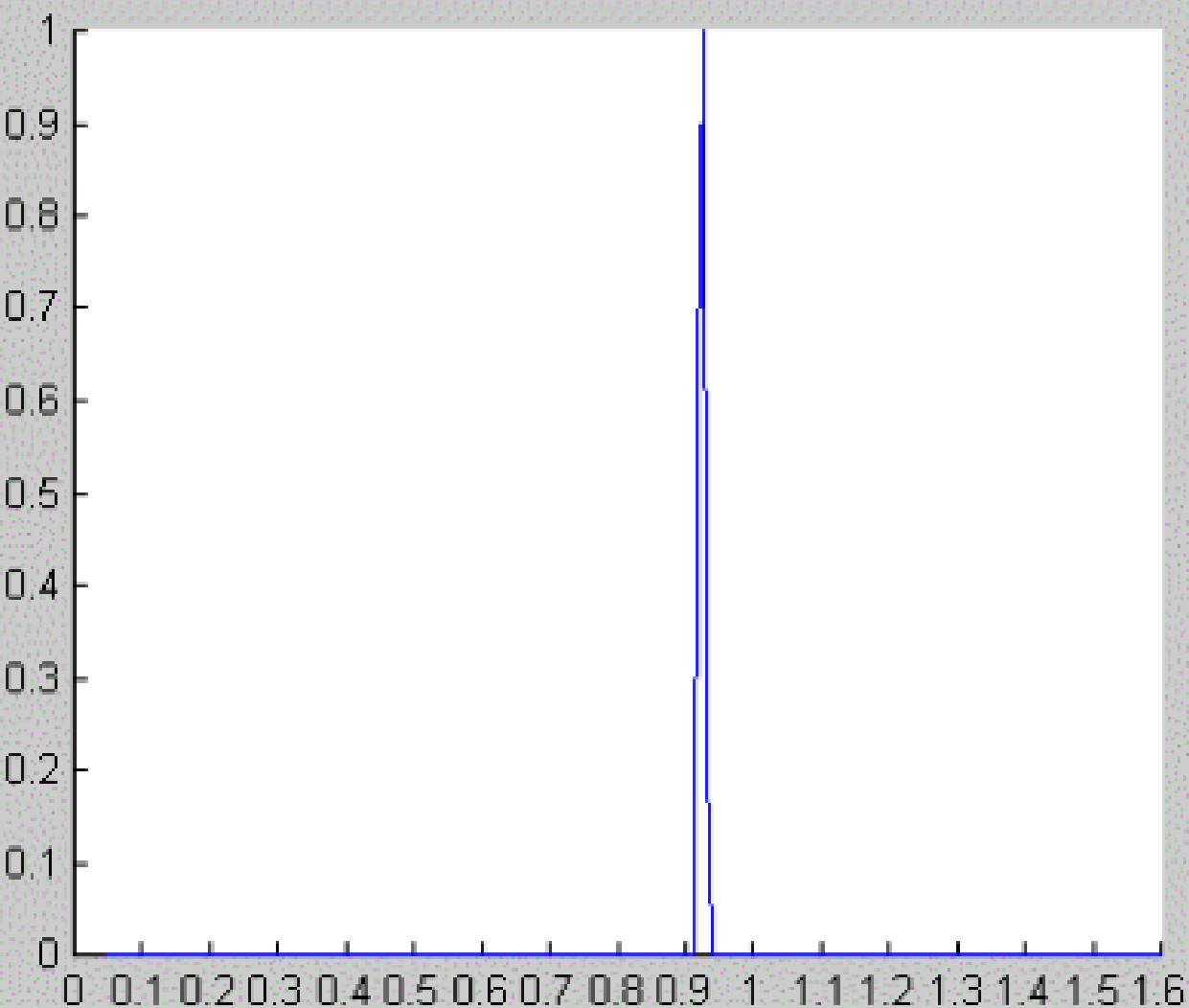


**Figure 1.** (a) Ratio between data and model from fitting a power law to the 0.5–11 keV data. (b) Ratio from fitting a power law and the empirical warm absorber model (see text). (c) Deconvolved spectrum of the Fe K $\alpha$  band, showing the total LAOR model and the continuum with and without (dashed) the reflection component for a model with reflection from an ionized disc. For clarity, the data have been rebinned and only the single-event data points are shown.

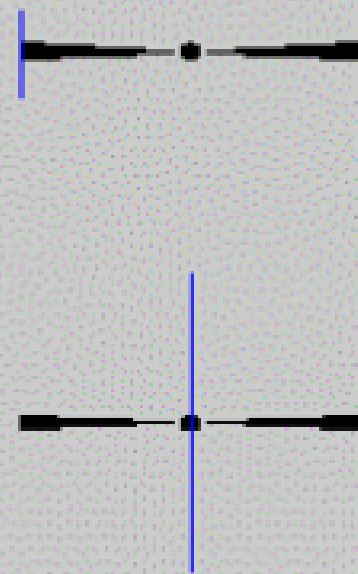
Figure No. 1

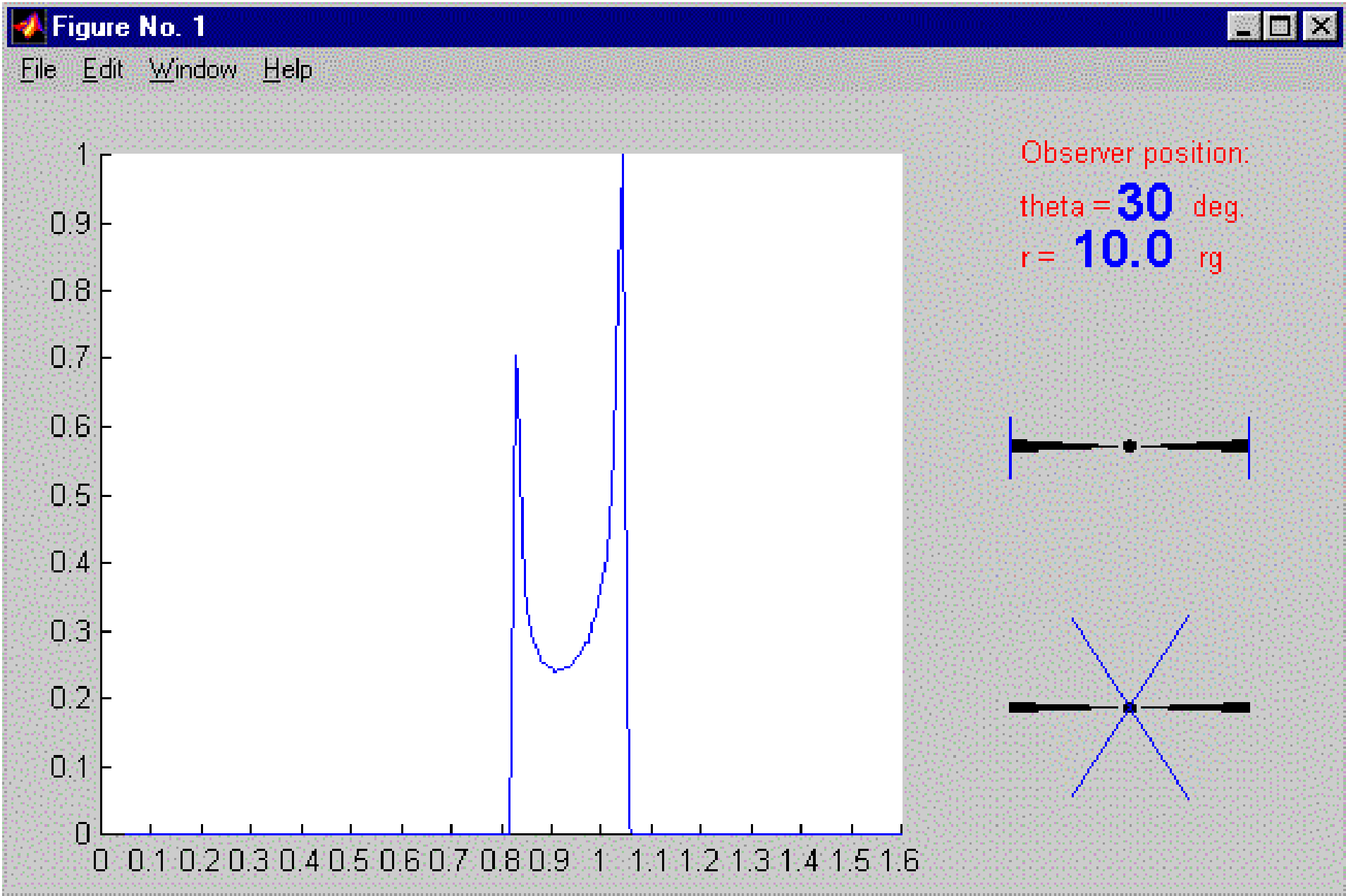


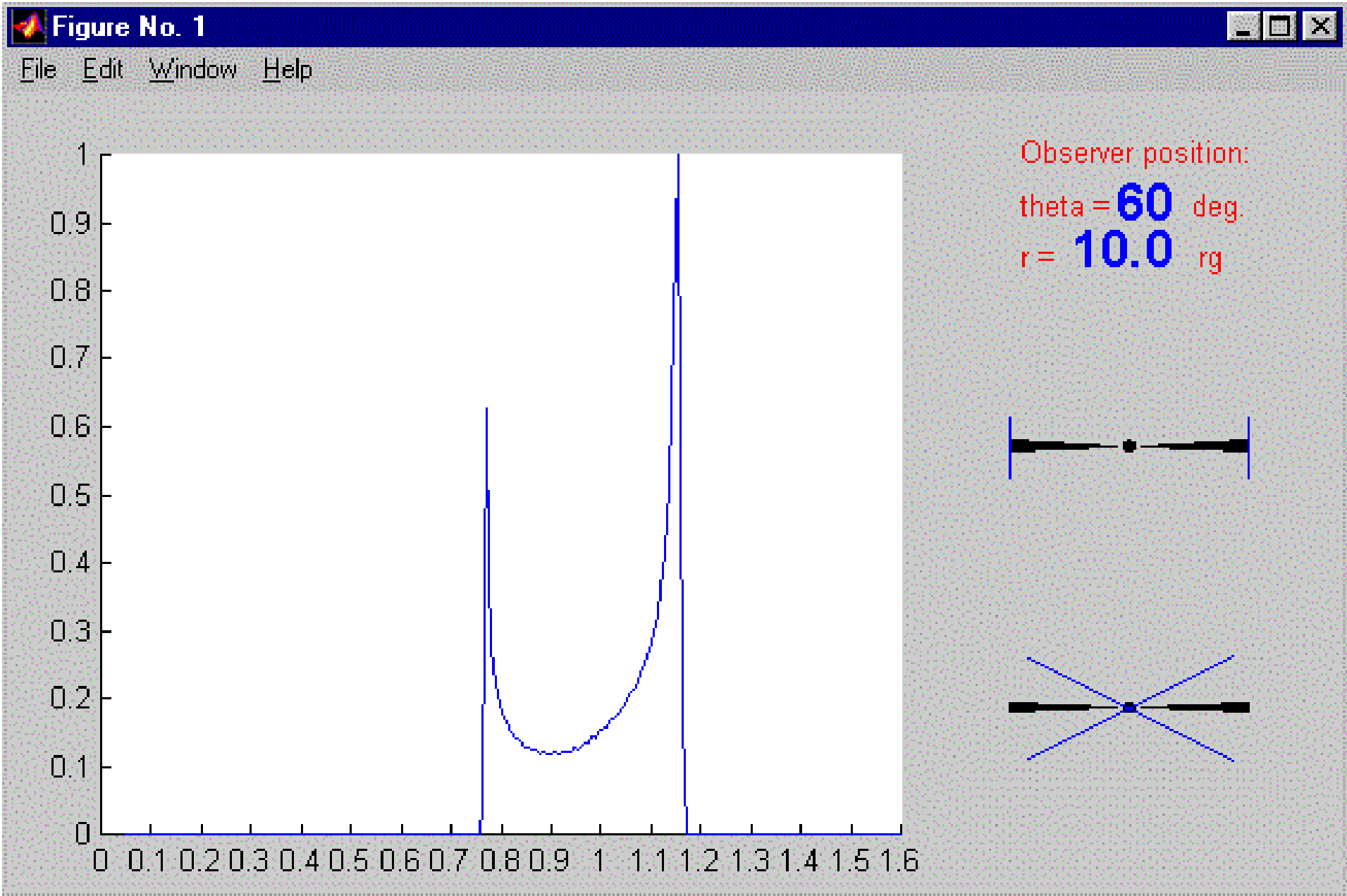
File Edit Window Help

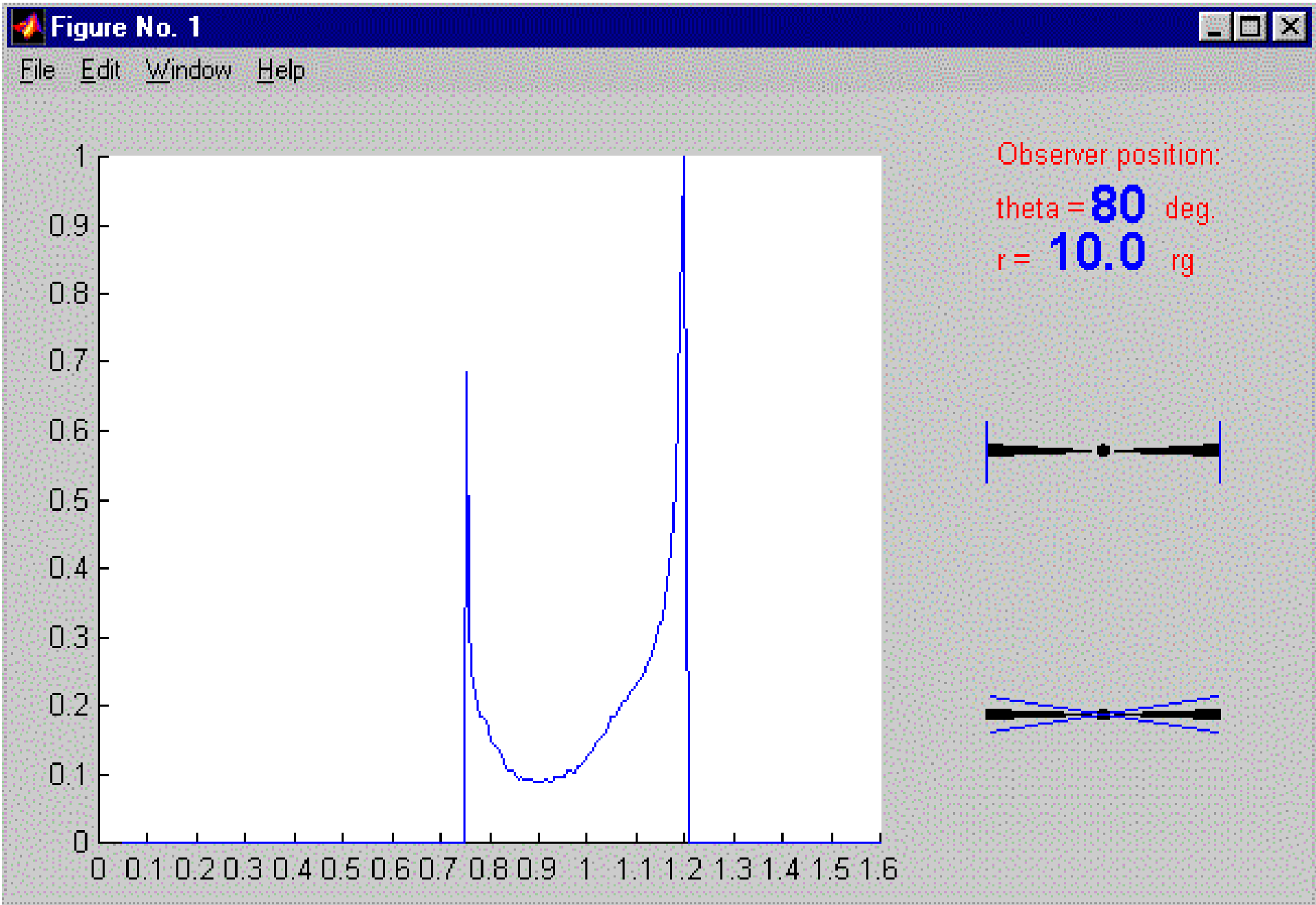


Observer position:  
theta = **0** deg.  
r = **10.0** rg



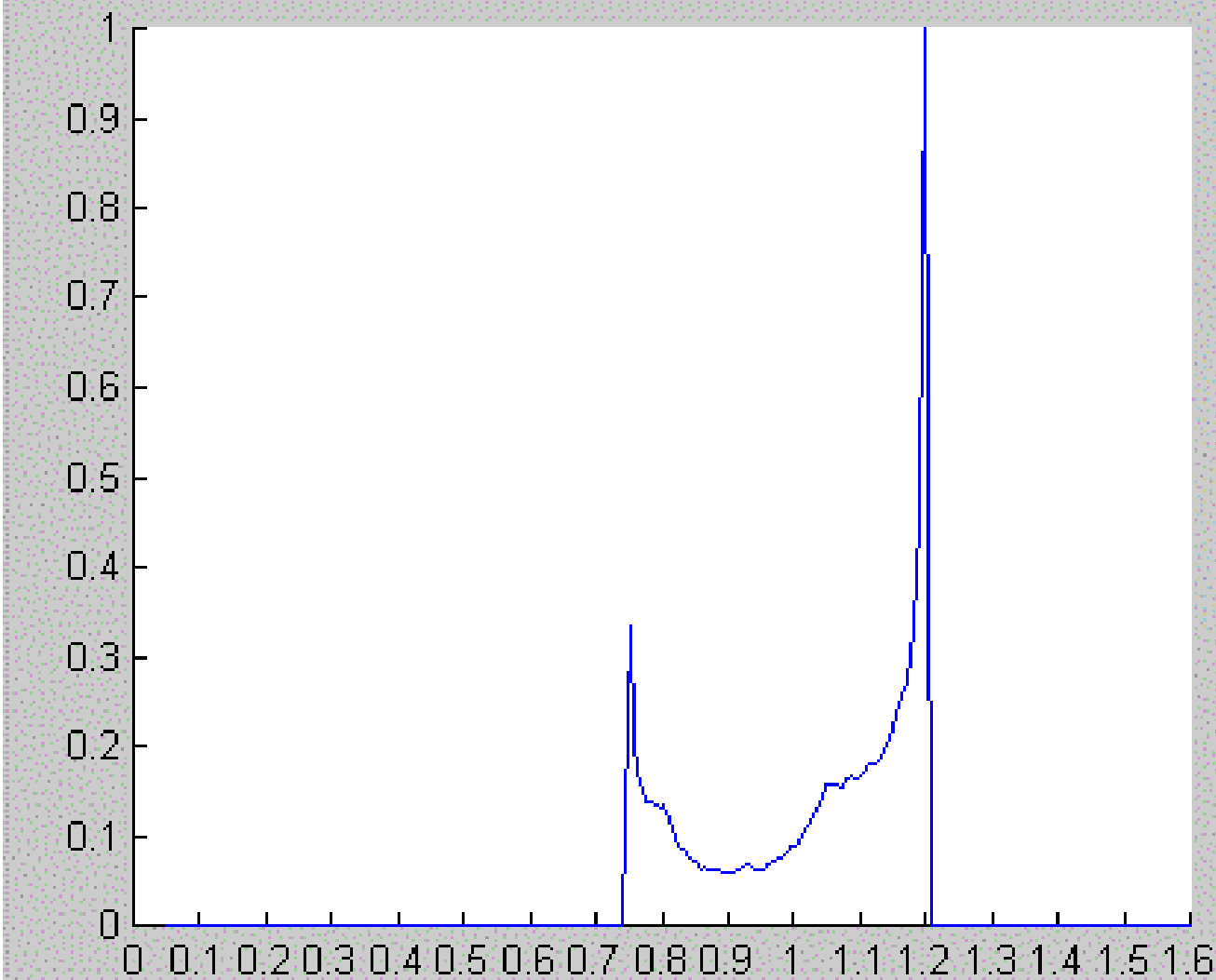




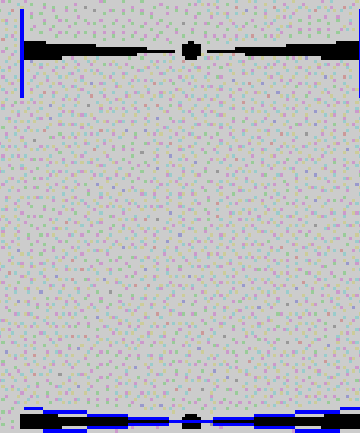




File Edit Window Help

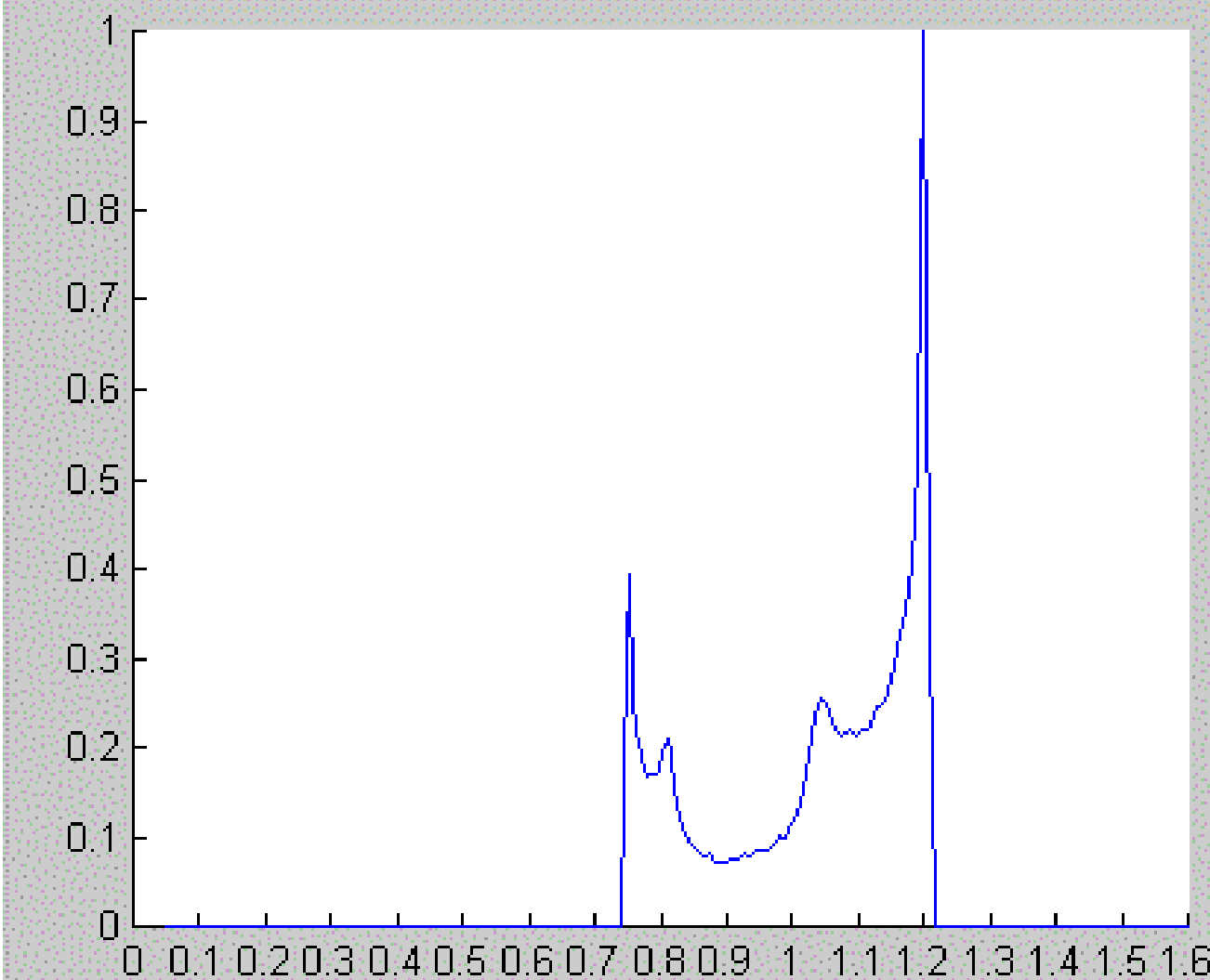


Observer position:  
theta = **85** deg.  
r = **10.0** rg

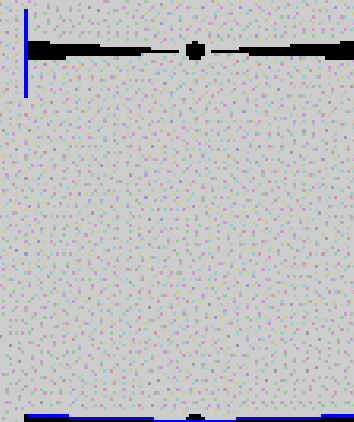




File Edit Window Help

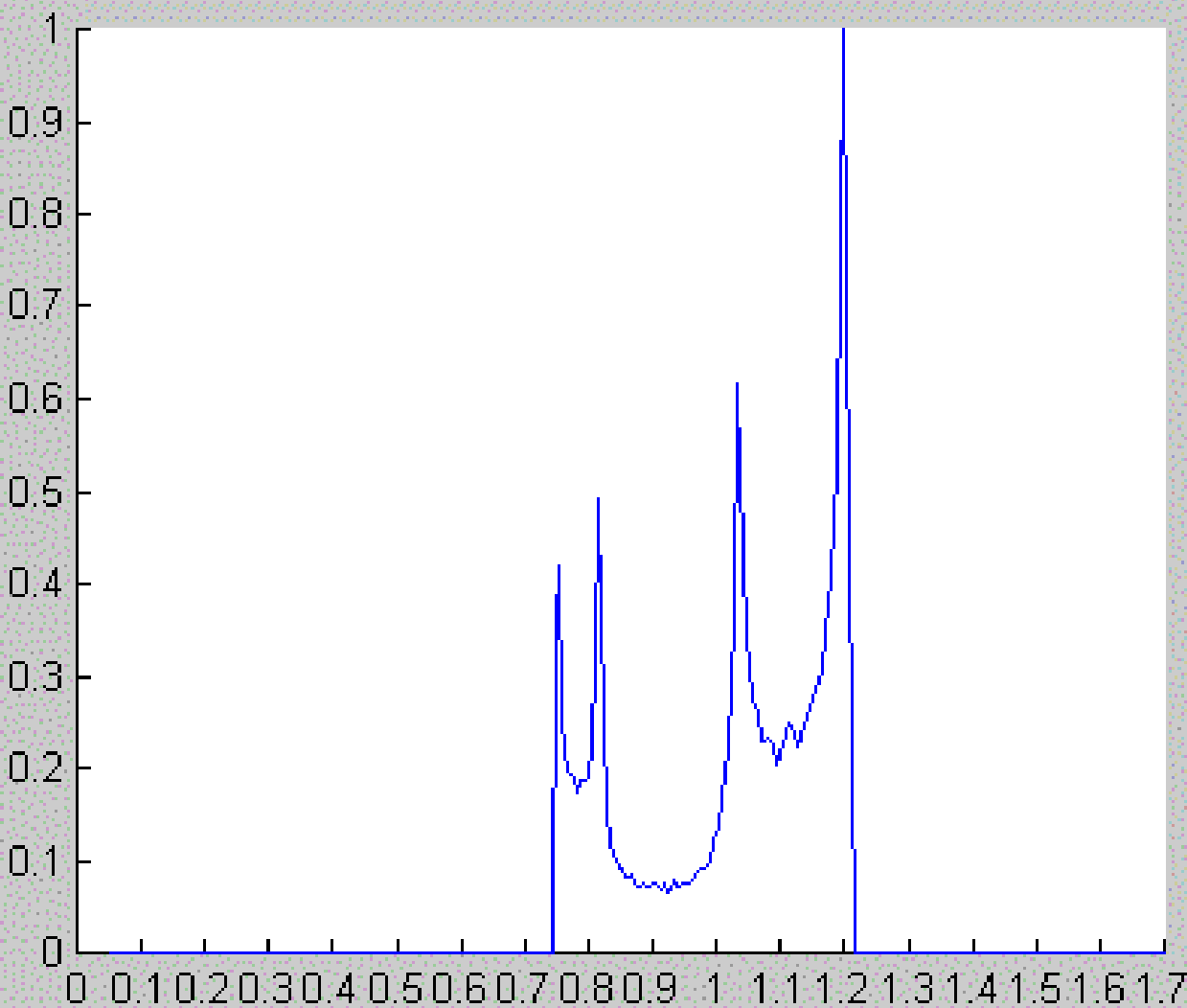


Observer position:  
theta = **88** deg.  
r = **10.0** rg

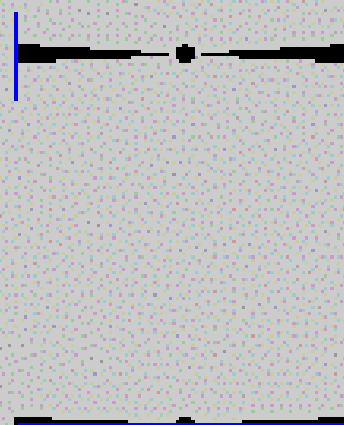


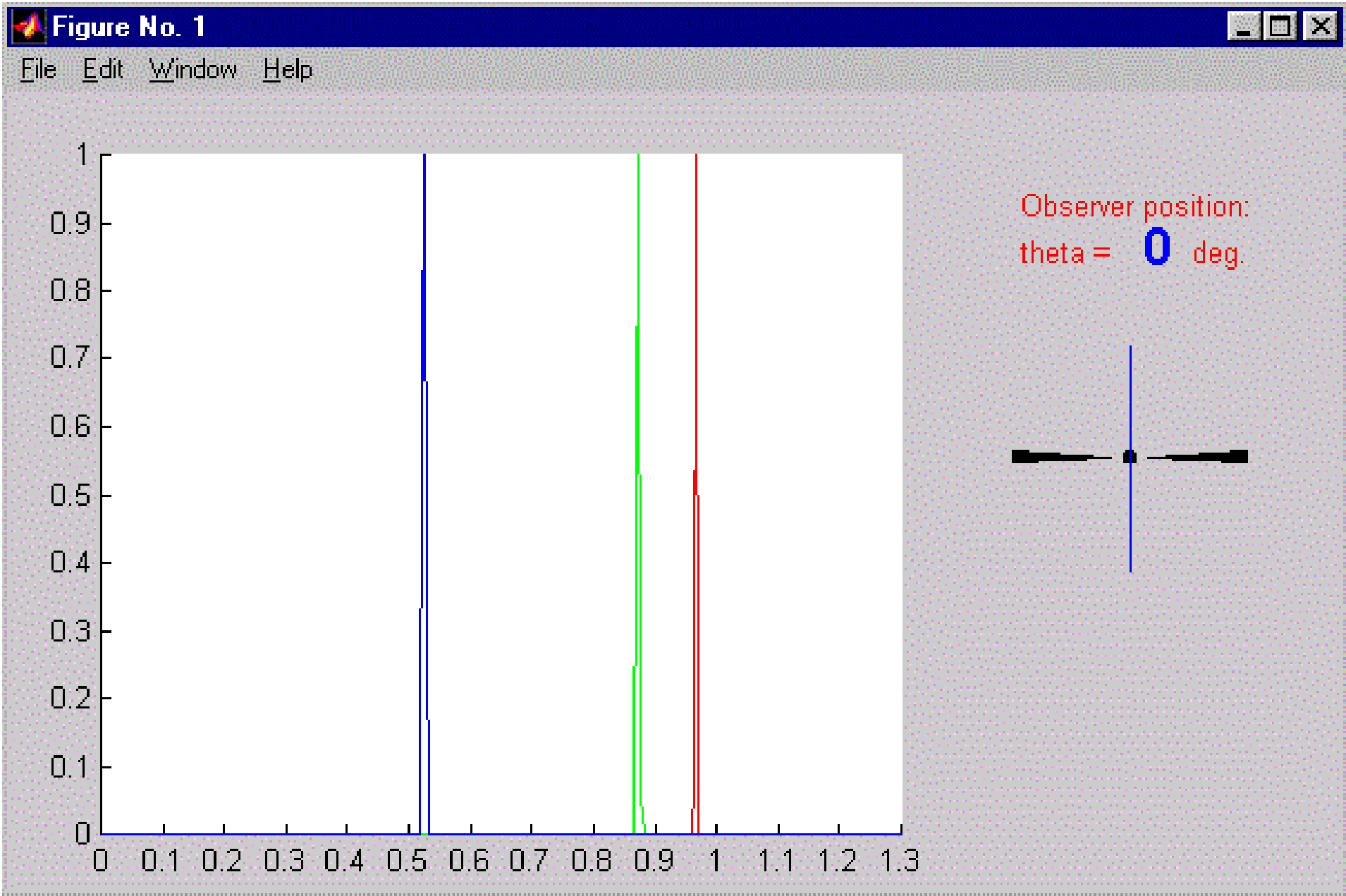


File Edit Window Help



Observer position:  
theta = **90** deg.  
 $r =$  **10.0** rg





- <http://www.gsfc.nasa.gov/gsfc/spacesci/pictures/blackhole/BH1m.jpg>



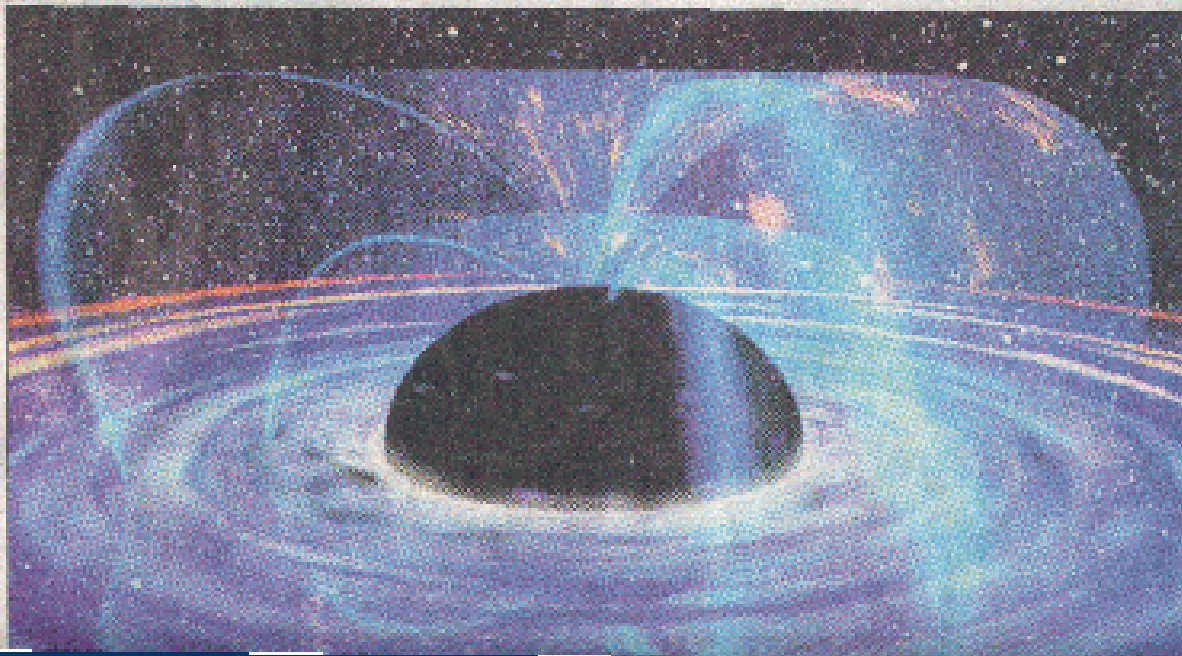
# What is a black hole?

# Everyone already seems to know!

# NATIONAL POST

REG. NO. 404 - THURSDAY, OCTOBER 29, 1964 [www.usatoday.com](http://www.usatoday.com)

Energy-spewing black hole puts on cosmic show for astronomers



WU WUPPEN 2014

*Annotate and use  
misification to be  
in the process*

• 11 KERPIK POKER

Minister of Health, was born  
Canton, January 1, 1860, and  
was educated at the local school  
and in Hong Kong. He has  
been a teacher, a druggist, a  
lawyer, a medical student, and  
is now a member of the Chinese  
Medical Association.

Diedrich has presented  
guitar and harmonica  
lessons through one book  
a year to thousands. He  
teaches his students to make  
music with their own  
German language and  
harmonica and guitar. The  
books, the tapes, the  
CDs, and the harmonicas  
are all produced by  
Diedrich's own company.

# Relativistic Fe K $\alpha$ Lines with *XMM-Newton*



Jörn Wilms  
(University of Warwick)

<http://astro.uni-tuebingen.de/~wilms>

# Mirages around Kerr black holes and retro-gravitational lenses

- Let us consider an illumination of black holes. Then retro-photons form caustics around black holes or mirages around black holes or boundaries around shadows.
- (Zakharov, Nucita, DePaolis, Ingrosso,
  - New Astronomy 10 (2005) (479-489);  
[astro-ph/0411511](http://arxiv.org/abs/astro-ph/0411511))

# RETRO-MACHOS: $\pi$ IN THE SKY?

DANIEL E. HOLZ

Institute for Theoretical Physics, University of California, Santa Barbara, CA 93106

AND

JOHN A. WHEELER

Department of Physics, Princeton University, Princeton, NJ 08544

*Draft version September 20, 2004*

## ABSTRACT

Shine a flashlight on a black hole, and one is greeted with the return of a series of concentric rings of light. For a point source of light, and for perfect alignment of the lens, source, and observer, the rings are of infinite brightness (in the limit of geometric optics). In this manner, distant black holes can be revealed through their reflection of light from the Sun. Such retro-MACHO events involve photons leaving the Sun, making a  $\pi$  rotation about the black hole, and then returning to be detected at the Earth. Our calculations show that, although the light return is quite small, it may nonetheless be detectable for stellar-mass black holes at the edge of our solar system. For example, all (unobscured) black holes of mass  $M$  or greater will be observable to a limiting magnitude  $\bar{m}$ , at a distance given by:  $0.02 \text{ pc} \times \sqrt[3]{10^{(\bar{m}-30)/2.5}} (M/10 M_\odot)^2$ . Discovery of a Retro-MACHO offers a way to *directly* image the presence of a black hole, and would be a stunning confirmation of strong-field general relativity.

*Subject headings:* gravitational lensing—black hole physics—relativity

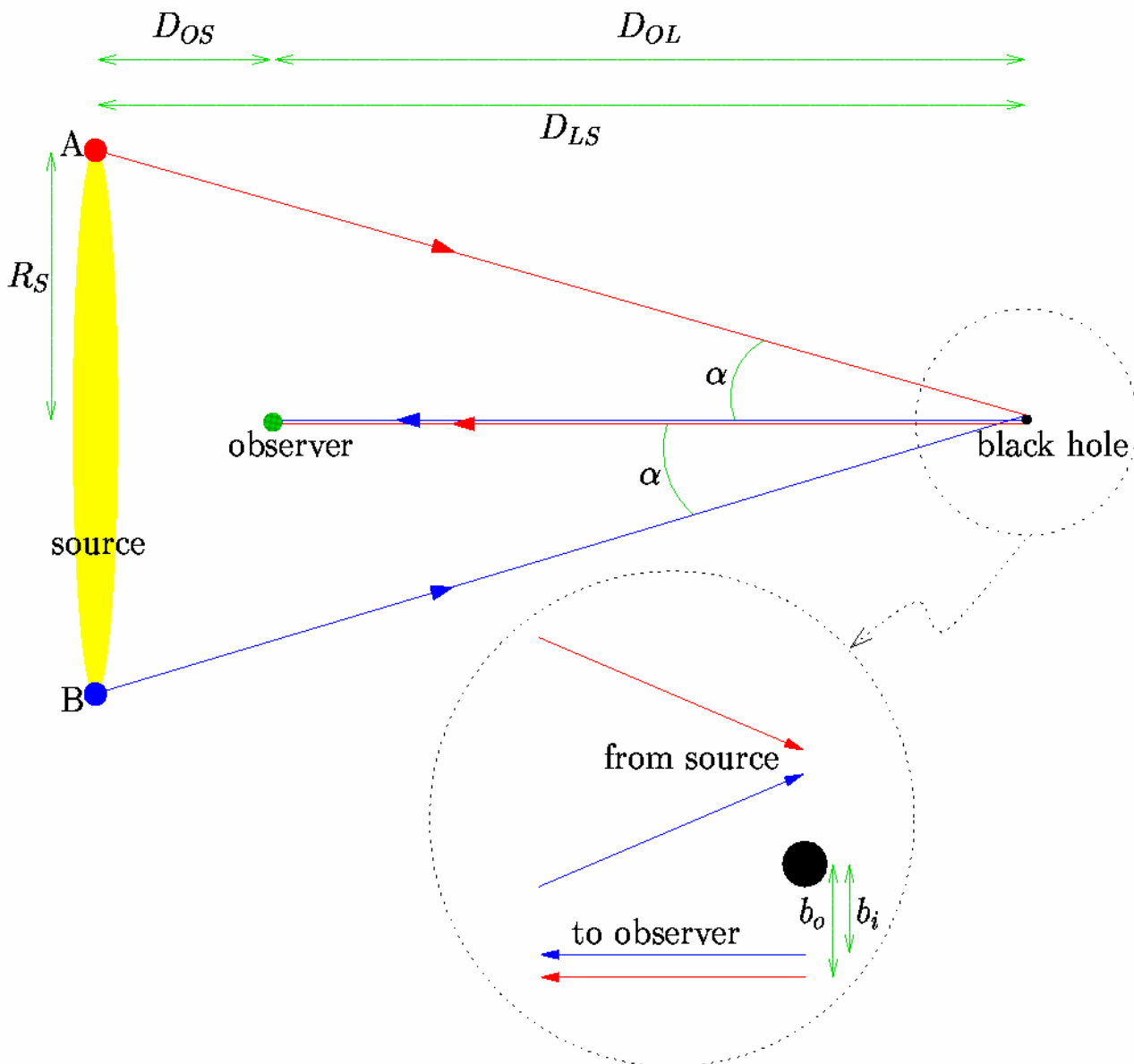


FIG. 1.— Perfect alignment: the (extended) source, observer, and lens are colinear. The resulting image of the source, as lensed by the black hole, is a ring. (The angles in this figure are greatly exaggerated.)

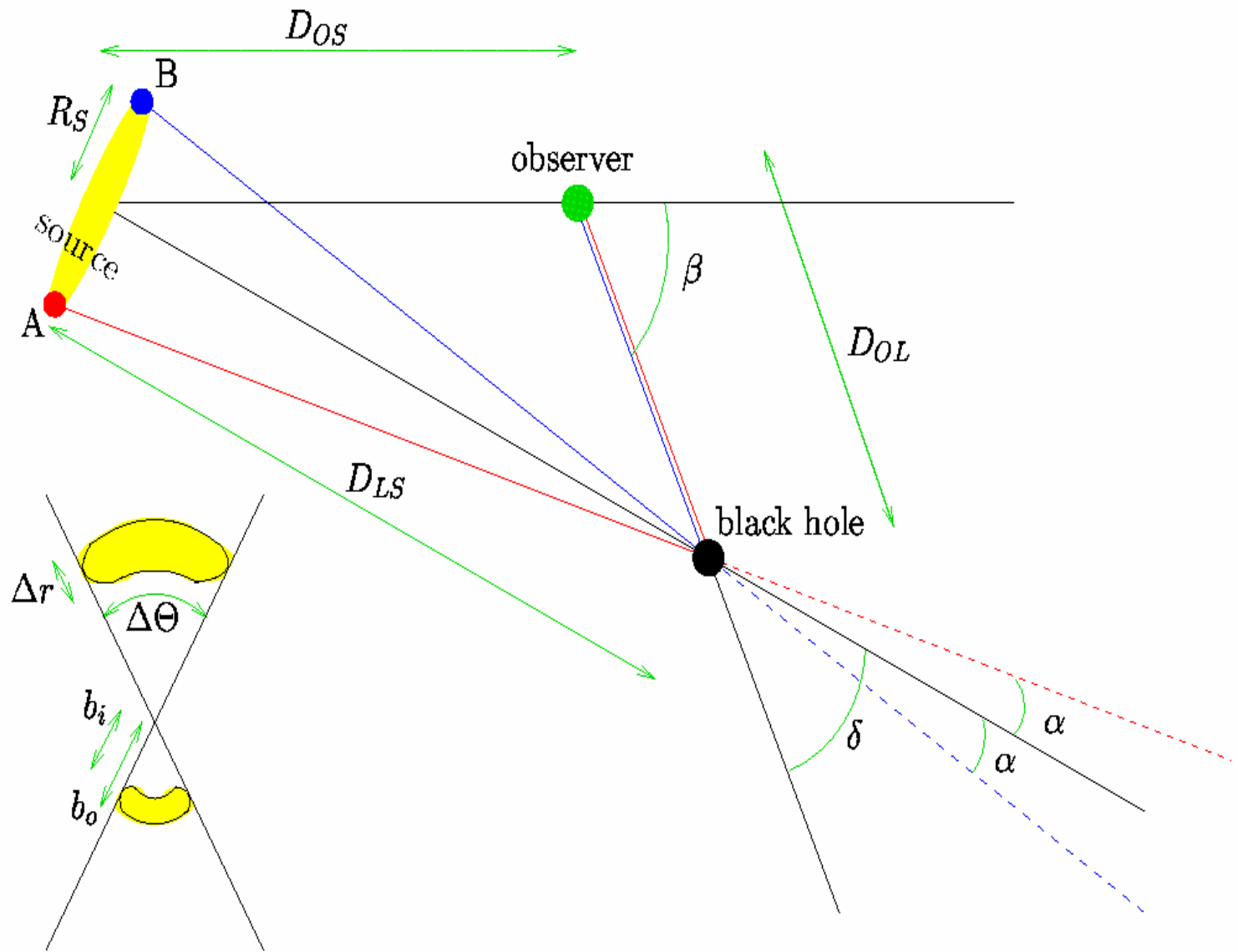


FIG. 2.— Imperfect alignment: the source, observer, and lens are not colinear. Pairs of images are produced, centered on the source–observer–lens plane, on opposite sides of the lens (see inset).

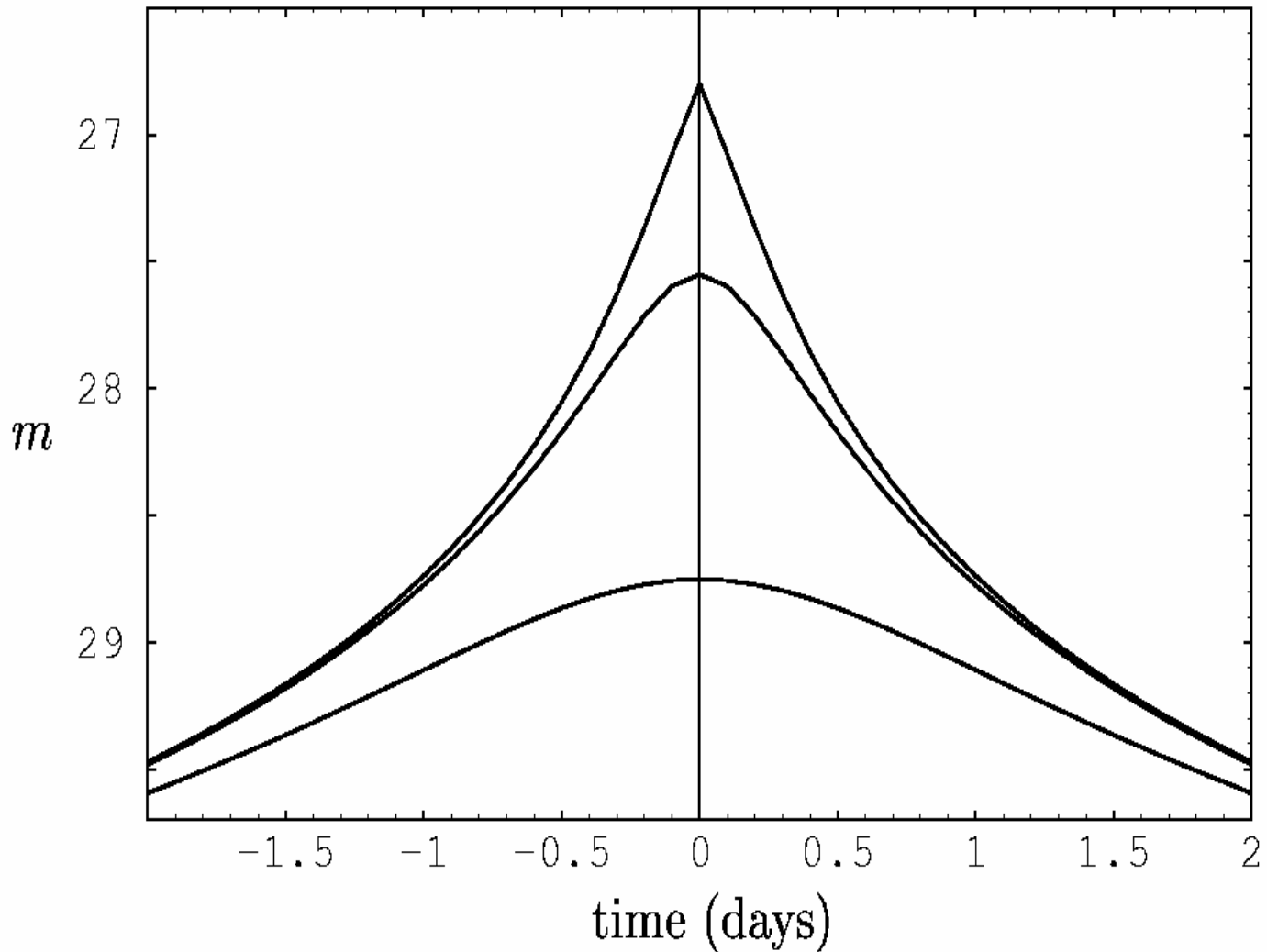


FIG. 3.— Solar retro-MACHO lightcurves: The apparent visual magnitude,  $m$ , of the Sun, imaged in a  $10 M_{\odot}$  black hole at a distance of 0.01 pc. The different curves are for the black hole at angular displacements from the ecliptic plane of 0,  $R_{\odot}/1 \text{ AU}$ , and  $1^{\circ}$  respectively (top to bottom).

TABLE 1  
RETRO-MACHO BRIGHTNESSES OF THE SUN

BH mass ( $M_{\odot}$ )	BH distance (pc)	$\beta = 0$ (perfect alignment)	$\beta = R_{\odot}/1 \text{ AU}$ (edge alignment)	$\beta = 1^\circ$	$\beta = \pi/4$	$\beta = \pi/2$ (max misalignment)
1	$10^{-2}$	31.0	32.6	34	38	38
1	$10^{-1}$	38.6	40.1	41	45	46
10	$10^{-2}$	26.1	27.6	29	33	33
10	$10^{-1}$	33.6	35.1	36	40	41
10	1	41.1	42.6	44	48	48

The full classification of geodesic types for Kerr metric is given by Zakharov (1986). As it was shown in this paper, there are three photon geodesic types: capture, scattering and critical curve which separates the first two sets. This classification fully depends only on two parameters  $\xi = L_z/E$  and  $\eta = Q/E^2$ , which are known as Chandrasekhar's constants (Chandrasekhar 1983). Here the Carter constant  $Q$  is given by Carter (1968)

$$Q = p_\theta^2 + \cos^2 \theta [a^2 (m^2 - E^2) + L_z^2/\sin^2 \theta], \quad (1)$$

where  $E = p_t$  is the particle energy at infinity,  $L_z = p_\phi$  is  $z$ -component of its angular momentum,  $m = p_i p^i$  is the particle mass. Therefore, since photons have  $m = 0$

$$\eta = p_\theta^2/E^2 + \cos^2 \theta [-a^2 + \xi^2/\sin^2 \theta]. \quad (2)$$

The first integral for the equation of photon motion (isotropic geodesics) for a radial coordinate in the Kerr metric is described by the following equation (Carter 1968; Chandrasekhar 1983; Zakharov 1986, 1991a)

$$\rho^4 (dr/d\lambda)^2 = R(r),$$

where

$$R(r) = r^4 + (a^2 - \xi^2 - \eta)r^2 + 2[\eta + (\xi - a)^2]r - a^2\eta, \quad (3)$$

and  $\rho^2 = r^2 + a^2 \cos^2 \theta$ ,  $\Delta = r^2 - 2r + a^2$ ,  $a = S/M^2$ . The constants  $M$  and  $S$  are the black hole mass and angular momentum, respectively. Eq. (3) is written in dimensionless variables (all lengths are expressed in black hole mass units  $M$ ).

If we fix a black hole spin parameter  $a$  and consider a plane  $(\xi, \eta)$  and different types of photon trajectories corresponding to  $(\xi, \eta)$ , namely, a capture region, a scatter region and the critical curve  $\eta_{\text{crit}}(\xi)$  separating the scatter and capture regions. The critical curve is a set of  $(\xi, \eta)$  where the polynomial  $R(r)$  has a multiple root (a double root for this case). Thus, the critical curve  $\eta_{\text{crit}}(\xi)$  could be determined from the system (Zakharov 1986, 1991a)

$$\begin{aligned} R(r) &= 0, \\ \frac{\partial R}{\partial r}(r) &= 0, \end{aligned} \tag{4}$$

for  $\eta \geq 0, r \geq r_+ = 1 + \sqrt{1 - a^2}$ , because by analysing of trajectories along the  $\theta$  coordinate we know that for  $\eta < 0$  we have  $M = \{(\xi, \eta) | \eta \geq -a^2 + 2a|\xi| - \xi^2, -a \leq \xi \leq a\}$  and for each point  $(\xi, \eta) \in M$  photons will be captured. If instead  $\eta < 0$  and  $(\xi, \eta) \notin M$ , photons cannot have such constants of motion, corresponding to the forbidden region (see, (Chandrasekhar 1983; Zakharov 1986) for details).

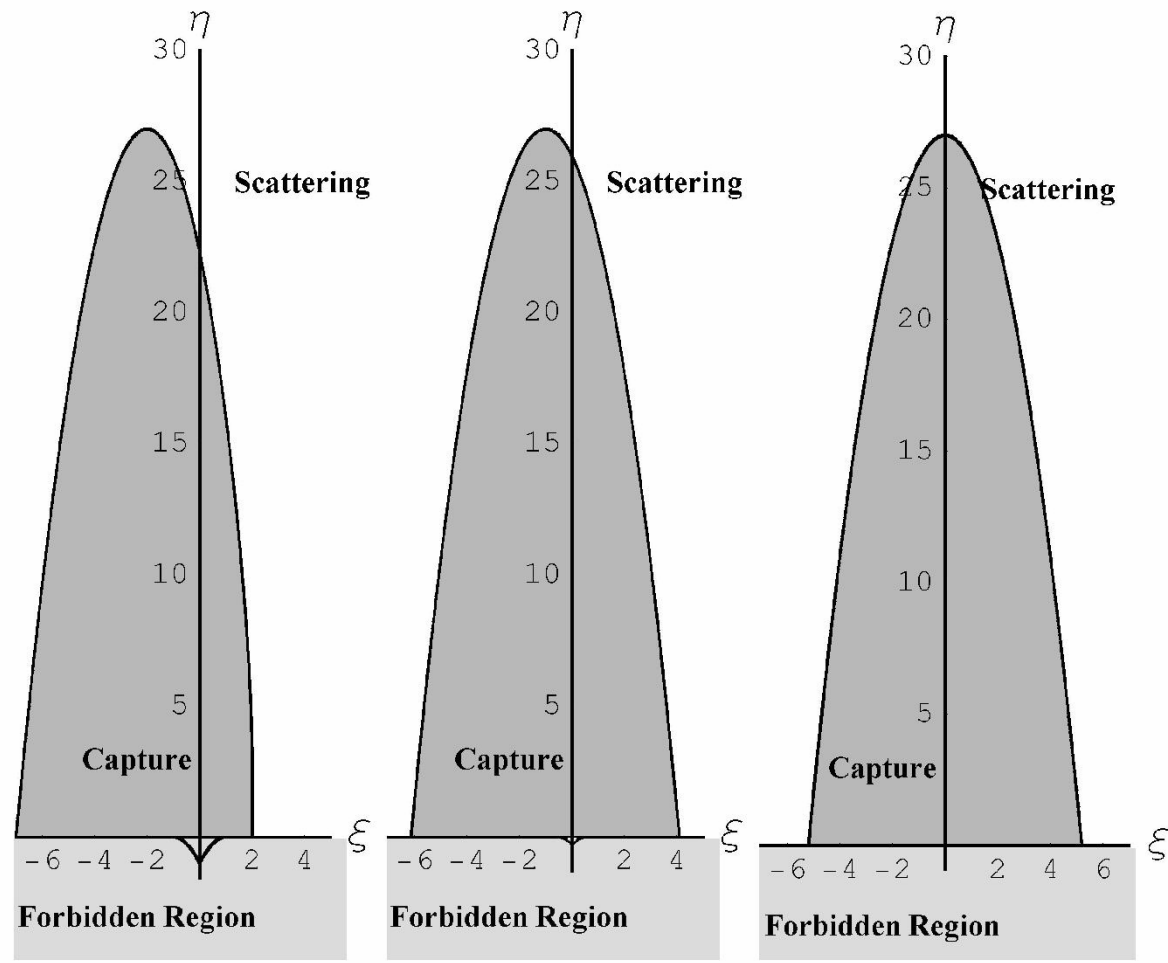


**Fig. 1.** Different types for photon trajectories and spin parameters ( $a = 1.$ ,  $a = 0.5$ ,  $a = 0.$ ). Critical curves separate capture and scatter regions. Here we show also the forbidden region corresponding to constants of motion  $\eta < 0$  and  $(\xi, \eta) \in M$  as it was discussed in the text.

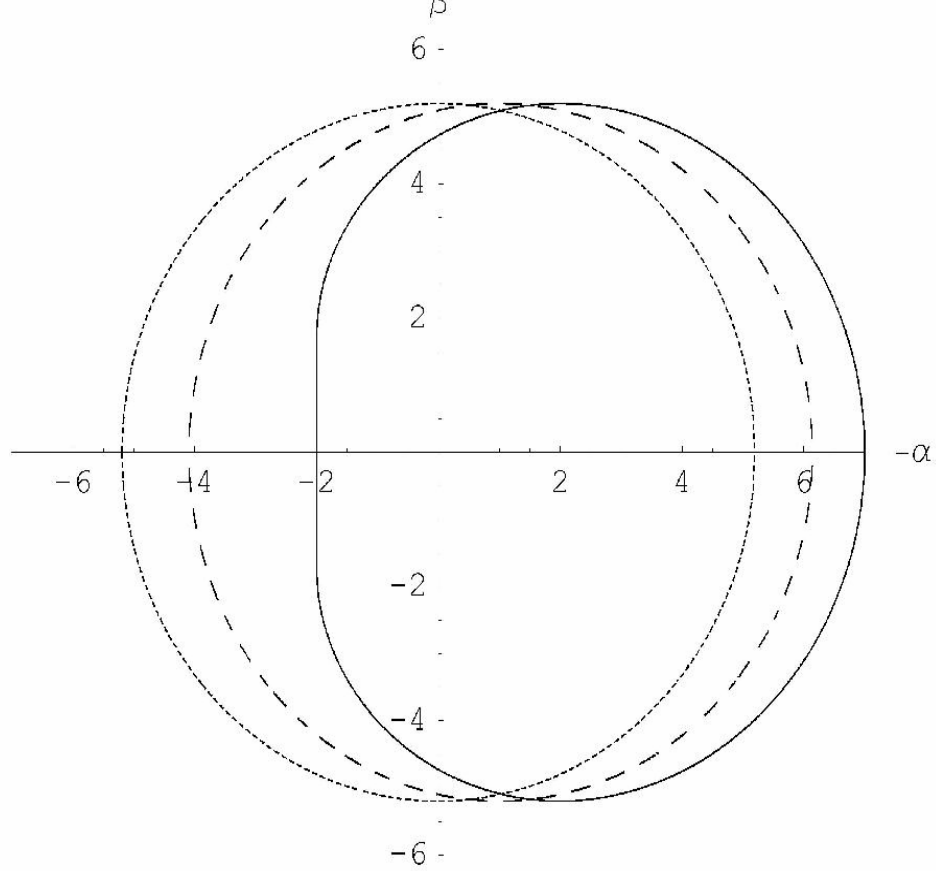


**Fig. 2.** Mirages around black hole for equatorial position of distant observer and different spin parameters. The solid line, the dashed line and the dotted line correspond to  $a = 1, a = 0.5, a = 0$  correspondingly

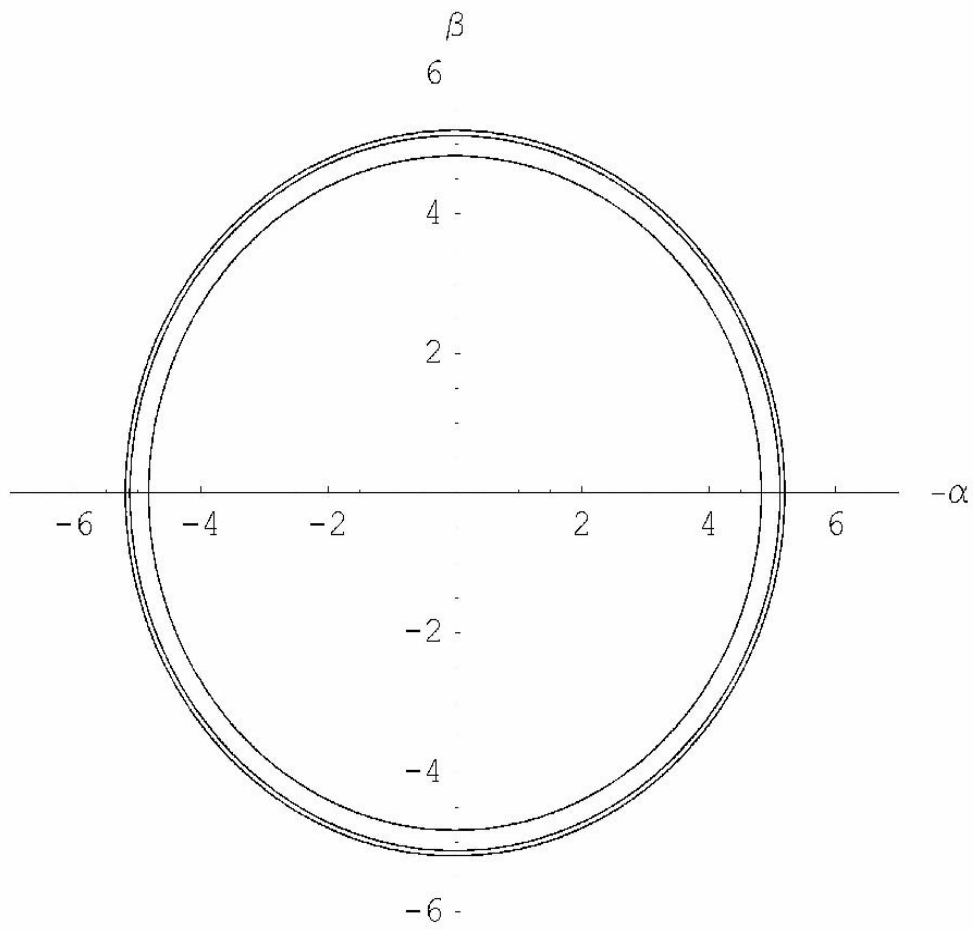


**Fig. 3.** Mirages around a black hole for the polar axis position of distant observer and different spin parameters ( $a = 0, a = 0.5, a = 1$ ). Smaller radii correspond to greater spin parameters.

**Table 1.** Dependence of  $\eta(0)$  and mirage radii  $R_{\text{circ}} = (\eta(0) + a^2)^{1/2}$  on spins.

$a$	0	0.2	0.4	0.5	0.6	0.8	1.
$\eta(0)$	27	26.839	26.348	25.970	25.495	24.210	22.314
$R_{\text{circ}}$	5.196	5.185	5.149	5.121	5.085	4.985	4.828

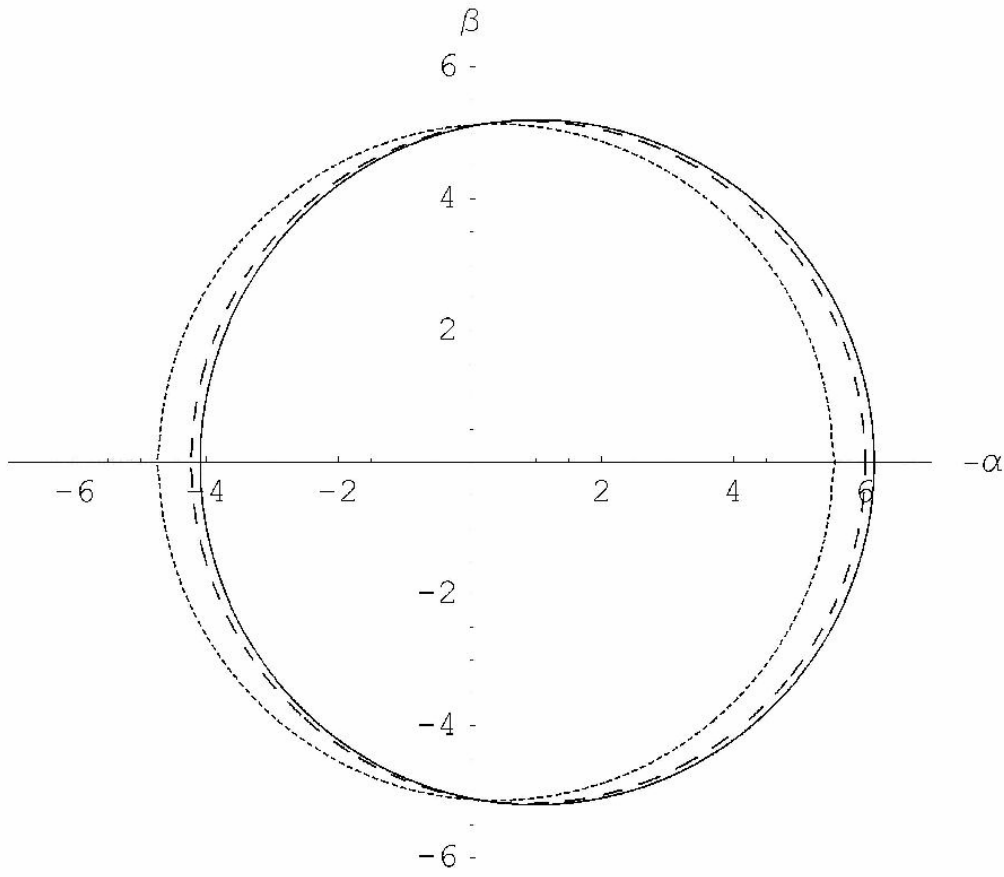


**Fig. 4.** Mirages around black hole for different angular positions of a distant observer and the spin  $a = 0.5$ . Solid, dashed and dotted lines correspond to  $\theta_0 = \pi/2, \pi/3$  and  $\pi/8$ , respectively.

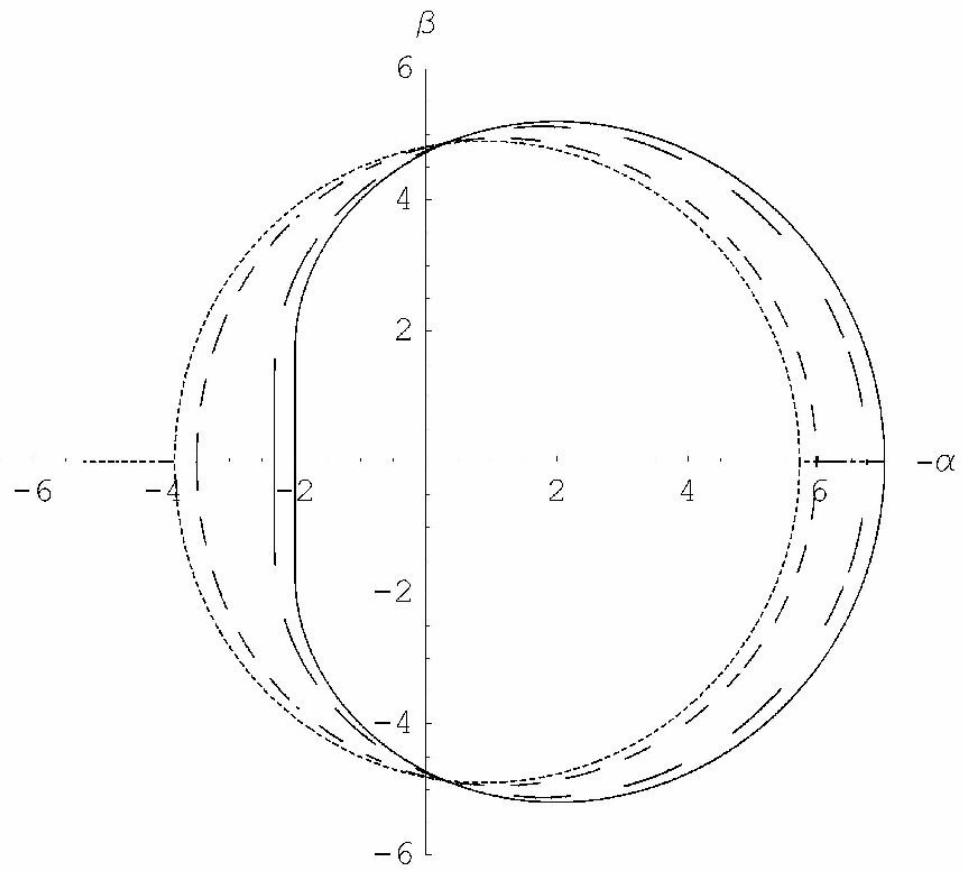


**Fig. 5.** Mirages around black hole for different angular positions of a distant observer and the spin  $a = 1$ . Solid, long dashed, short dashed and dotted lines correspond to  $\theta_0 = \pi/2, \pi/3, \pi/6$  and  $\pi/8$ , respectively.

# Direct Measurements of Black Hole Charge with Future Astrometrical Missions

A.F. Zakharov<sup>1,2,3</sup>, F. De Paolis<sup>4</sup>, G. Ingrosso<sup>4</sup>, A.A. Nucita<sup>4</sup>

<sup>1</sup> Institute of Theoretical and Experimental Physics, 25, B.Cheremushkinskaya st., Moscow, 117259, Russia,

<sup>2</sup> Astro Space Centre of Lebedev Physics Institute, 84/32, Profsoyuznaya st., Moscow, 117810, Russia,

<sup>3</sup> Joint Institute for Nuclear Research, Dubna, Russia

<sup>4</sup> Department of Physics, University of Lecce and INFN, Section of Lecce, Via Arnesano, I-73100 Lecce, Italy

Received / accepted

**Abstract.** Recently, Zakharov et al. (2005a) considered the possibility of evaluating the spin parameter and the inclination angle for Kerr black holes in nearby galactic centers by using future advanced astrometrical instruments. A similar approach which uses the characteristic properties of gravitational retro-lensing images can be followed to measure the charge of Reissner-Nordström black hole. Indeed, in spite of the fact that their formation might be problematic, charged black holes are objects of intensive investigations. From the theoretical point of view it is well-known that a black hole is described by only three parameters, namely, its mass  $M$ , angular momentum  $J$  and charge  $Q$ . Therefore, it would be important to have a method for measuring all these parameters, preferably by model independent way. In this paper, we propose a procedure to measure the black hole charge by using the size of the retro-lensing images that can be revealed by future astrometrical missions. A discussion of the Kerr-Newmann black hole case is also offered.

In this paper we focus on the possibility to measure the black hole charge as well and we present an analytical dependence of mirage size on the black hole charge. Indeed, future space missions like Radioastron in radio band or MAXIM in X-ray band have angular resolution close to the shadow size for massive black holes in the center of our and nearby galaxies.

## 2. Basic Definitions and Equations

The expression for the Reissner - Nordström metric in natural units ( $G = c = 1$ ) has the form

$$ds^2 = -(1 - 2M/r + Q^2/r^2)dt^2 + (1 - 2M/r + Q^2/r^2)^{-1}dr^2 + r^2(d\theta^2 + \sin^2\theta d\phi^2). \quad (1)$$

$$R(r_{max}) = 0, \quad \frac{\partial R}{\partial r}(r_{max}) = 0, \quad (6)$$

as it was done, for example, by Chandrasekhar (1983) to solve similar problems.

Introducing the notation  $\xi^2 = l, Q^2 = q$ , we obtain

$$R(r) = r^4 - lr^2 + 2lr - qr. \quad (7)$$

The discriminant  $\Delta$  of the polynomial  $R(r)$  has the form (as it was shown by Zakharov (1991a,b, 1994a)):

$$\Delta = 16l^3[l^2(1 - q) + l(-8q^2 + 36q - 27) - 16q^3]. \quad (8)$$

The polynomial  $R(r)$  thus has a multiple root if and only if

$$l^3[l^2(1 - q) + l(-8q^2 + 36q - 27) - 16q^3] = 0. \quad (9)$$

Excluding the case  $l = 0$ , which corresponds to a multiple root at  $r = 0$ , we find that the polynomial  $R(r)$  has a multiple root for  $r \geq r_+$  if and only if

$$l^2(1 - q) + l(-8q^2 + 36q - 27) - 16q^3 = 0. \quad (10)$$

If  $q = 0$ , we obtain the well-known result for a Schwarzschild black hole (Misner, Thorne and Wheeler 1973; Wald 1984; Lightman et al. 1975),  $l = 27$ , or  $L_{cr} = 3\sqrt{3}$ . If  $q = 1$ , then  $l = 16$ , or  $L_{cr} = 4$ , which also corresponds to numerical results given by Young (1976).

The photon capture cross section for an extreme charged black hole turns out to be considerably smaller than the capture cross section of a Schwarzschild black hole. The critical value of the impact parameter, characterizing the capture cross section for a Reissner - Nordström black hole, is determined by the equation (Zakharov 1991a,b, 1994a)

$$l = \frac{(8q^2 - 36q + 27) + \sqrt{(8q^2 - 36q + 27)^2 + 64q^3(1 - q)}}{2(1 - q)}. \quad (11)$$

As it was explained by Zakharov et al. (2005a,b) this leads to the formation of shadows described by the critical value of  $L_{cr}$  or, in other words, in the spherically symmetric case, shadows are circles with radii  $L_{cr}$ . Therefore, measuring the shadow size, one could evaluate the black hole charge in black hole mass units  $M$ .

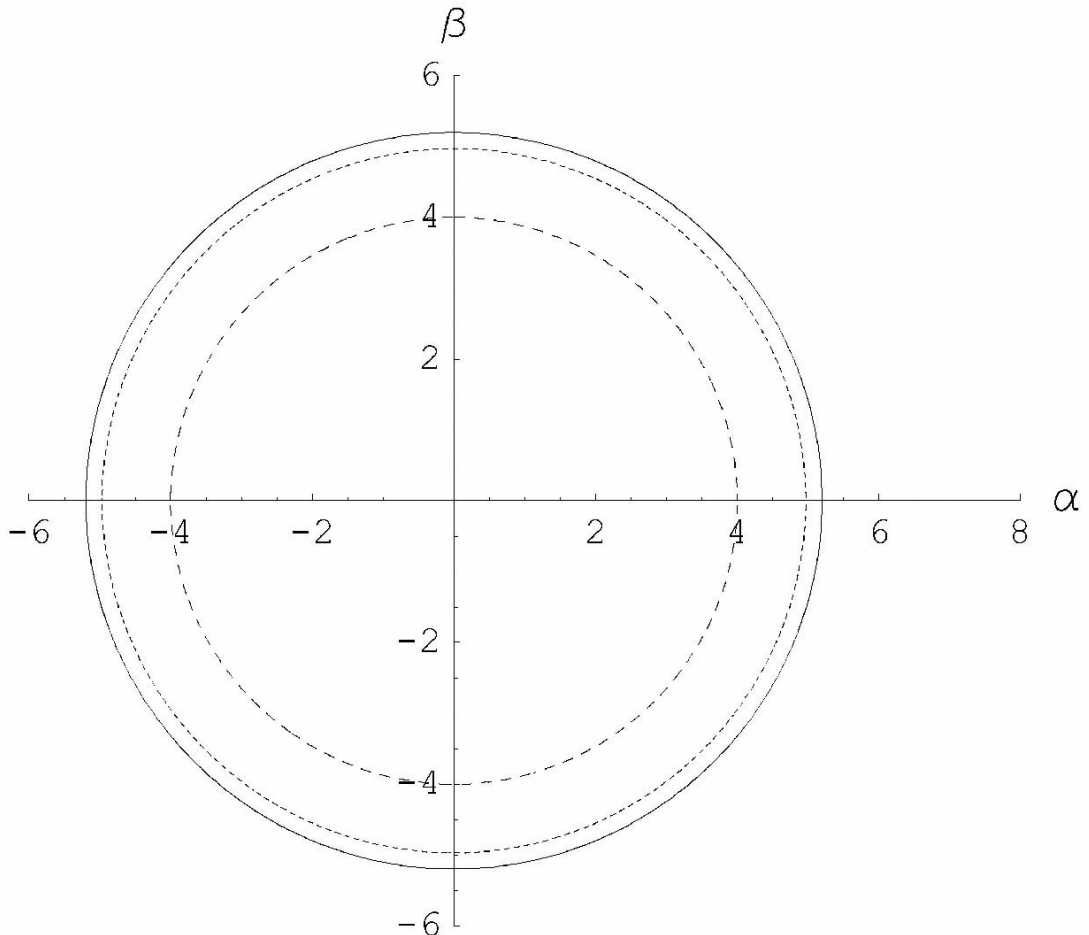
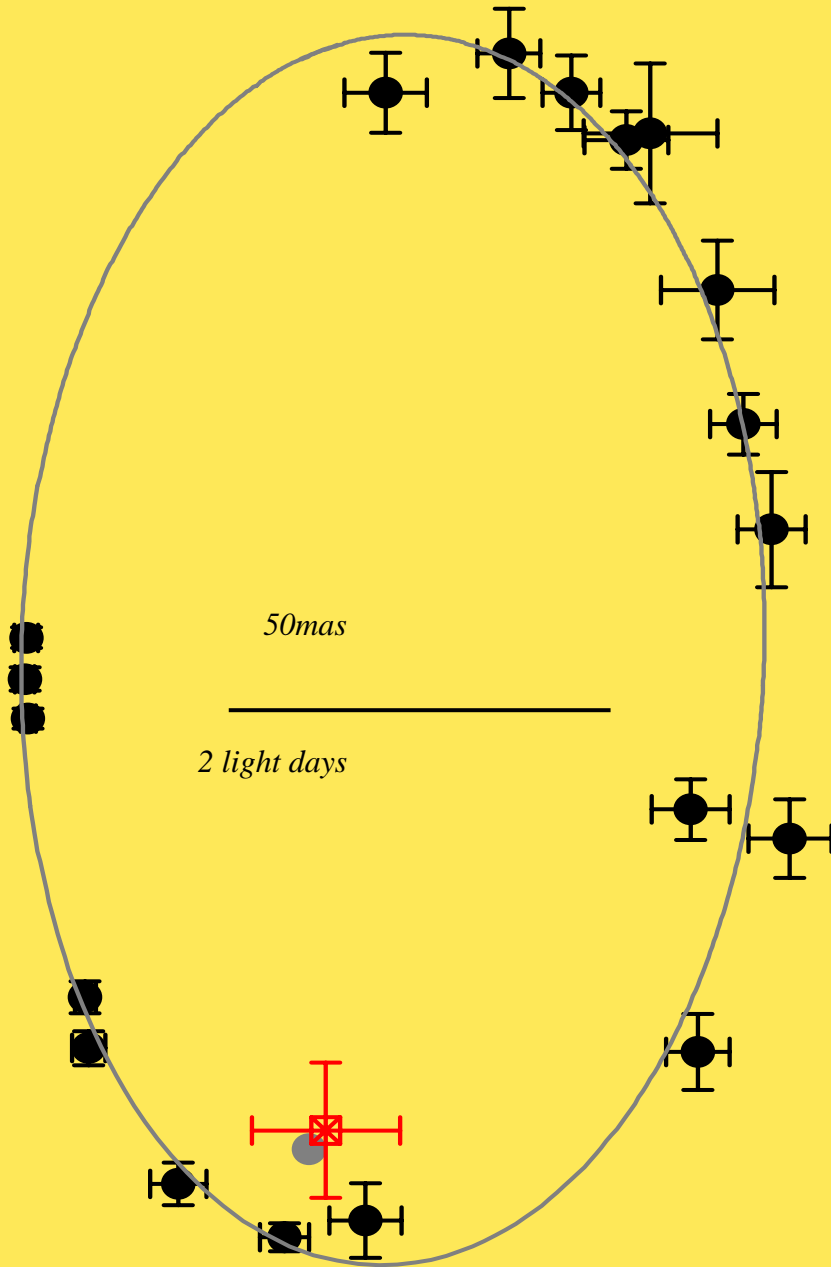
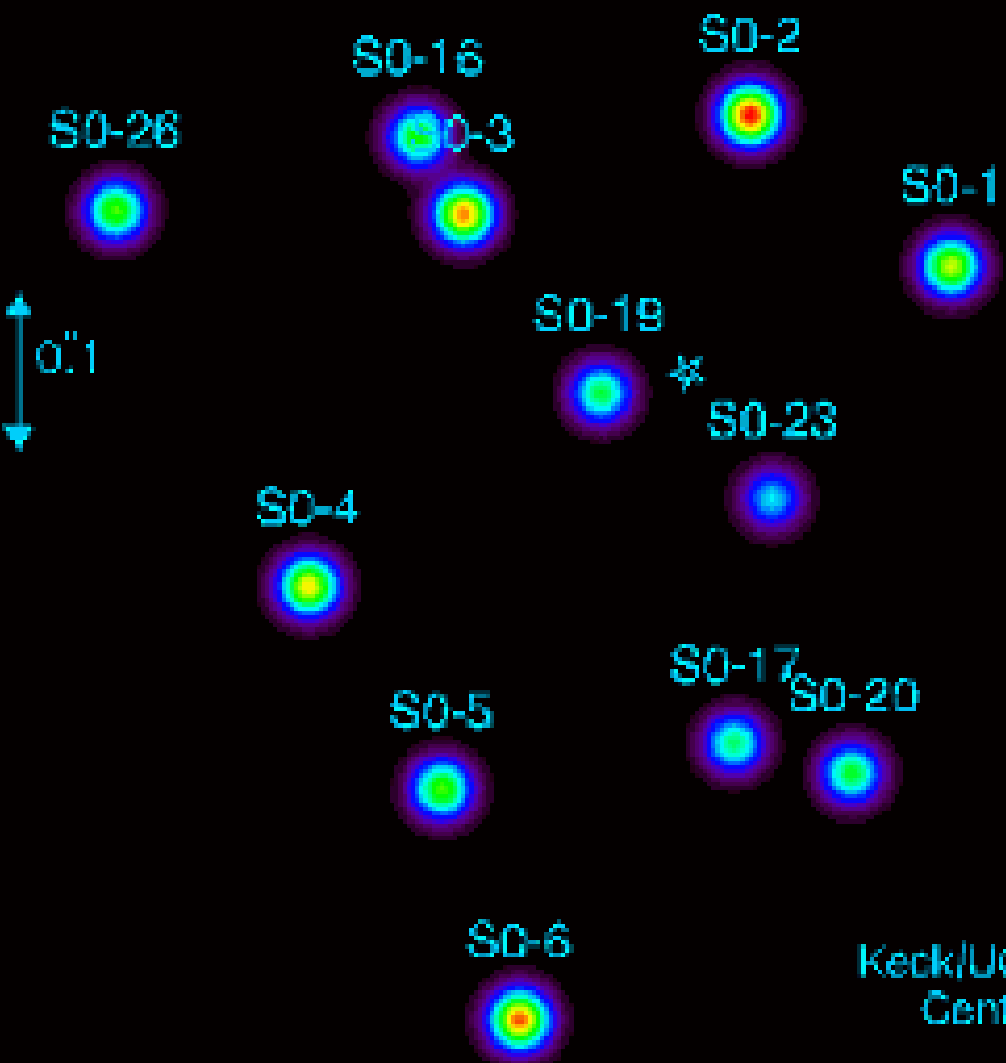


**Fig. 1.** Shadow (mirage) sizes are shown for selected charges of black holes  $Q = 0$  (solid line),  $Q = 0.5$  (short dashed line) and  $Q = 1$  (long dashed line).

A.F. Zakharov & F. De Paolis, A.A. Nucita,  
G.Ingrossi, **Astron. & Astrophys.**, **442**, 795  
**(2005)**

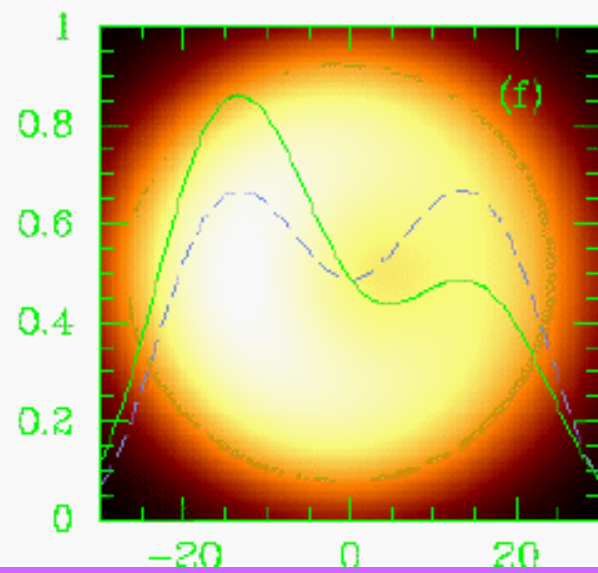
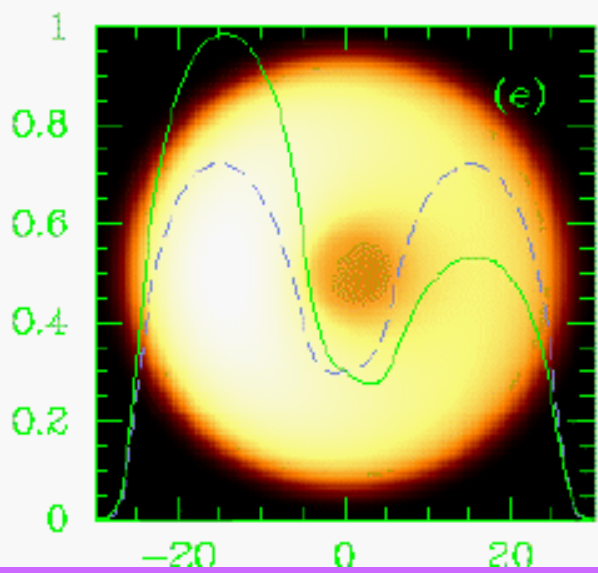
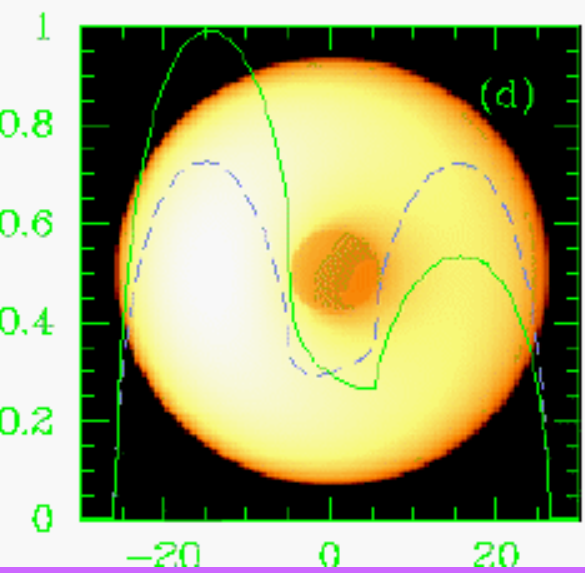
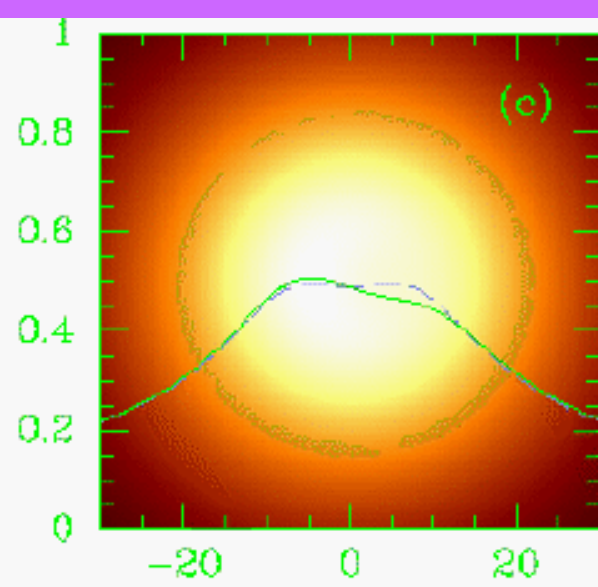
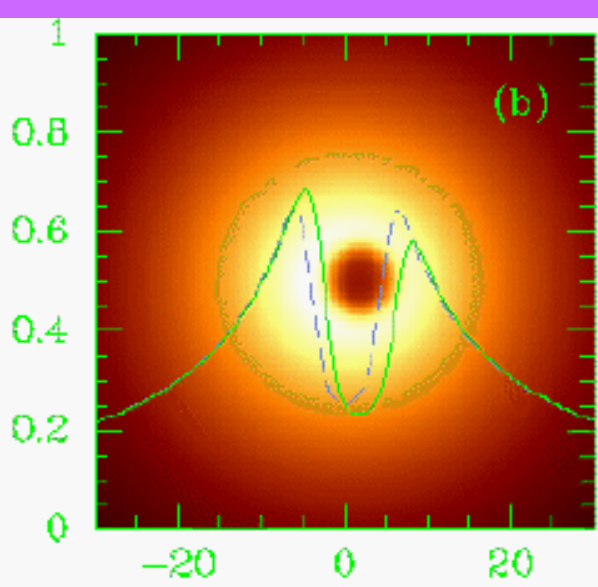
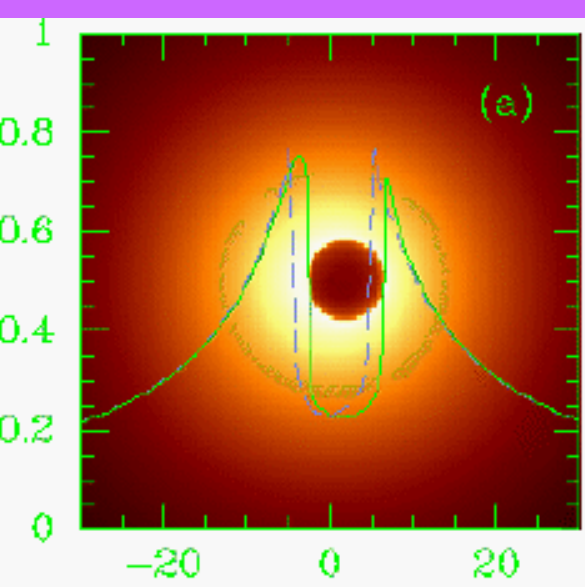


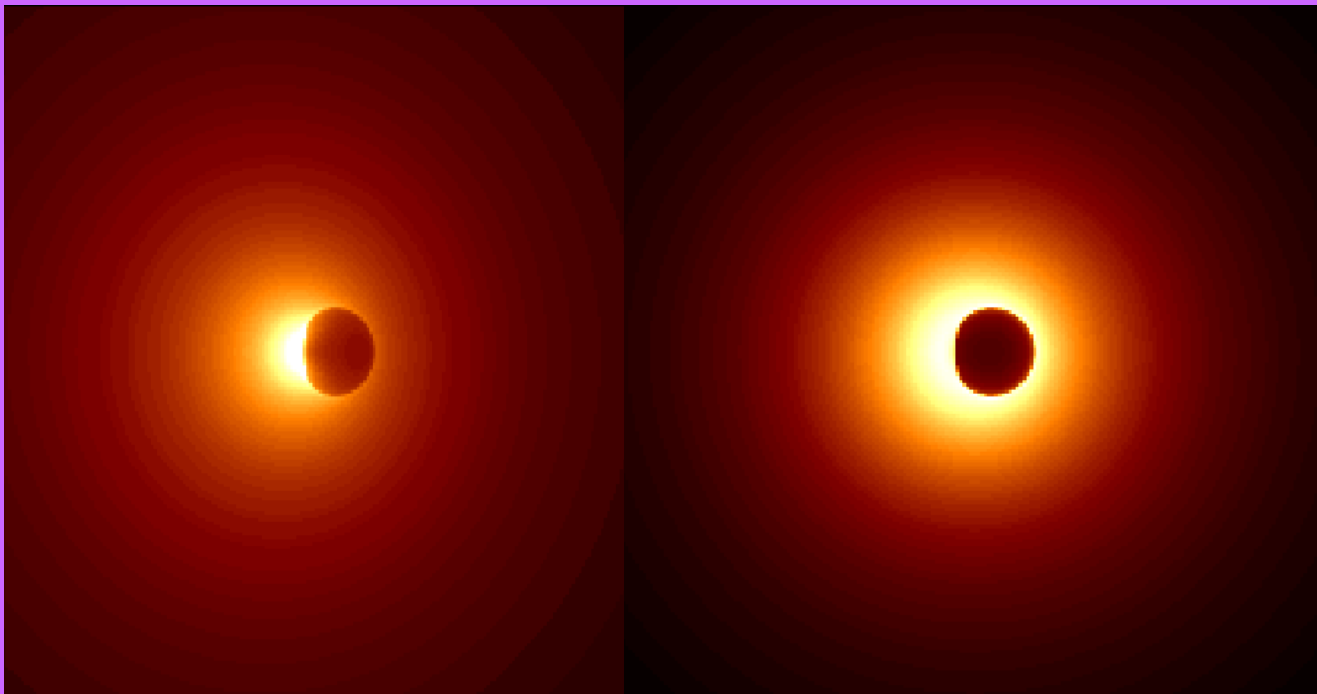
1995.50



Keck/UCLA Galactic  
Center Group

Similarly to Falcke, Melia & Agol (2000) we propose to use VLBI technique to observe the discussed mirages around black holes. They used ray-tracing calculations to evaluate the shapes of shadows. The boundaries of the shadows are black hole mirages (glories or "faces") analyzed earlier. We use the length parameter  $r_g = \frac{GM}{c^2} = 6 \times 10^{11}$  cm to calculate all values in these units as it was explained in the text. If we take into account the distance towards the Galactic Center  $D_{\text{GC}} = 8$  kpc then the length  $r_g$  corresponds to angular sizes  $\sim 5\mu\text{as}$ . Since the minimum arc size for the considered mirages are about  $2r_g$ , the standard RADIOASTRON resolution of about  $8\mu\text{as}$  is comparable with the required precision. The resolution in the case of the higher orbit and shortest wavelength is  $\sim 1\mu\text{as}$  (Table 2) good enough to reconstruct the shapes. Therefore, in principle it will be possible to evaluate  $a$  and  $\theta$  parameters after mirage shape reconstructions from observational data even if we will observe only the bright part of the image (the bright arc) corresponding to positive parameters  $\alpha$ . However, Gammie, Shapiro & McKinney (2004)





**ALMA Memo 499**

**20 May 2004**

**An Approach Detecting the Event Horizon of SgrA\***

Makoto MIYOSHI, Seiji KAMENO, José K. ISHITSUKA

*National Astronomical Observatory, 2-21-1 Osawa, Mitaka, Tokyo 181-8588*

*makoto.miyoshi@nao.ac.jp, kameno@hotaka.mtk.nao.ac.jp, pepe@hotaka.mtk.nao.ac.jp*

Zhi-Qiang SHEN

*Shanghai Astronomical Observatory, Chinese Academy of Sciences, Shanghai 200030*

*zshen@shao.ac.cn*

Rohta TAKAHASHI

*Yukawa Institute for Theoretical Physics, Kyoto University,*

*Sakyo-Ku, Kyoto 606-8502, Japan*

*rohta@yukawa.kyoto-u.ac.jp*

and

Shinji HORIUCHI

*Center for Astrophysics and Supercomputing, Swinburne University of Technology,*

*Mail stops 31 P. O. Box 218 Hawthorn, Victoria, 3122, Australia*

*shoriuchi@swin.edu.au*

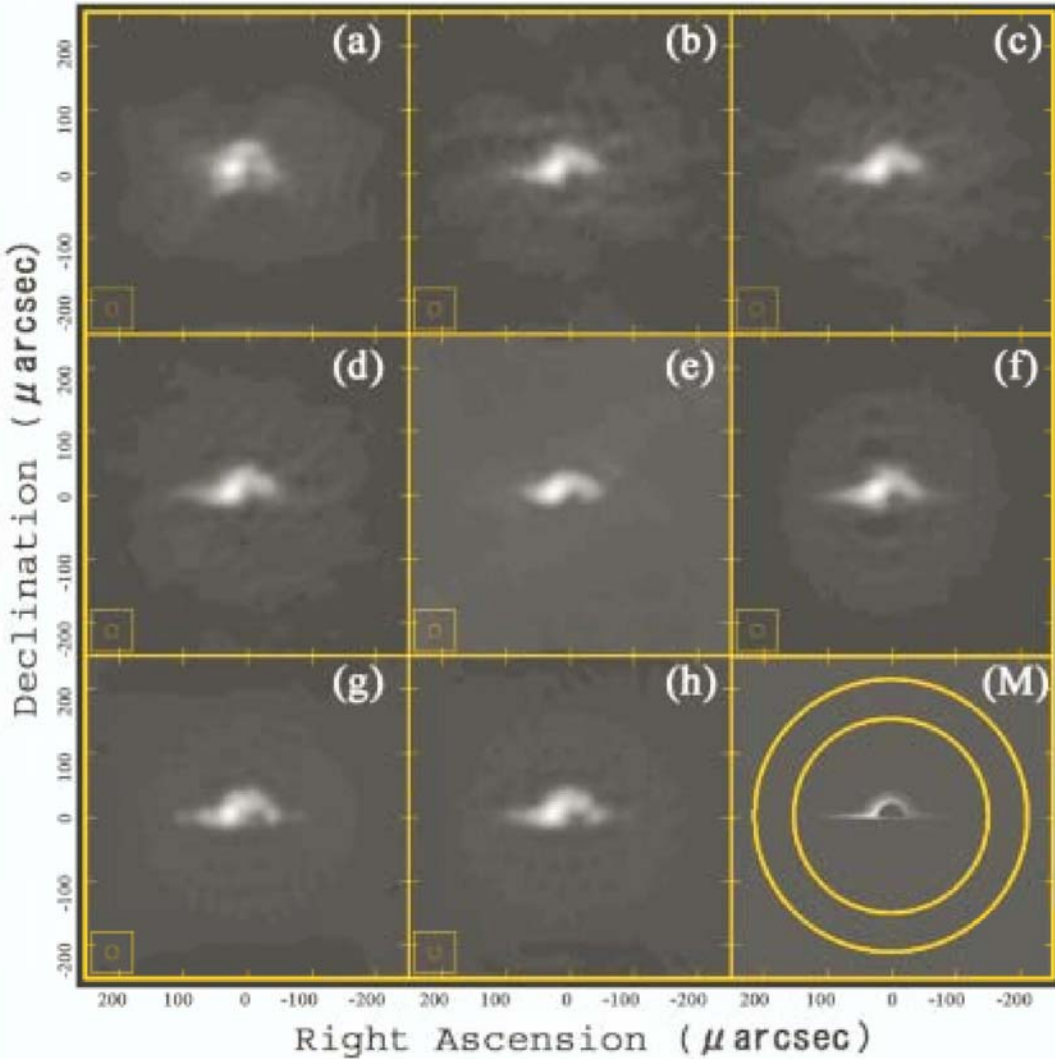


**Fig. 4.** Clean results from simulations for the image model B (edge on view of a standard disk plus dark halo). (a) Array A, (b) Array B, (c) Array C, (d) Array D, (e) Array E, (f) Array F, (g) Array G and (h) Array H and (M) the image model B. The two contours show 0.01% (outside) and 0.1% (inside) level of the peak brightness. The span of each side is  $250\mu\text{asec}$ . The inset in every panel shows the used restoring beam size.

## LETTERS

## A size of $\sim 1$ AU for the radio source Sgr A\* at the centre of the Milky Way

Zhi-Qiang Shen<sup>1</sup>, K. Y. Lo<sup>2</sup>, M.-C. Liang<sup>3</sup>, Paul T. P. Ho<sup>4,5</sup> & J.-H. Zhao<sup>4</sup>

Although it is widely accepted that most galaxies have supermassive black holes at their centres<sup>1–3</sup>, concrete proof has proved elusive. Sagittarius A\* (Sgr A\*)<sup>4</sup>, an extremely compact radio source at the centre of our Galaxy, is the best candidate for proof<sup>5–7</sup>, because it is the closest. Previous very-long-baseline interferometry observations (at 7 mm wavelength) reported that Sgr A\* is  $\sim 2$  astronomical units (AU) in size<sup>8</sup>, but this is still larger than the ‘shadow’ (a remarkably dim inner region encircled by a bright ring) that should arise from general relativistic effects near the event horizon of the black hole<sup>9</sup>. Moreover, the measured size is wavelength dependent<sup>10</sup>. Here we report a radio image of Sgr A\* at a wavelength of 3.5 mm, demonstrating that its size is  $\sim 1$  AU. When combined with the lower limit on its mass<sup>11</sup>, the lower limit on the mass density is  $6.5 \times 10^{21} M_{\odot} \text{ pc}^{-3}$  (where  $M_{\odot}$  is the solar mass), which provides strong evidence that Sgr A\* is a supermassive black hole. The power-law relationship between wavelength and intrinsic size ( $\text{size} \propto \text{wavelength}^{1.09}$ ) explicitly rules out explanations other than those emission models with stratified structure, which predict a smaller emitting region observed at a shorter radio wavelength.

Past very-long-baseline interferometry (VLBI) observations<sup>12–16</sup> of Sgr A\* have revealed an east–west elongated structure whose apparent angular size at longer wavelengths is dominated by the interstellar scattering angle, that is,  $\theta_{\text{obs}} = \theta_{\text{obs}}^{\text{1 cm}} \lambda^2$ , where  $\theta_{\text{obs}}$  is the observed size in milliarcseconds (mas) at wavelength  $\lambda$  in cm, and equals  $\theta_{\text{obs}}^{\text{1 cm}}$  at 1 cm. Thus, VLBI observations at shorter millimetre wavelengths, where the intrinsic structure of Sgr A\* could become comparable to the pure scattering size, are expected to show deviations of the observed size from the scattering law. This has been demonstrated by the recent detection of the intrinsic size at 7 mm (ref. 8). On 20 November 2002, we successfully carried out an observation of Sgr A\* with the Very Long Baseline Array (VLBA) at its shortest wavelength of 3.5 mm (ref. 10). Our observation, with the steadily improved performance of the VLBA system, has produced the first (to our knowledge) high-resolution image of Sgr A\* made at 3.5 mm (Fig. 1), which exhibits an elongated structure too.

To yield a quantitative description of the observed structure, we tried a model fitting procedure<sup>17</sup> in which the amplitude closure relation is applied. Compared to the conventional VLBI

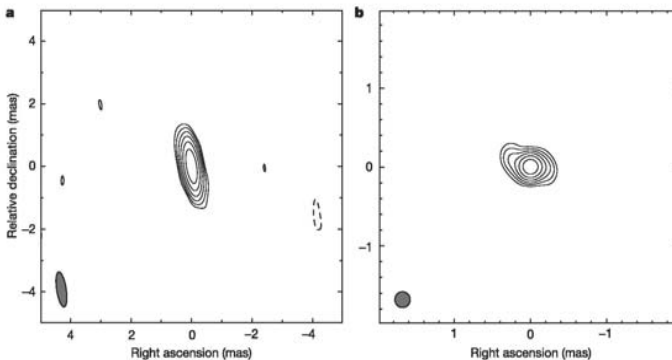


**Figure 1 | High-resolution VLBI image of Sgr A\* at 3.5 mm obtained with the VLBA on 20 November 2002.** The observations were flexibly scheduled to ensure good weather conditions at most sites, and the data were recorded at the highest possible recording rate of 512 Mbit s<sup>-1</sup>. Standard visibility amplitude calibration including the elevation-dependent opacity correction was done, and the final image was obtained after several iterations of the self-calibration and cleaning procedures. The calibrated total flux density is

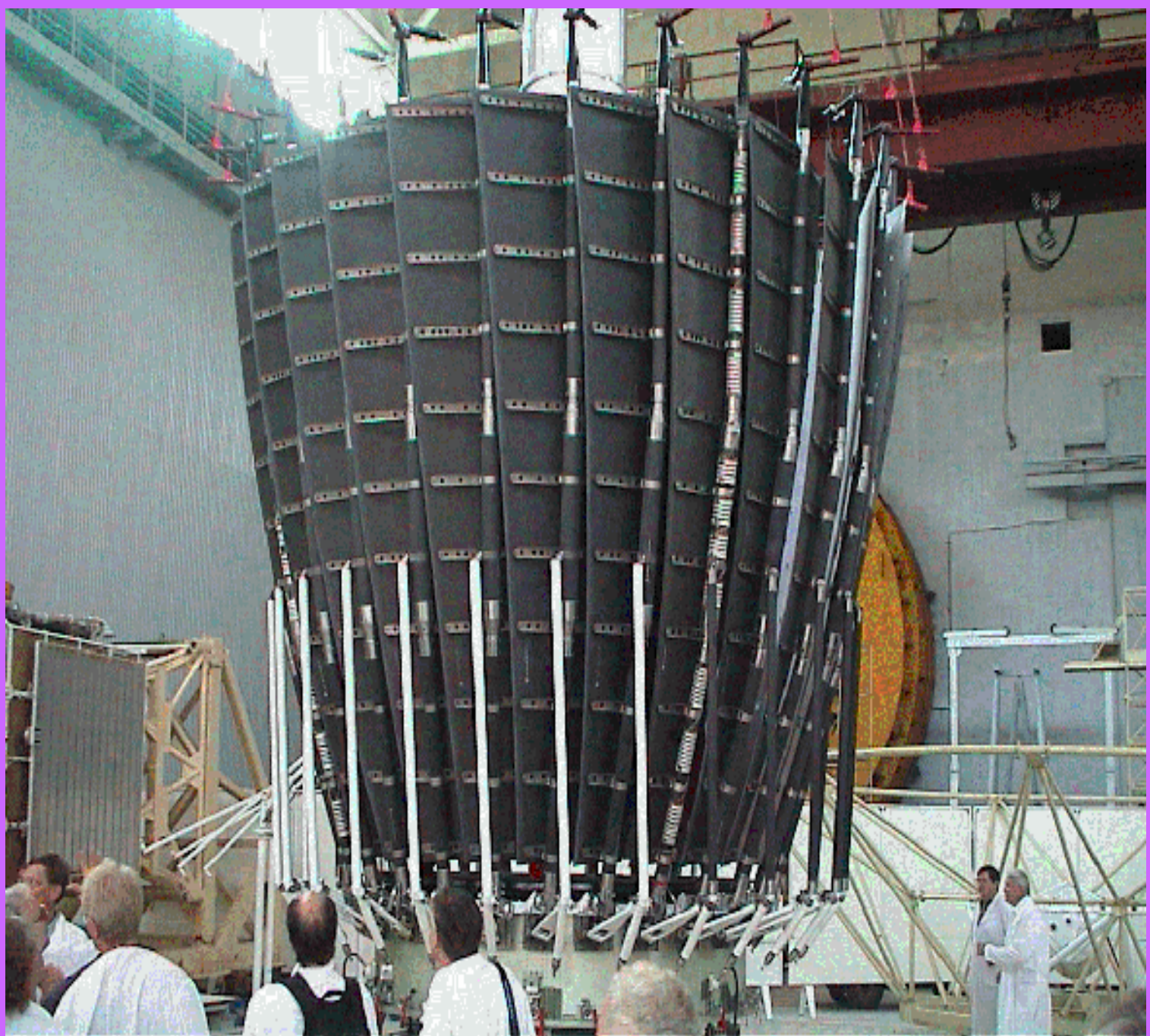
about 1.2 Jy. **a**, A uniformly weighted image with the restoring beam (indicated at the lower left corner) of 1.13 mas  $\times$  0.32 mas at 9°. The peak flux density is 1.08 Jy beam<sup>-1</sup>. Contour levels are drawn at  $3\sigma \times (-1, 1, 2, 4, 8, 16, 32)$ ;  $3\sigma = 17.5$  mJy beam<sup>-1</sup>. **b**, A super-resolution image with a circular beam of 0.20 mas from which an east–west elongated structure can be seen (see Table 1). Note the different scales. The contour levels are the same as that in **a** with the corresponding peak flux density of 1.01 Jy beam<sup>-1</sup>.

<sup>1</sup>Shanghai Astronomical Observatory, 80 Nandan Road, Shanghai 200030, China. <sup>2</sup>National Radio Astronomy Observatory, 520 Edgemont Road, Charlottesville, Virginia 22903, USA. <sup>3</sup>Division of Geological and Planetary Sciences, California Institute of Technology, Pasadena, California 91125, USA. <sup>4</sup>Harvard-Smithsonian CfA, 60 Garden Street, Cambridge, Massachusetts 02138, USA. <sup>5</sup>Institute of Astronomy & Astrophysics, Academia Sinica, PO Box 23-141, Taipei 106, Taiwan, China.

**Table 2.** The fringe sizes (in micro arc seconds) for the standard and advanced apogees  $B_{max}$  (350 000 and 3 200 000 km correspondingly).

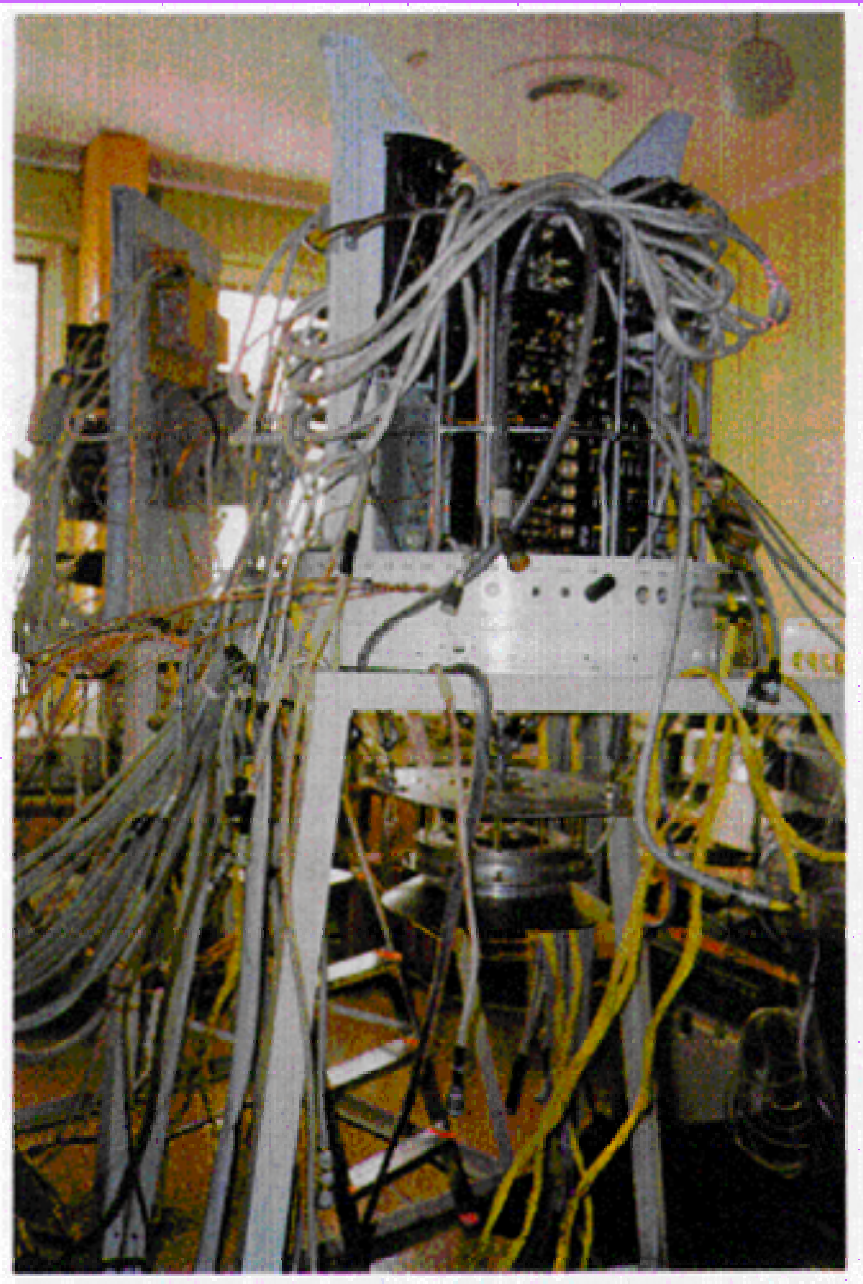
$B_{max}$ (km)\lambda(cm)	92	18	6.2	1.35
$3.5 \times 10^5$	540	106	37	8
$3.2 \times 10^6$	59	12	4	0.9











SRT electronics - under testing in ASC

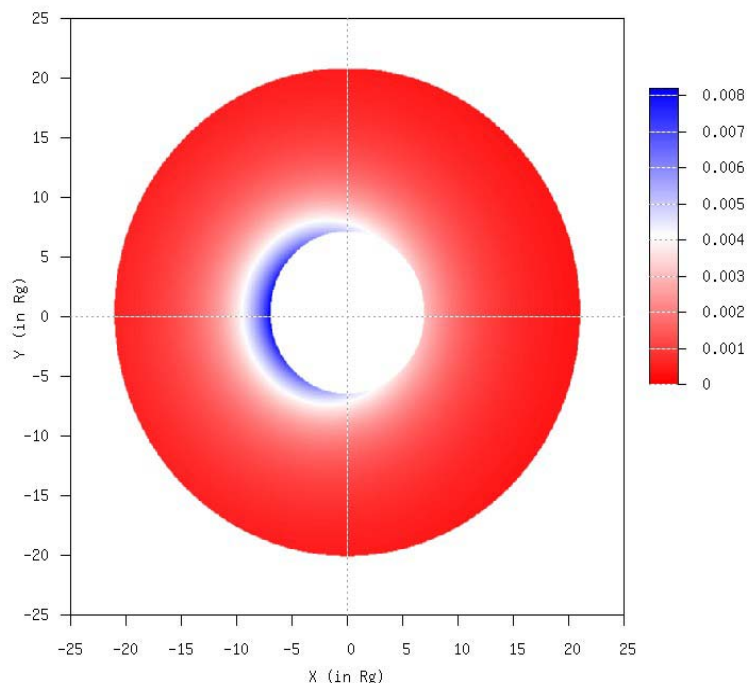
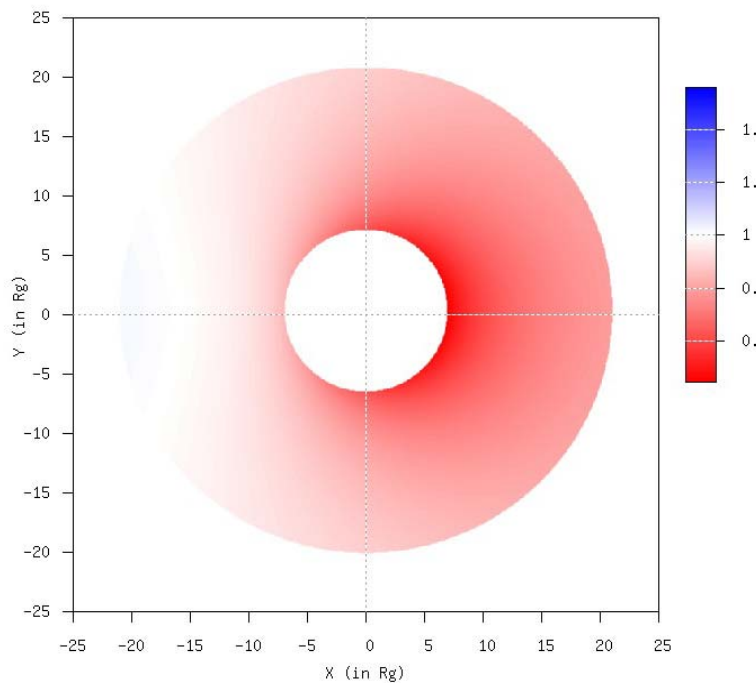




# Schwarzschild black hole images (A.F. Zakharov & P. Jovanovic in preparation)

- $\theta=15$  deg
- Redshift map

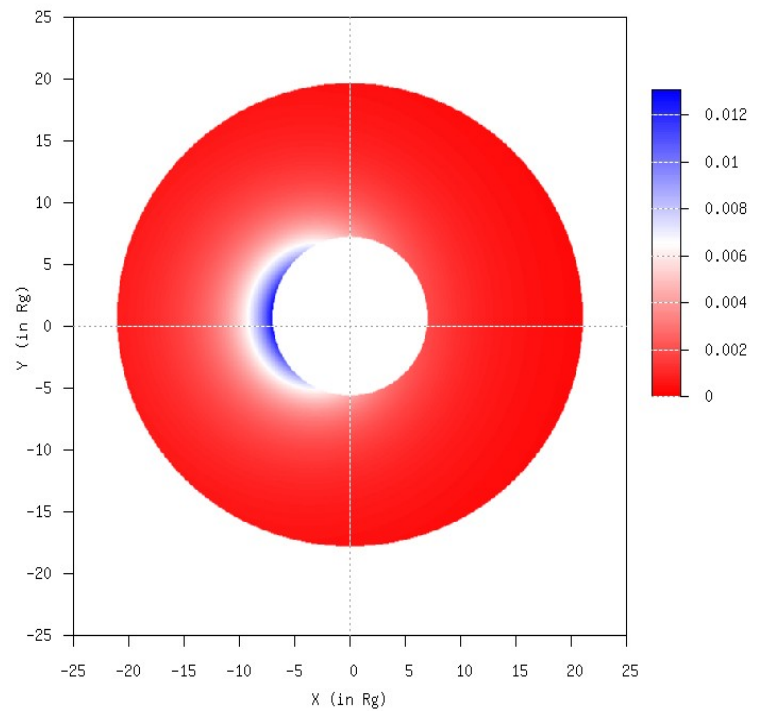
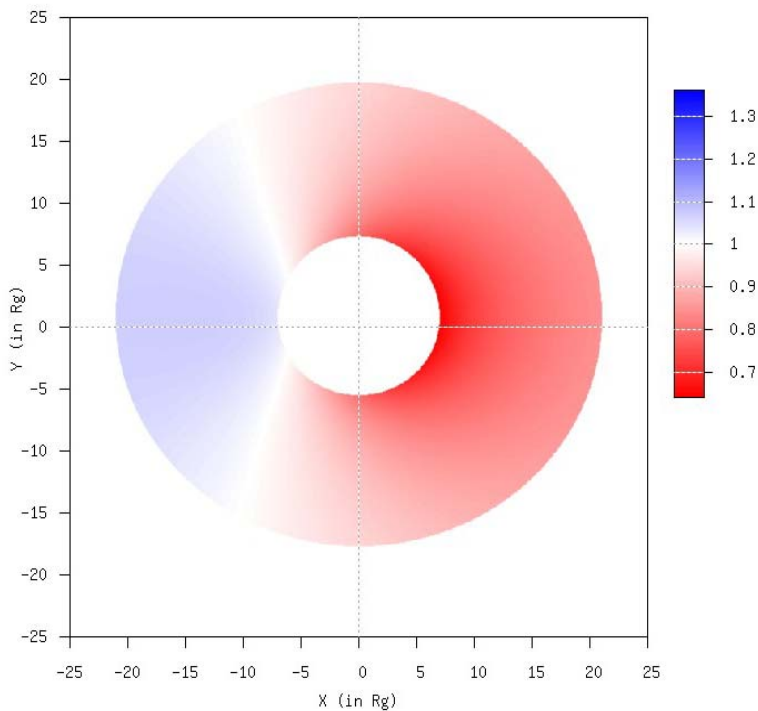
Intensity map



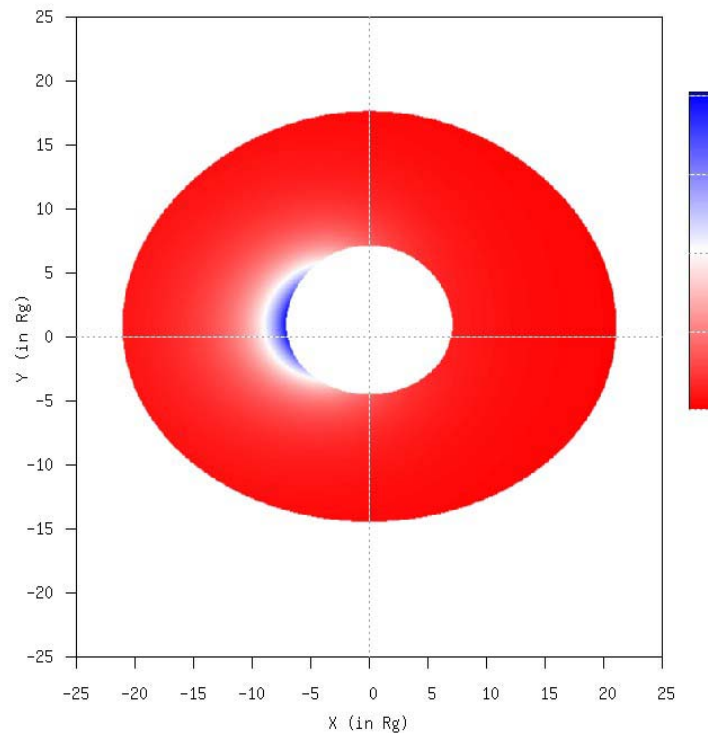
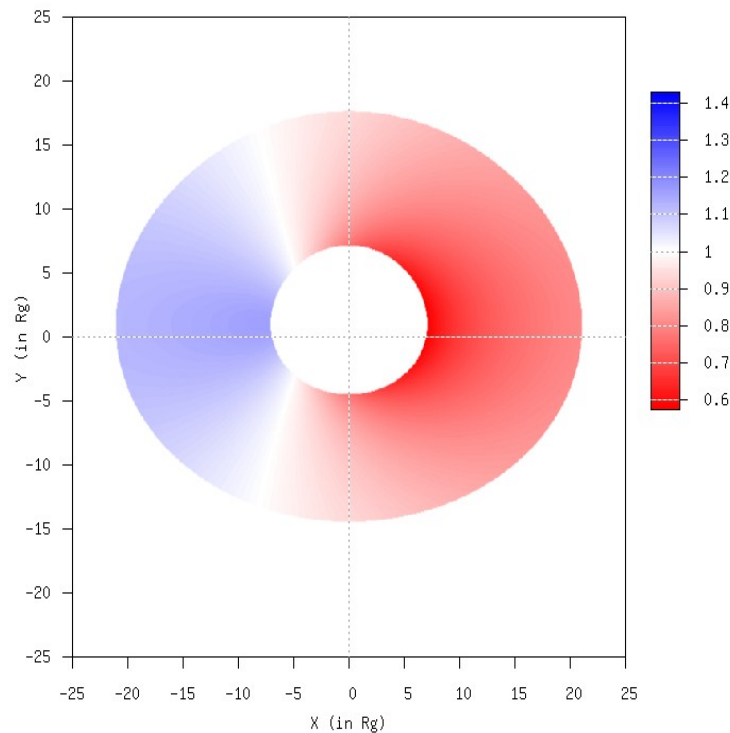
# Schwarzschild black hole images

- $\theta=30$  deg
- Redshift map

Intensity map



# Schwarzschild black hole images: $\theta=45$ deg

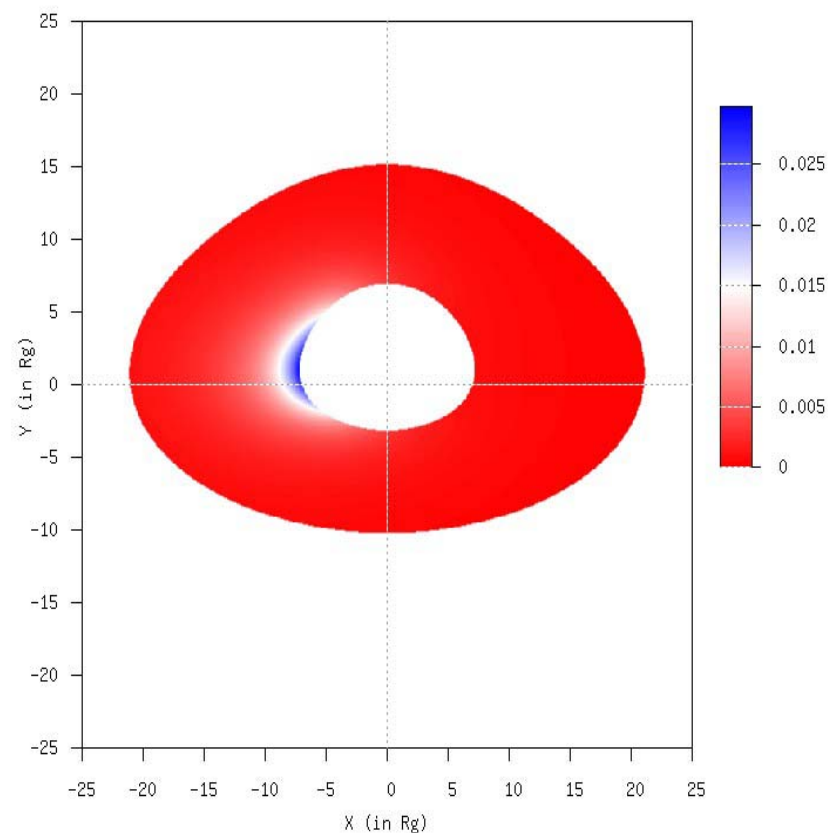
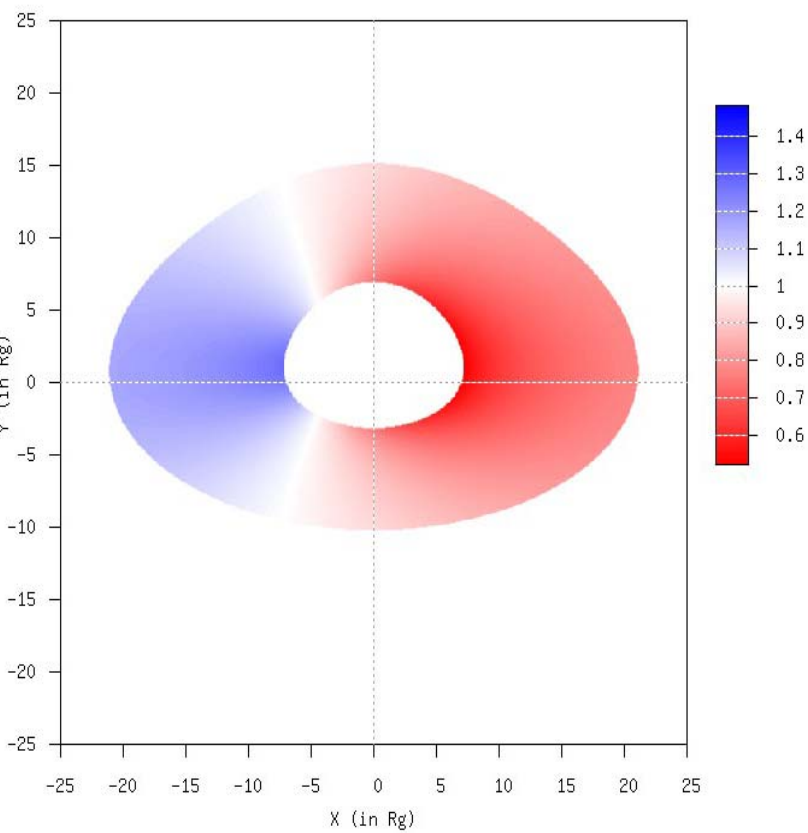


# Schwarzschild black hole images: $\theta=60$ deg

- Redshift map

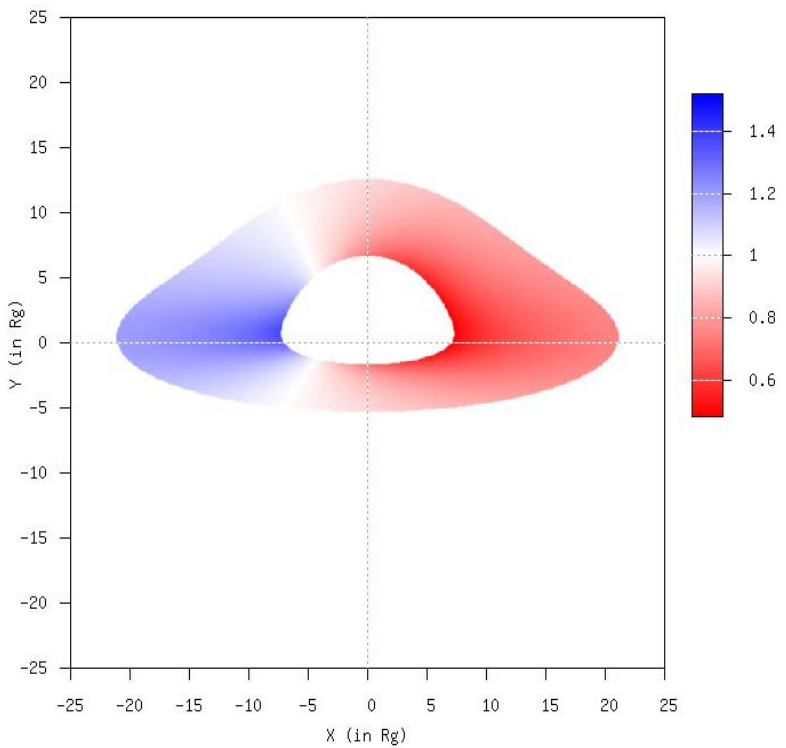
- 

- Intensity map



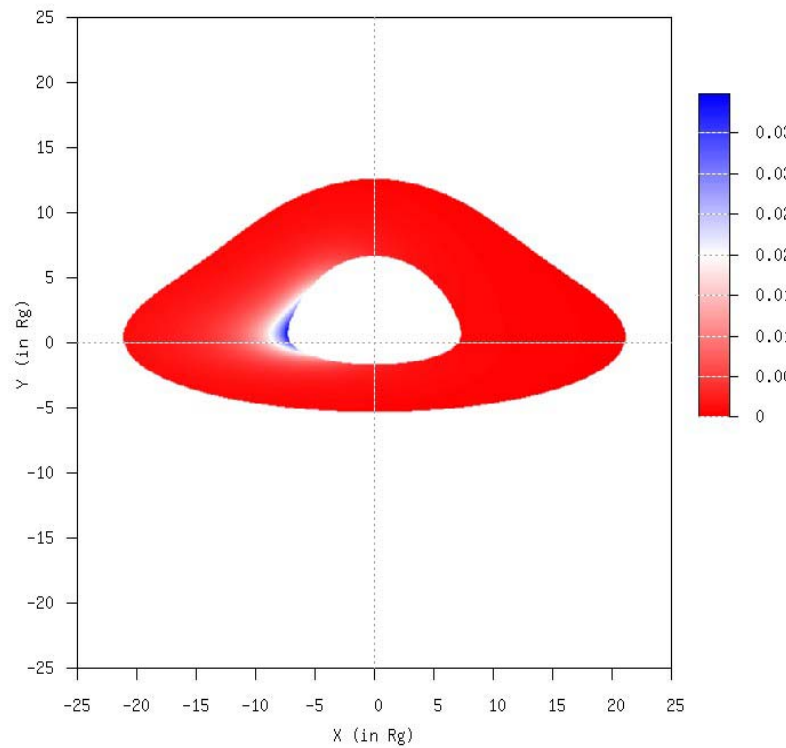
# Schwarzschild black hole images: $\theta=75$ deg

- Redshift map



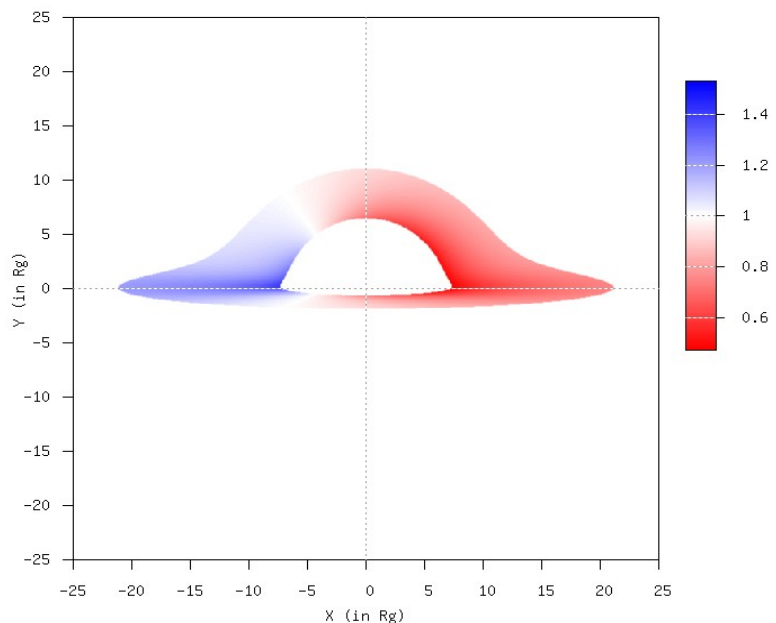
- 

- Intensity map

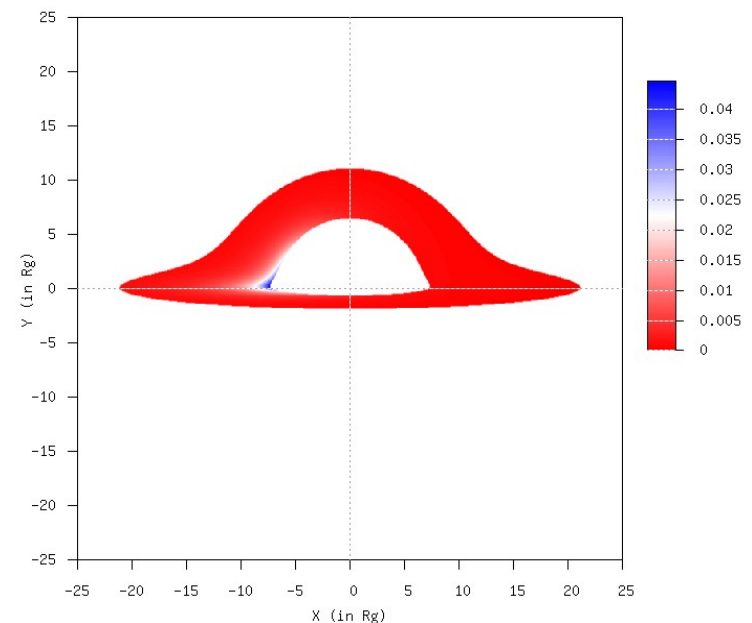


# Schwarzschild black hole images: $\theta=85$ deg

- Redshift map

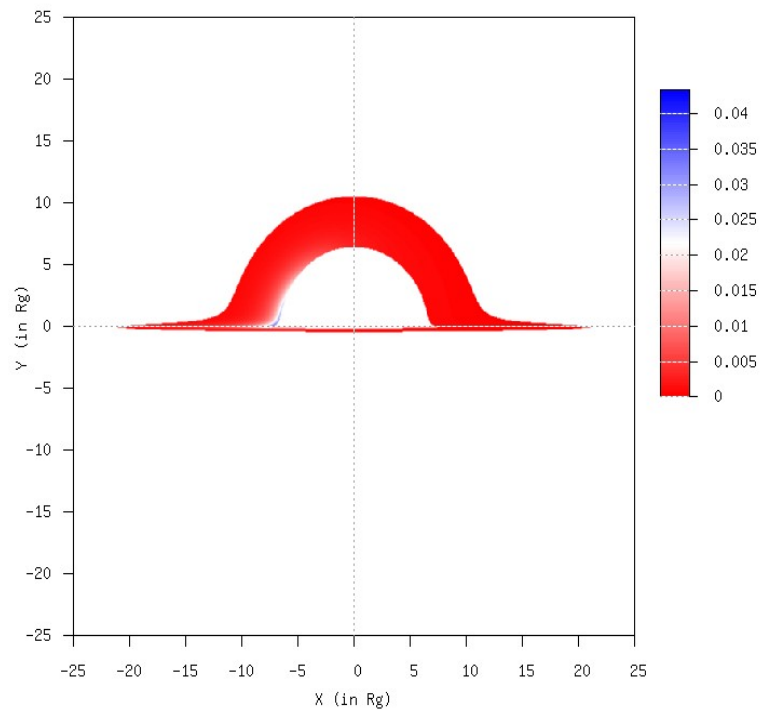
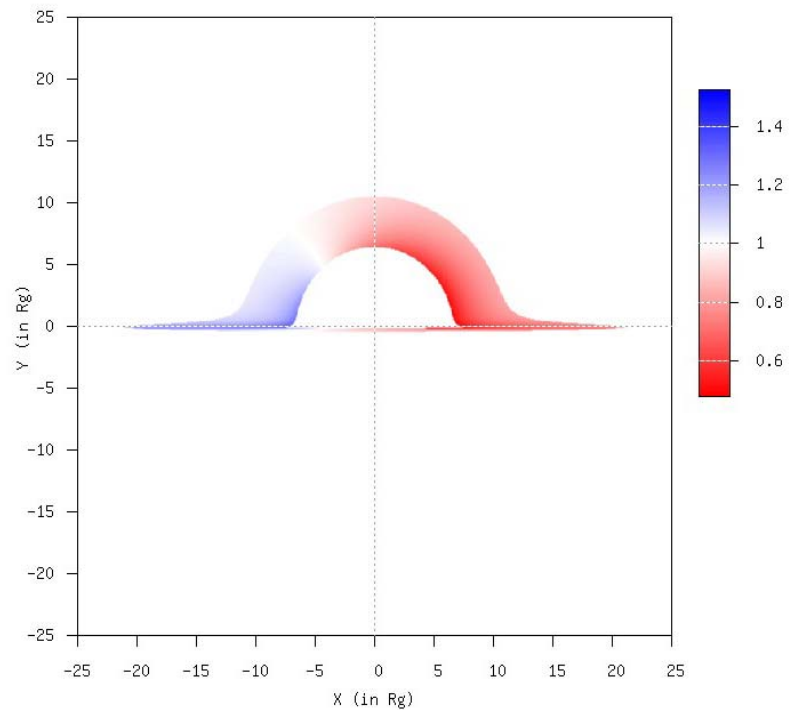


- Intensity map



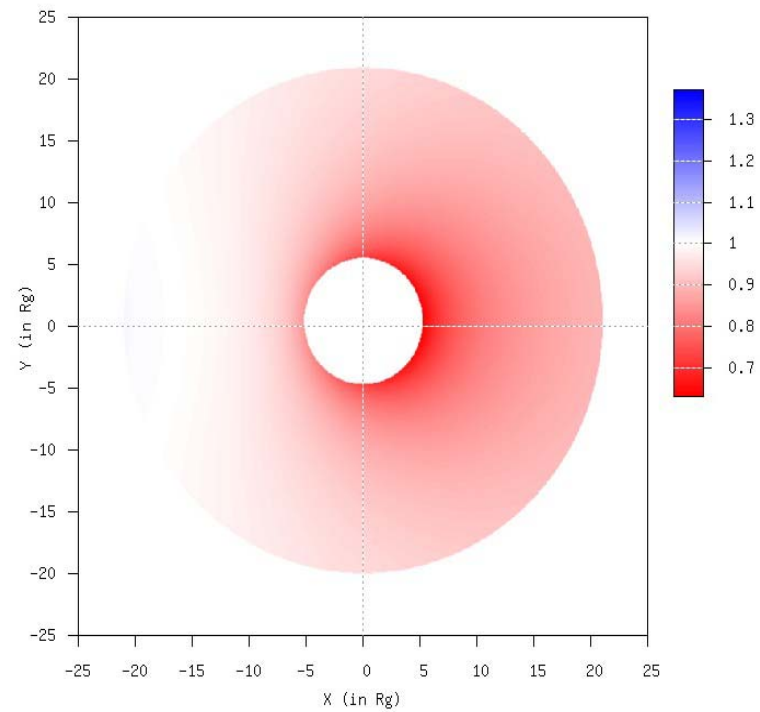
# Schwarzschild black hole images: $\theta=89$ deg

- Redshift map



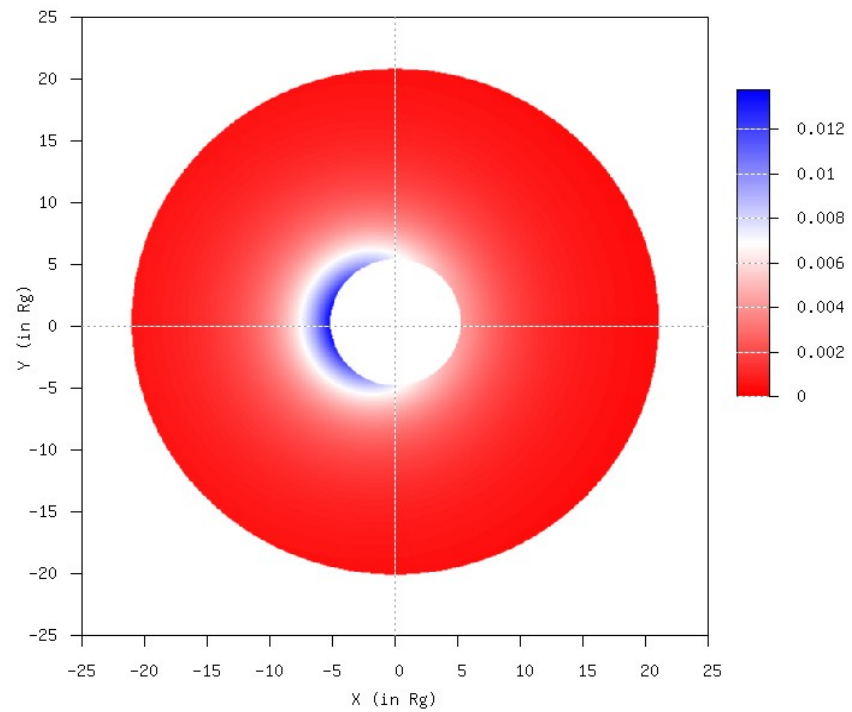
# Kerr black hole images ( $a=0.5$ ): $\theta=15$ deg

- Redshift map



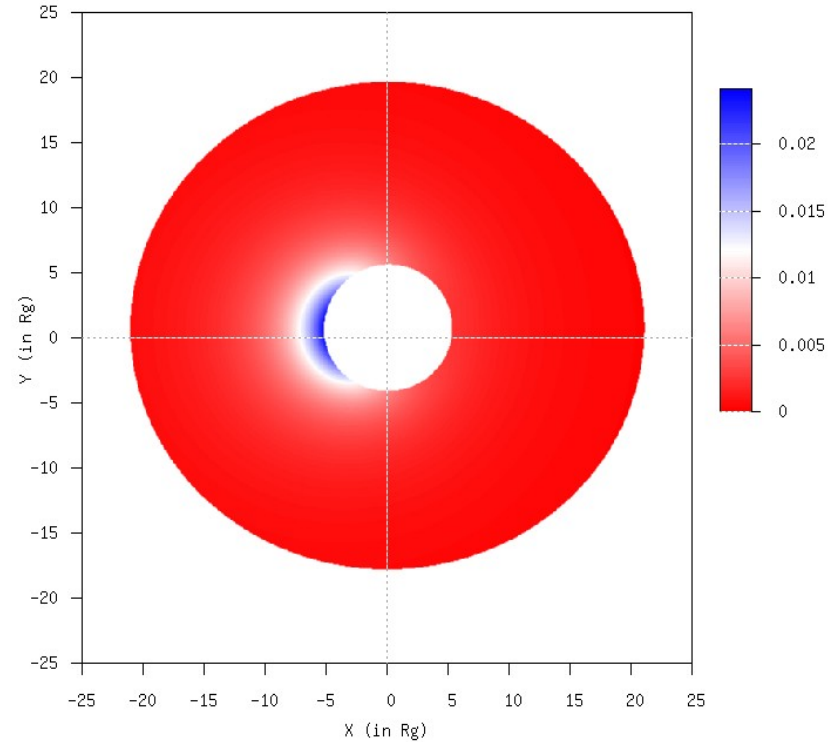
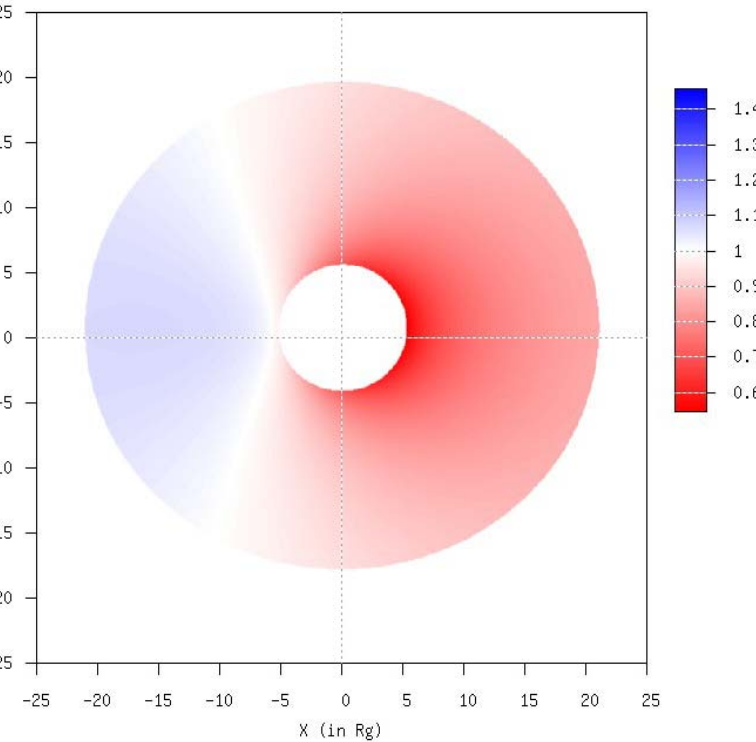
- 

- Intensity map



# Kerr black hole images ( $a=0.5$ ): $\theta=30$ deg

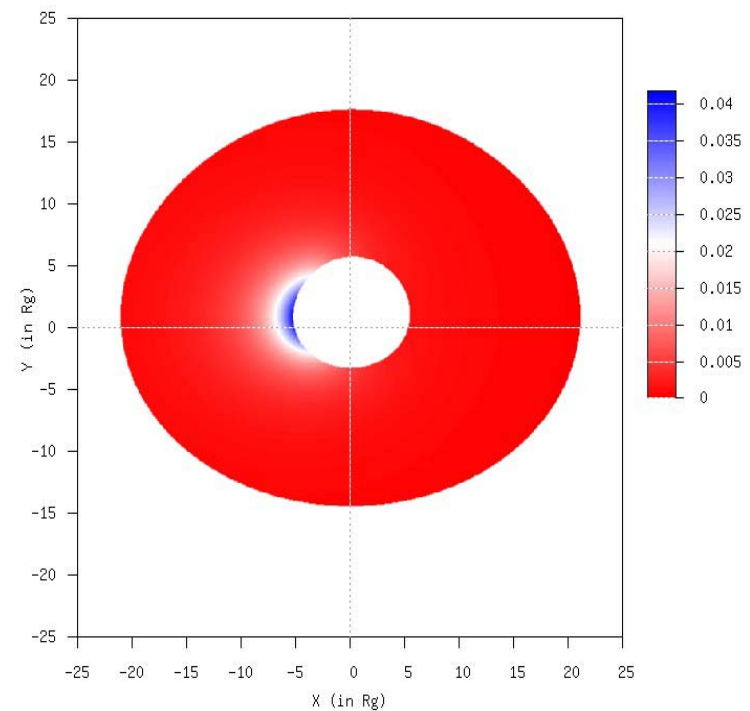
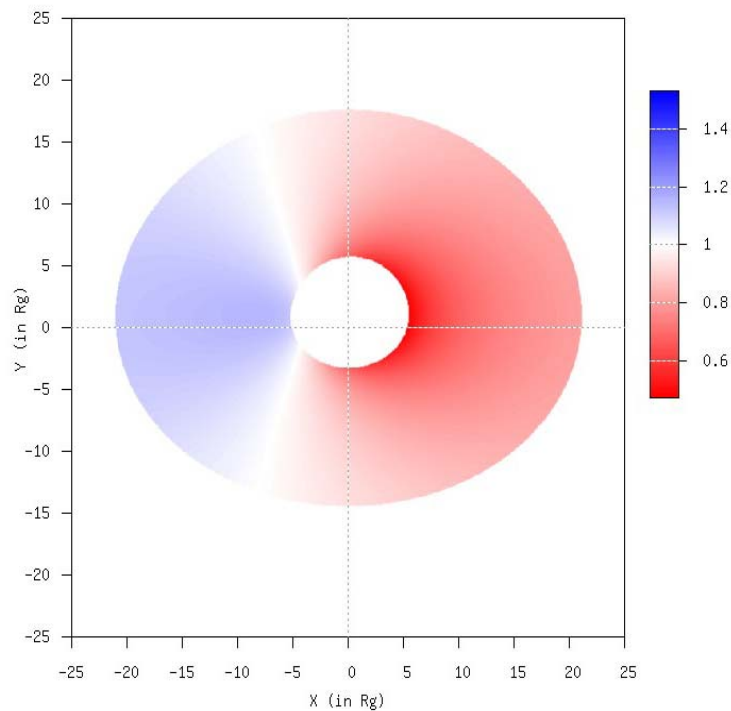
- Redshift map
- Intensity map



# Kerr black hole images ( $a=0.5$ ): $\theta=45$ deg

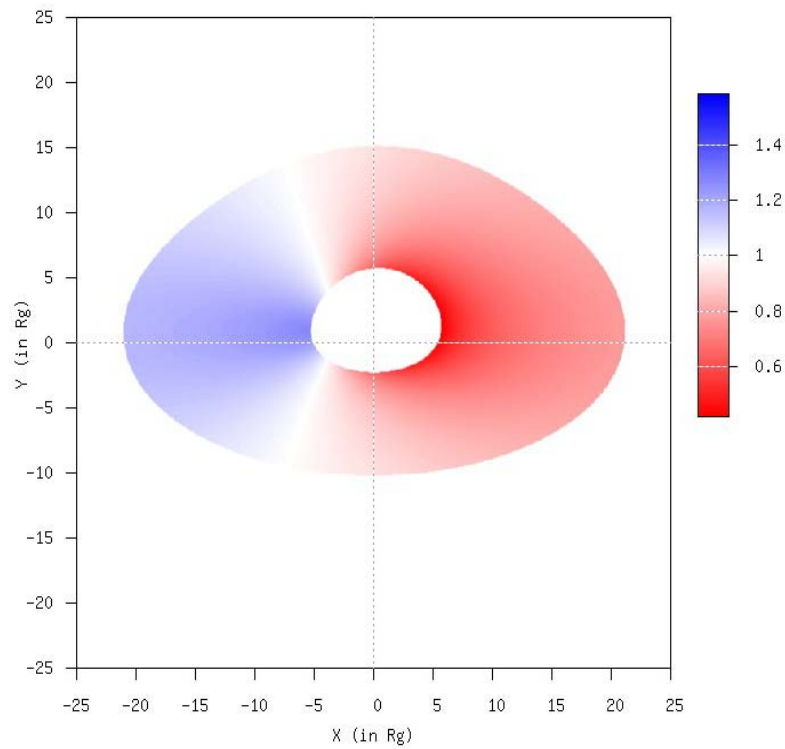
- Redshift map

- Intensity map



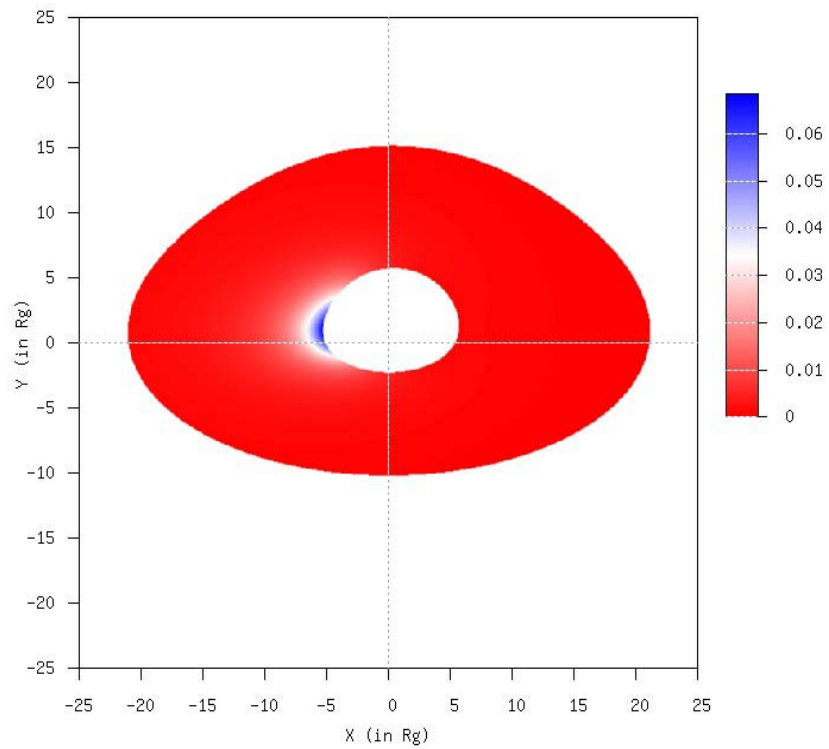
# Kerr black hole images ( $a=0.5$ ): $\theta=60$ deg

- Redshift map



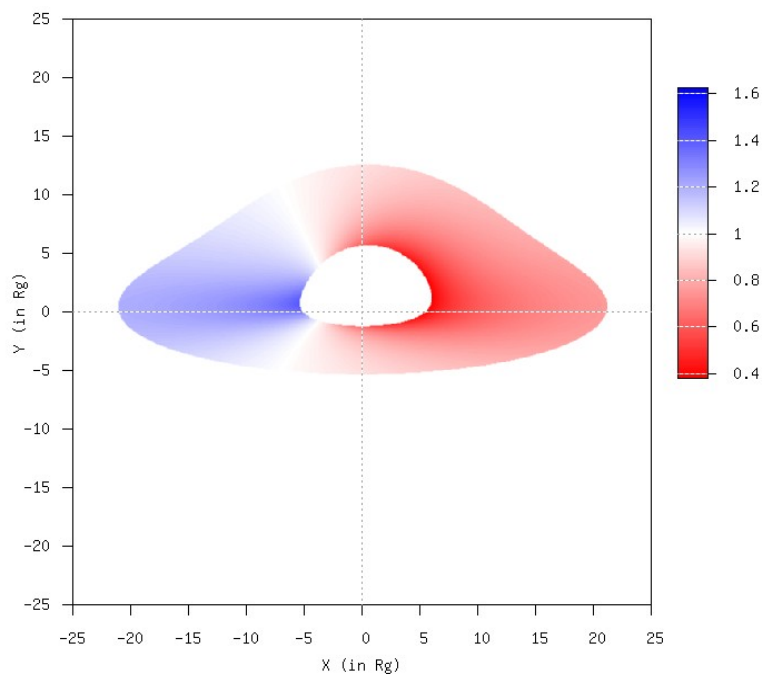
- 

- Intensity map



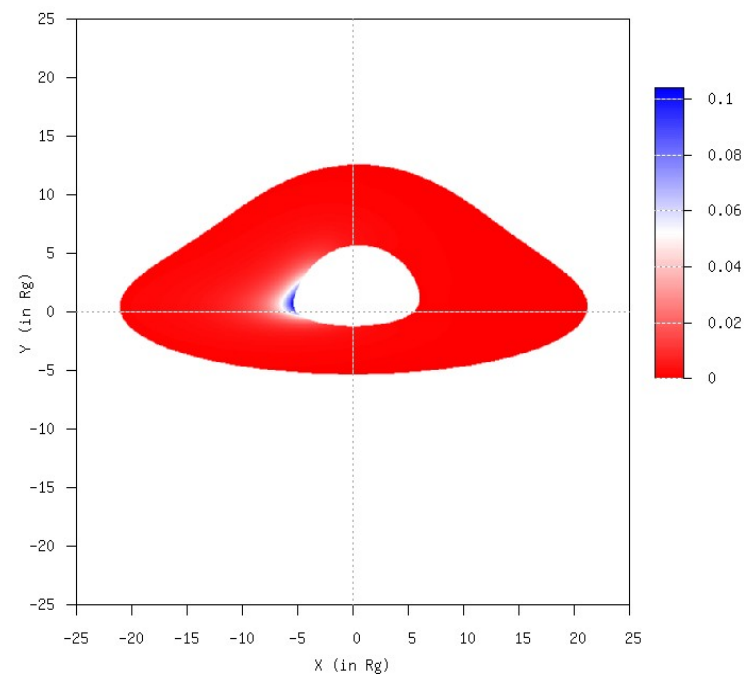
# Kerr black hole images ( $a=0.5$ ): $\theta=75$ deg

- Redshift map



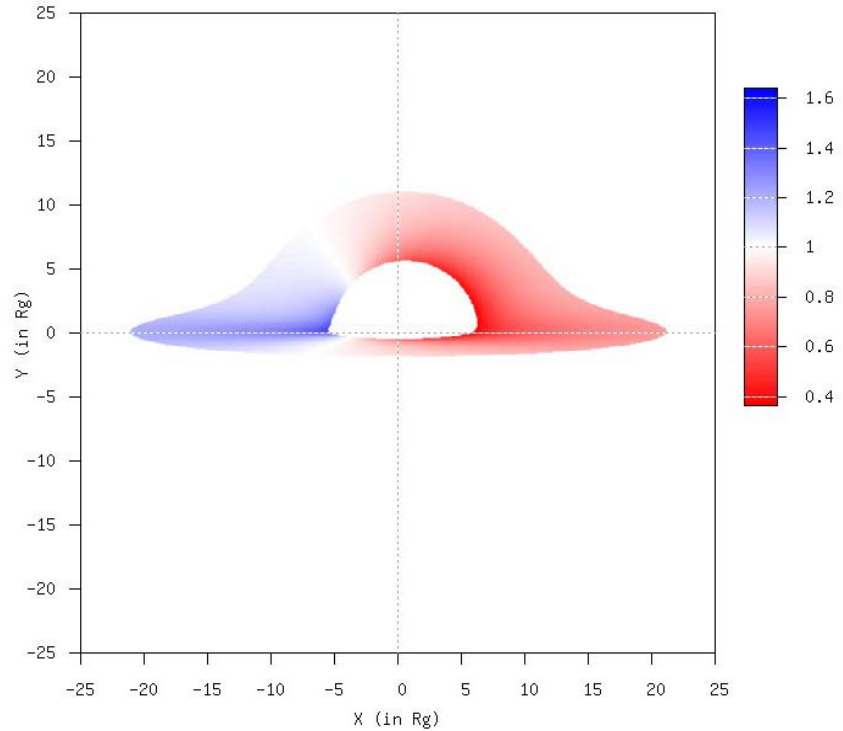
- 

- Intensity map

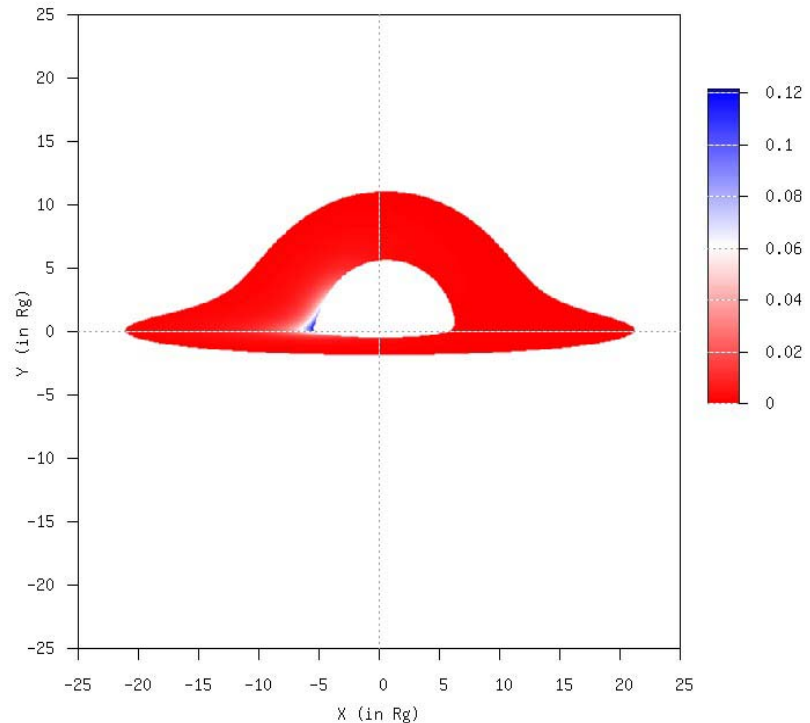


# Kerr black hole images ( $a=0.5$ ): $\theta=85$ deg

- Redshift map

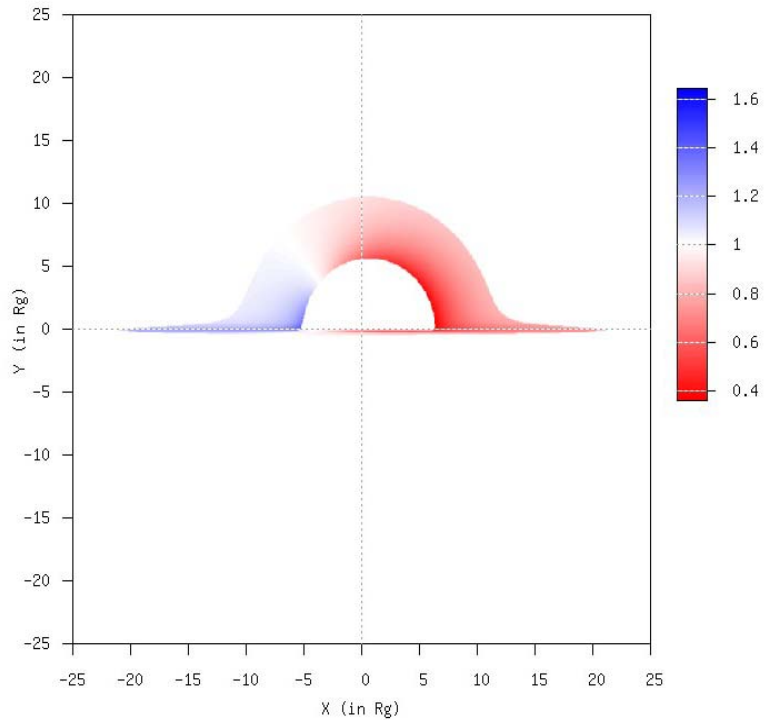


- Intensity map



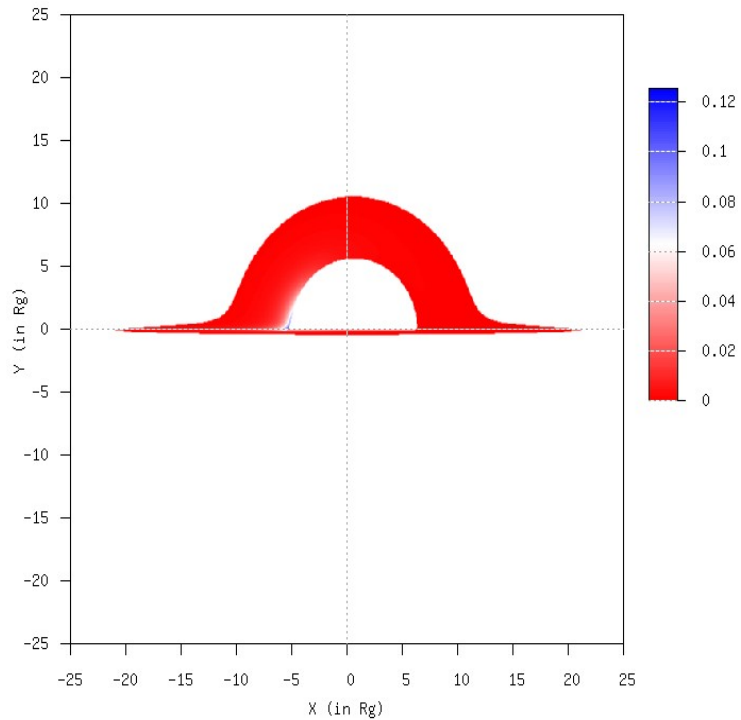
# Kerr black hole images ( $a=0.5$ ): $\theta=89$ deg

- Redshift map



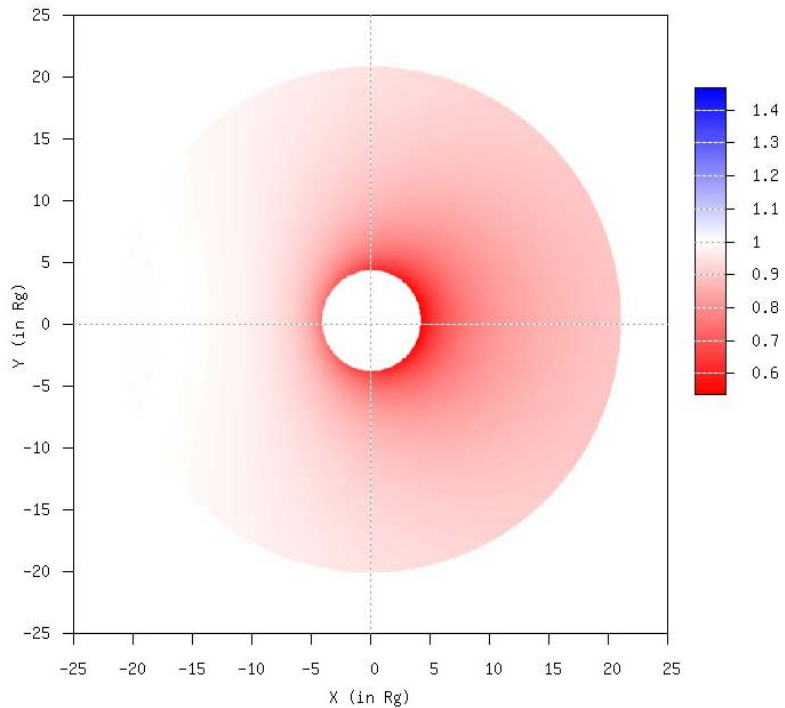
- 

- Intensity map

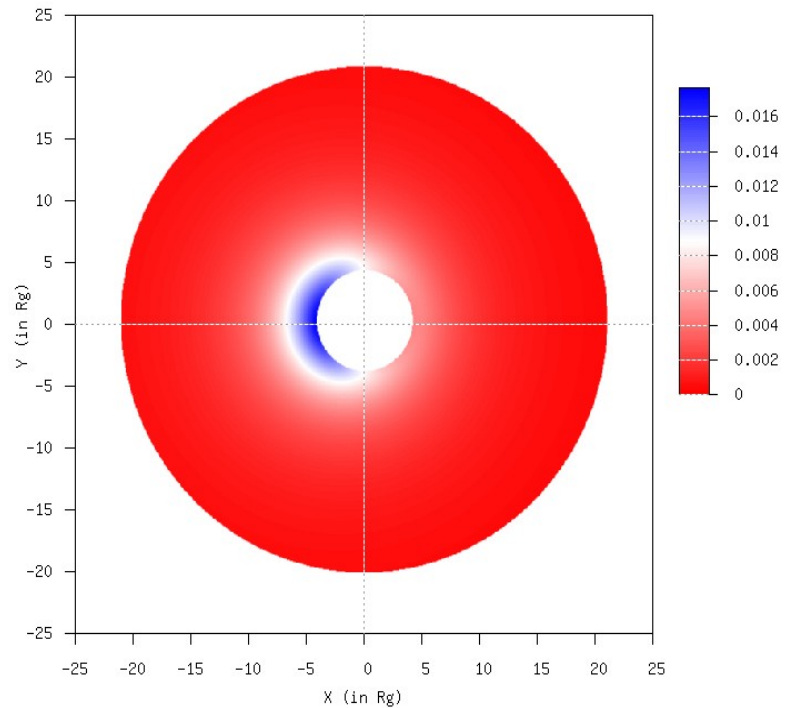


# Kerr black hole images ( $a=0.75$ ): $\theta=15$ deg

- Redshift map

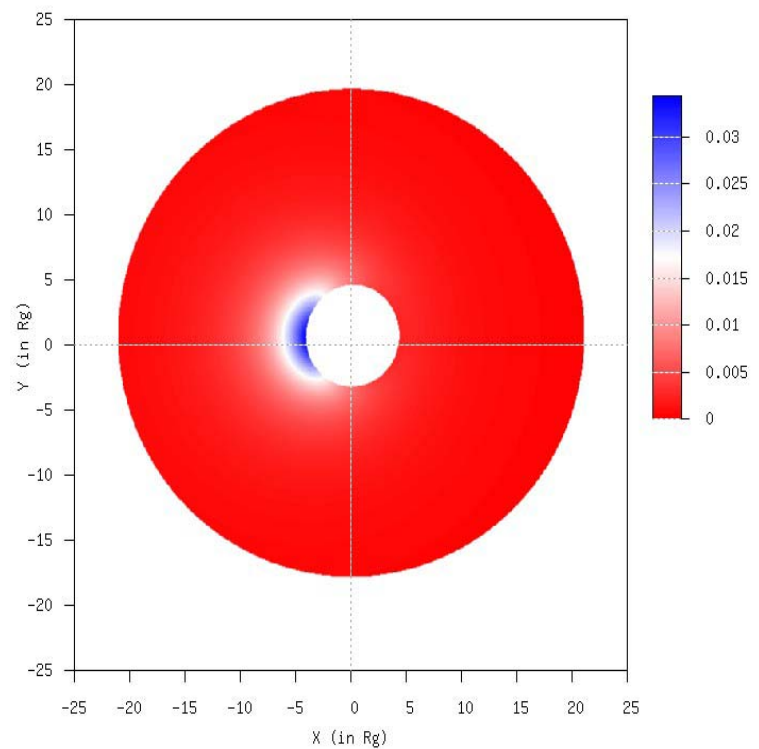
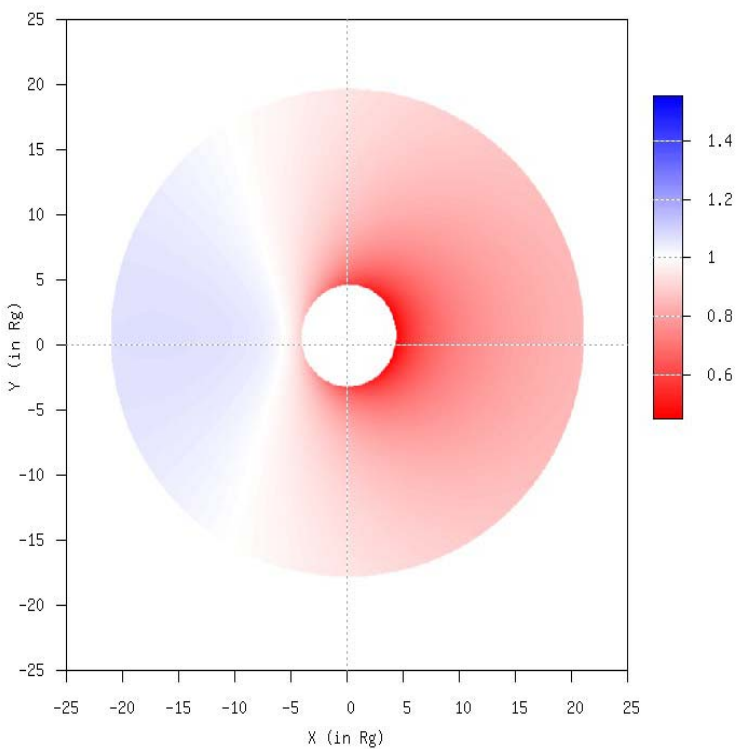


- Intensity map



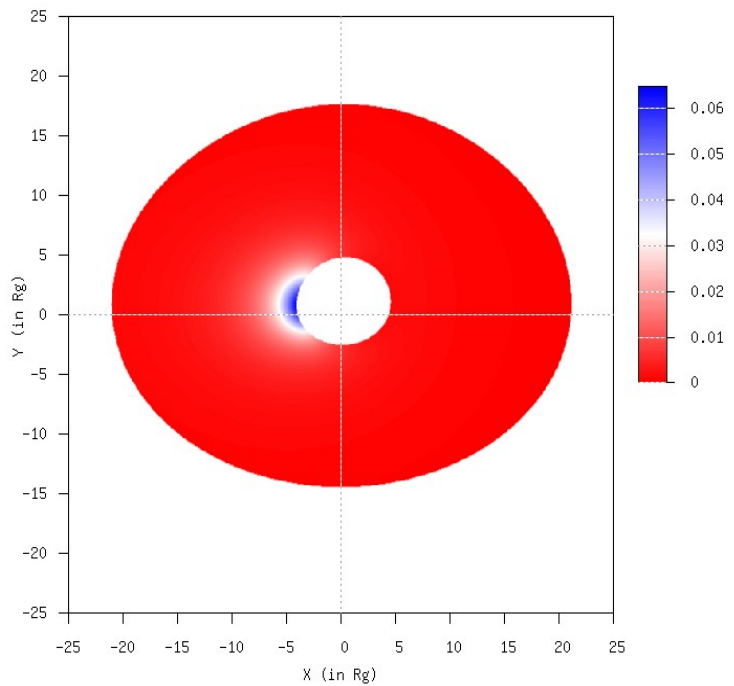
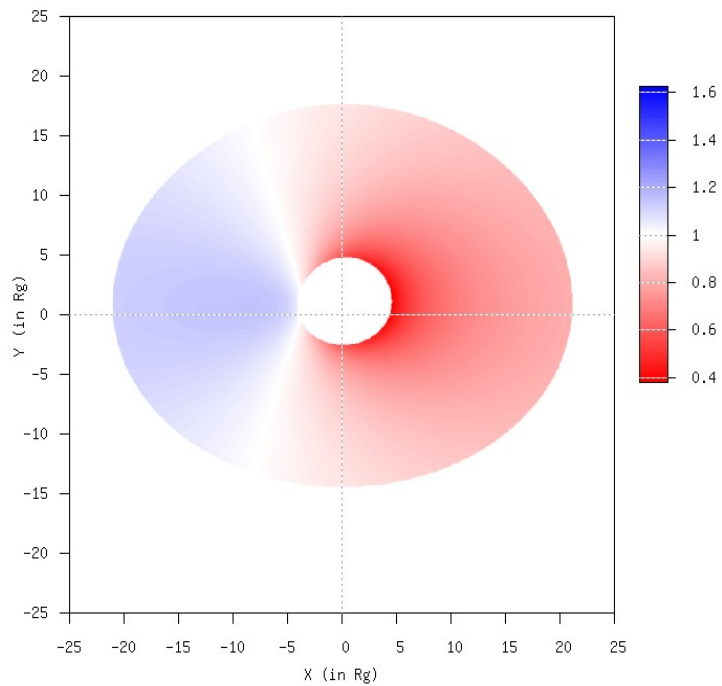
# Kerr black hole images ( $a=0.75$ ): $\theta=30$ deg

- Redshift map
- Intensity map



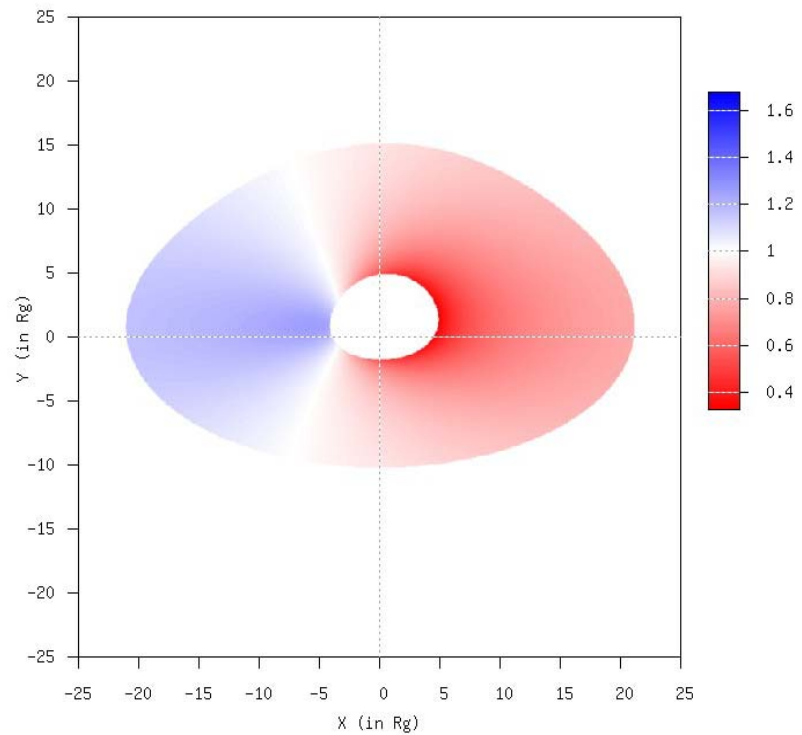
# Kerr black hole images ( $a=0.75$ ): $\theta=45$ deg

- Redshift map
- Intensity map



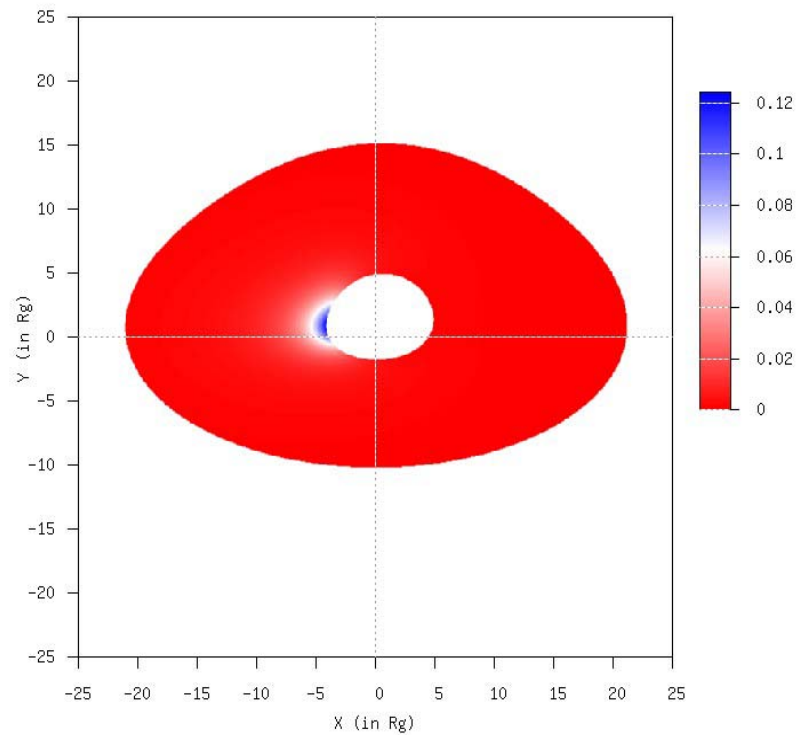
# Kerr black hole images ( $a=0.75$ ): $\theta=60$ deg

- Redshift map



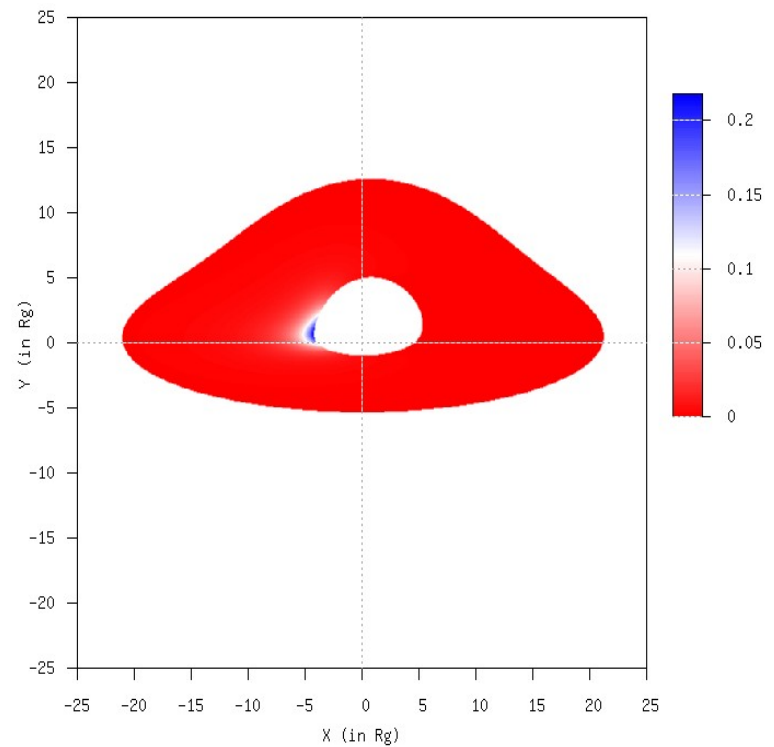
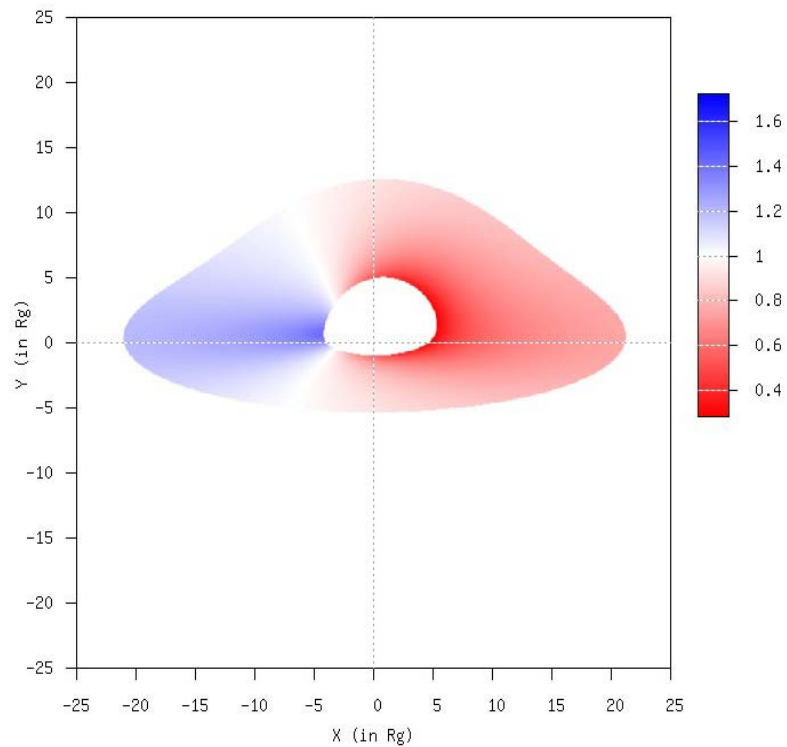
- 

- Intensity map



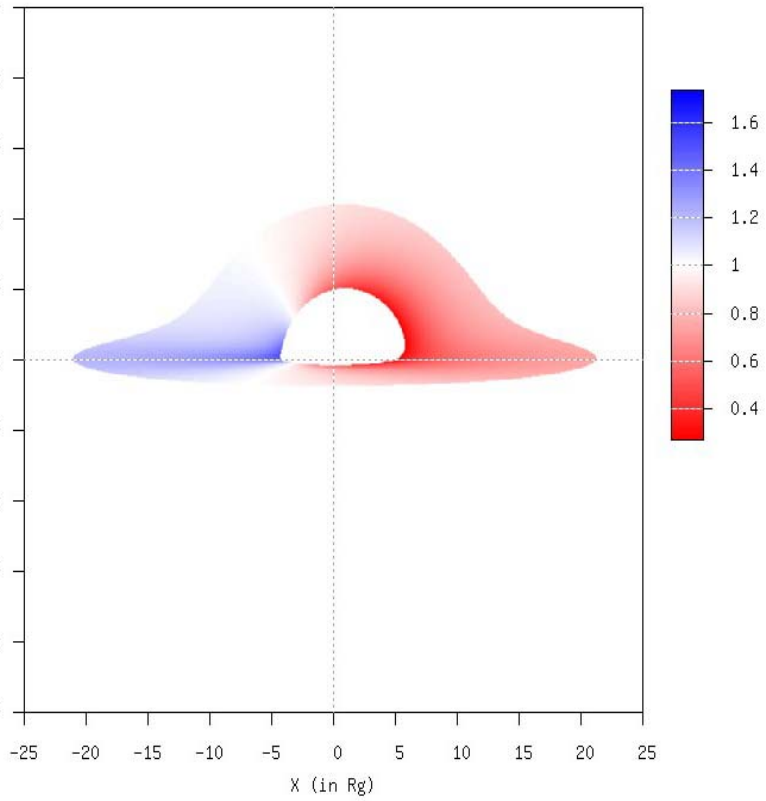
# Kerr black hole images ( $a=0.75$ ): $\theta=75$ deg

- Redshift map
- Intensity map

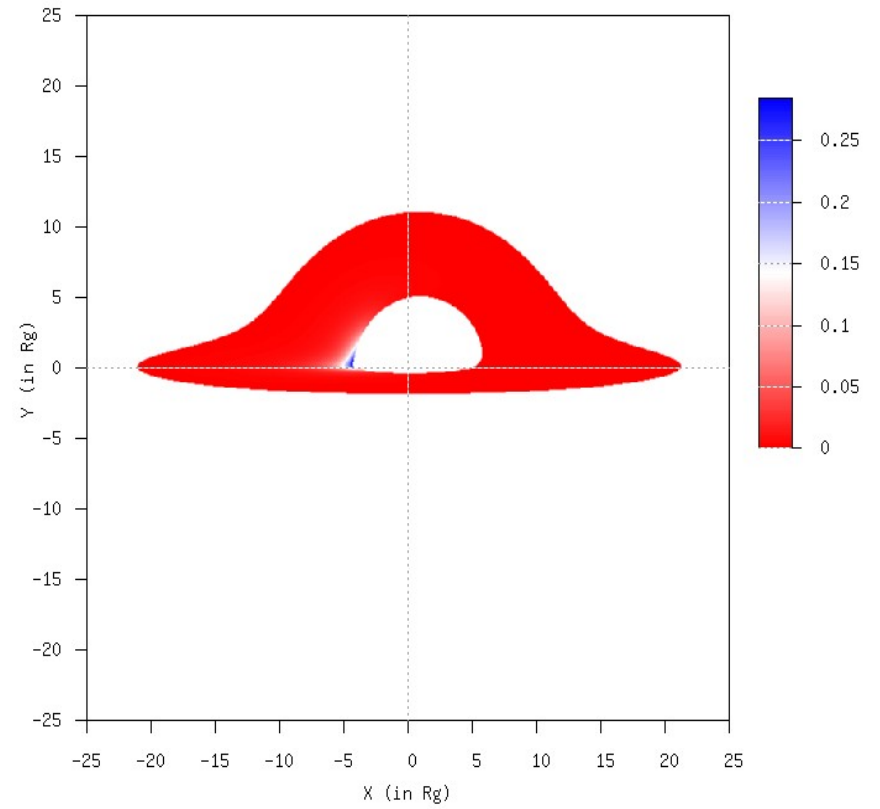


# Kerr black hole images ( $a=0.75$ ): $\theta=85$ deg

- Redshift map

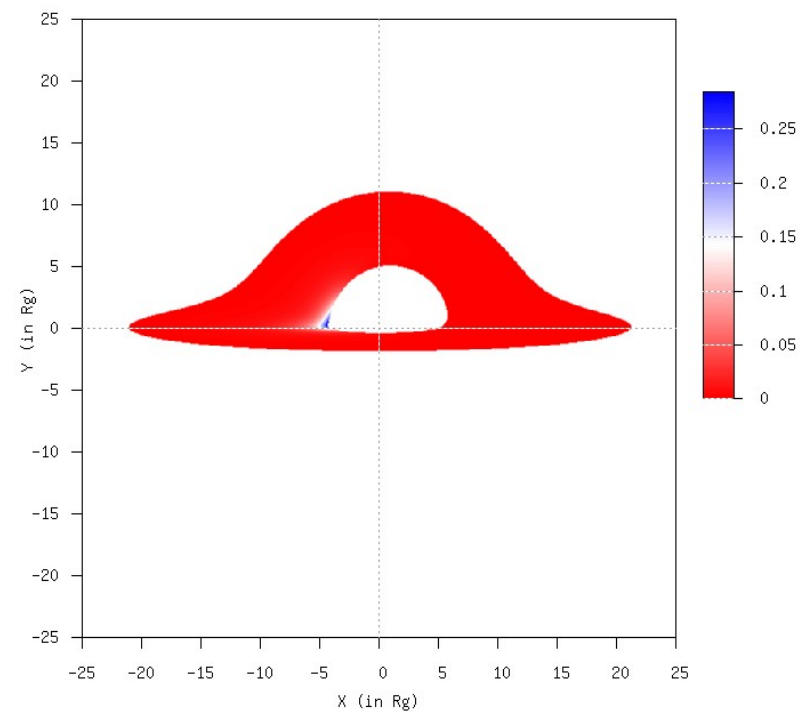
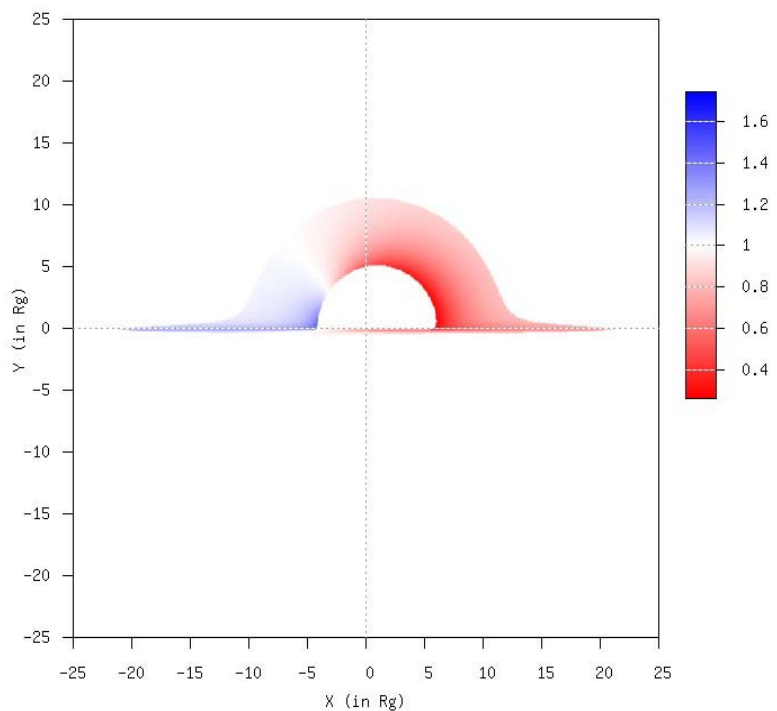


- Intensity map



# Kerr black hole images ( $a=0.75$ ): $\theta=89$ deg

- Redshift map
- Intensity map

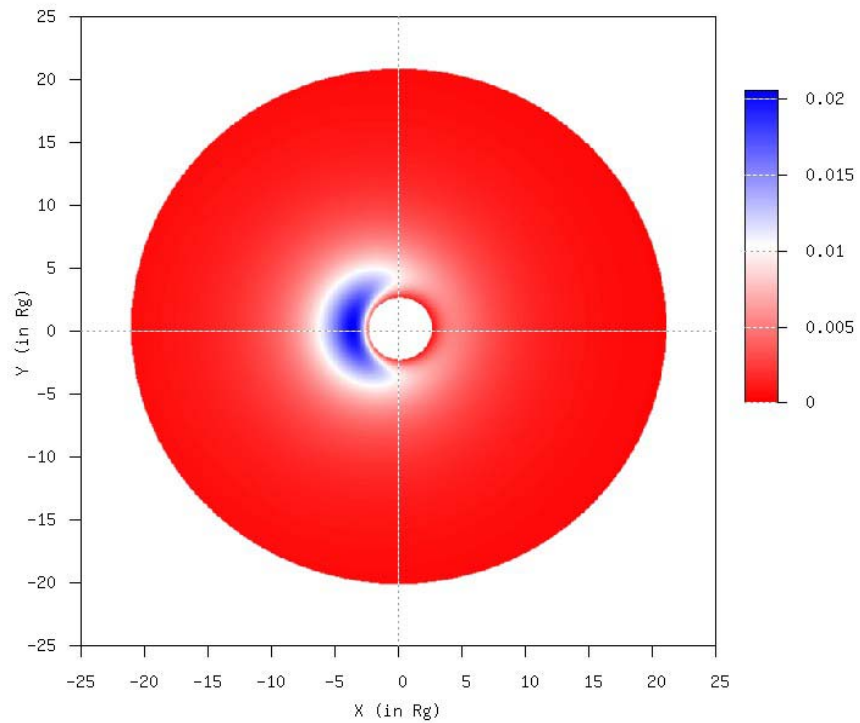
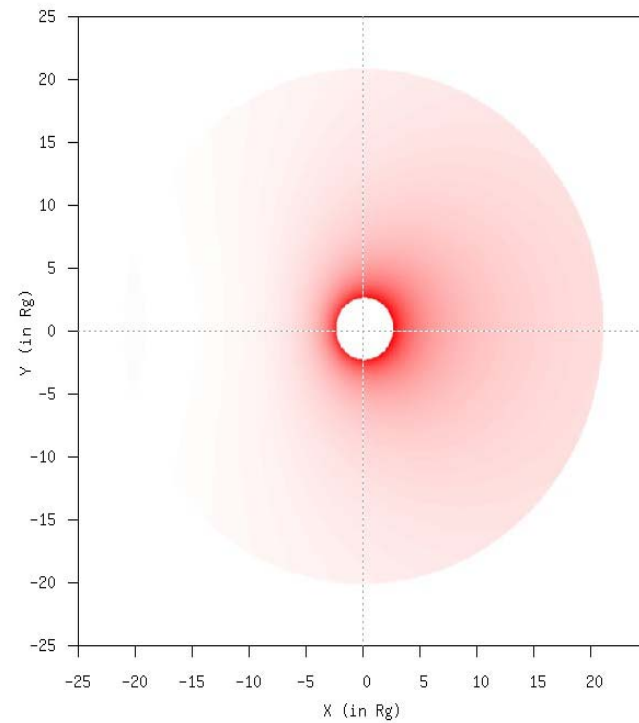


# Kerr black hole images ( $a=0.99$ ): $\theta=15$ deg

- Redshift map

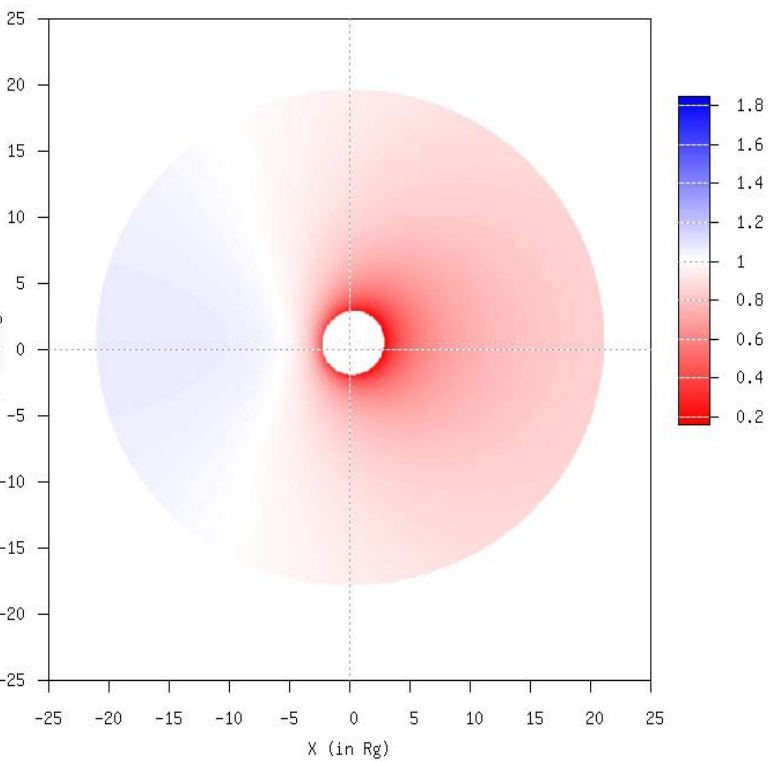
- 

- Intensity map

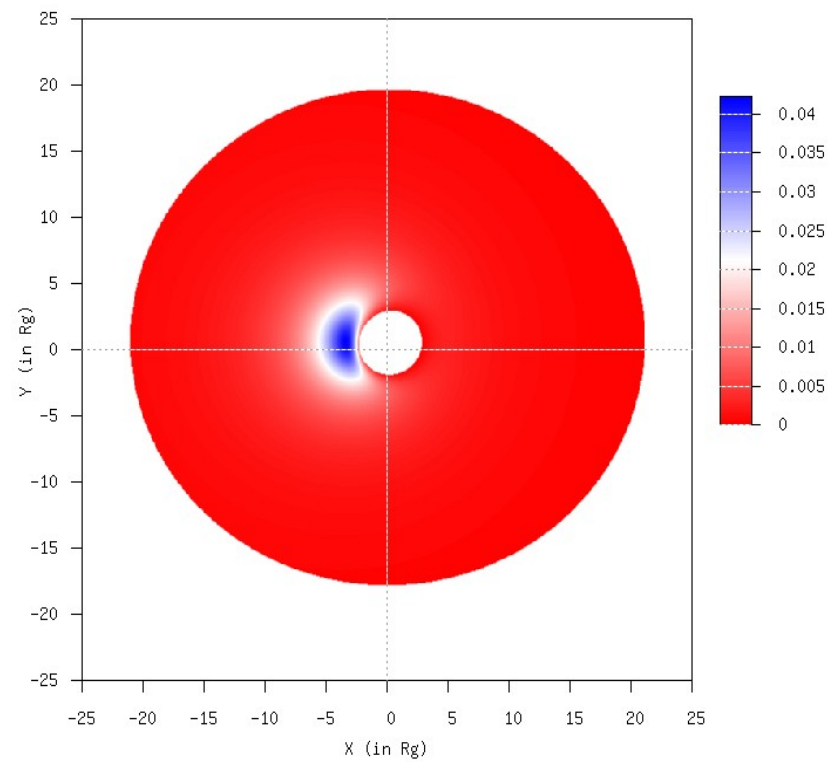


# Kerr black hole images ( $a=0.99$ ): $\theta=30$ deg

- Redshift map



- Intensity map

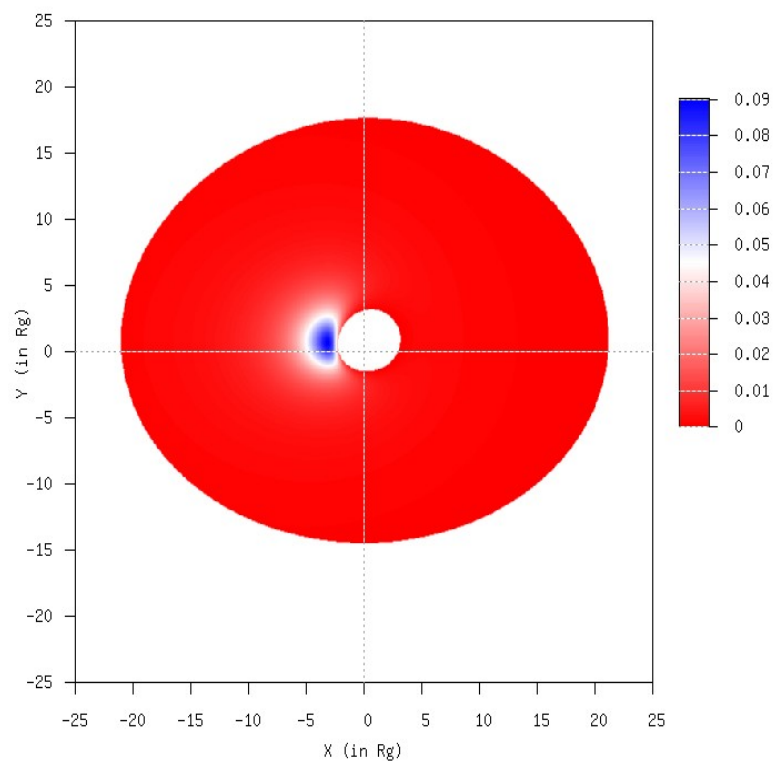
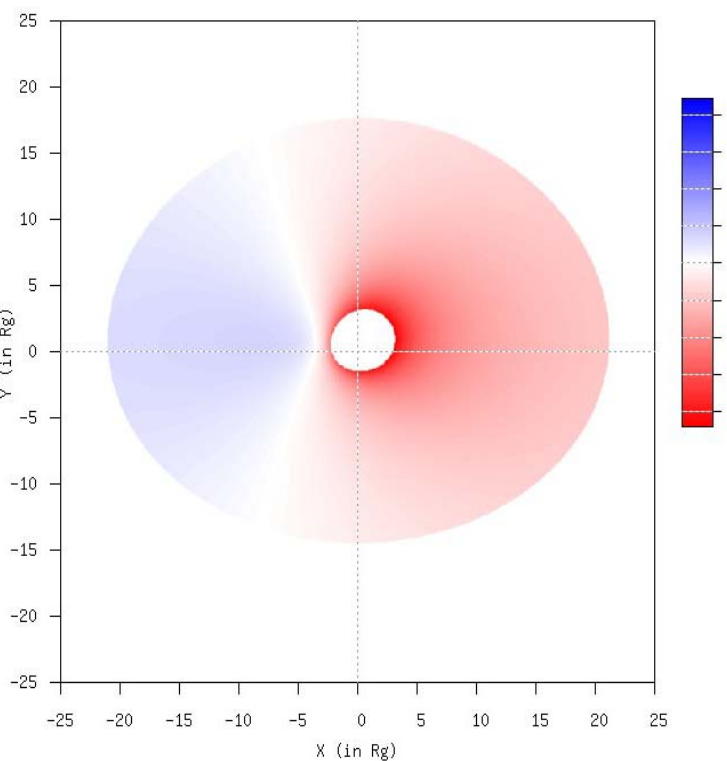


# Kerr black hole images ( $a=0.99$ ): $\theta=45$ deg

- Redshift map

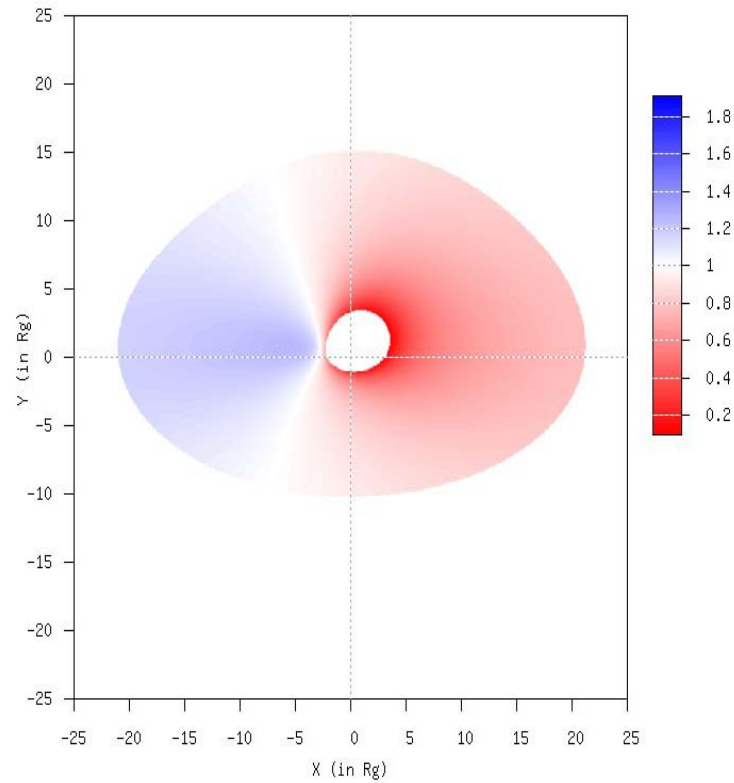
- 

- Intensity map



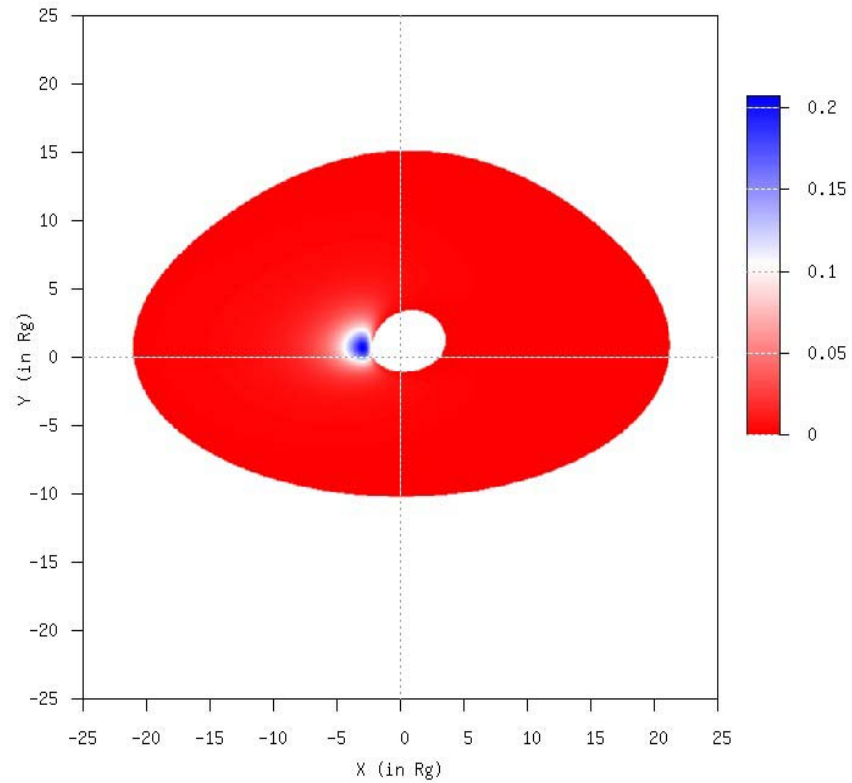
# Kerr black hole images ( $a=0.99$ ): $\theta=60$ deg

- Redshift map



- 

- Intensity map

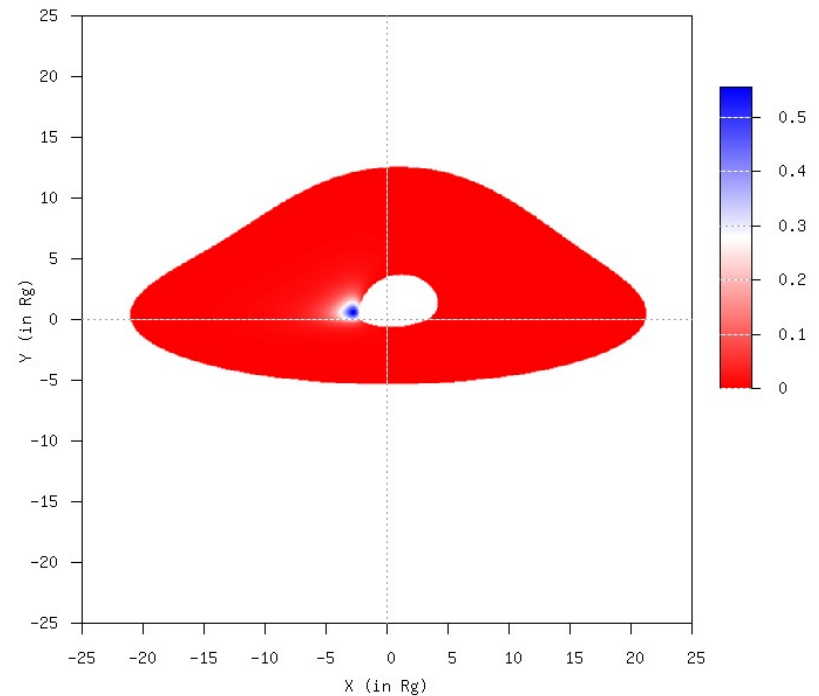
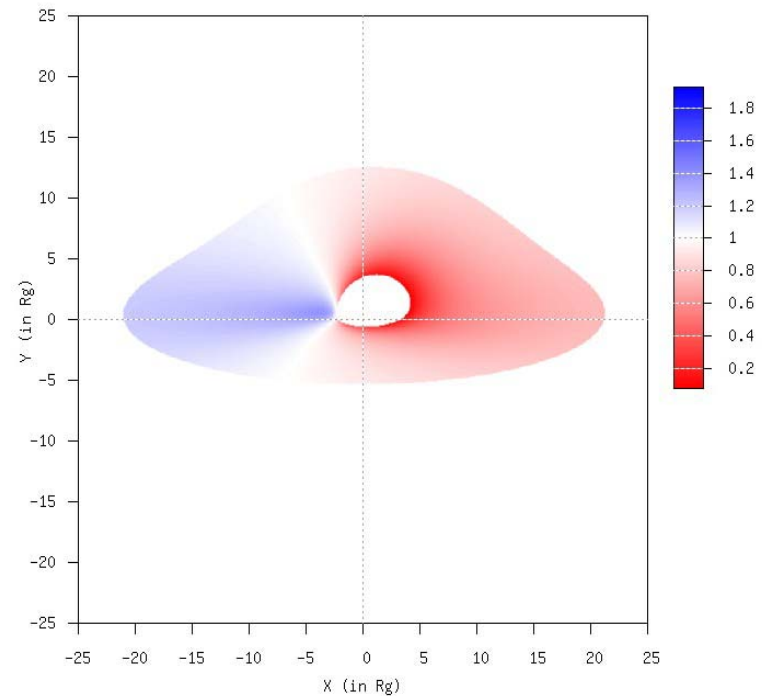


# Kerr black hole images ( $a=0.99$ ): $\theta=75$ deg

- Redshift map

- 

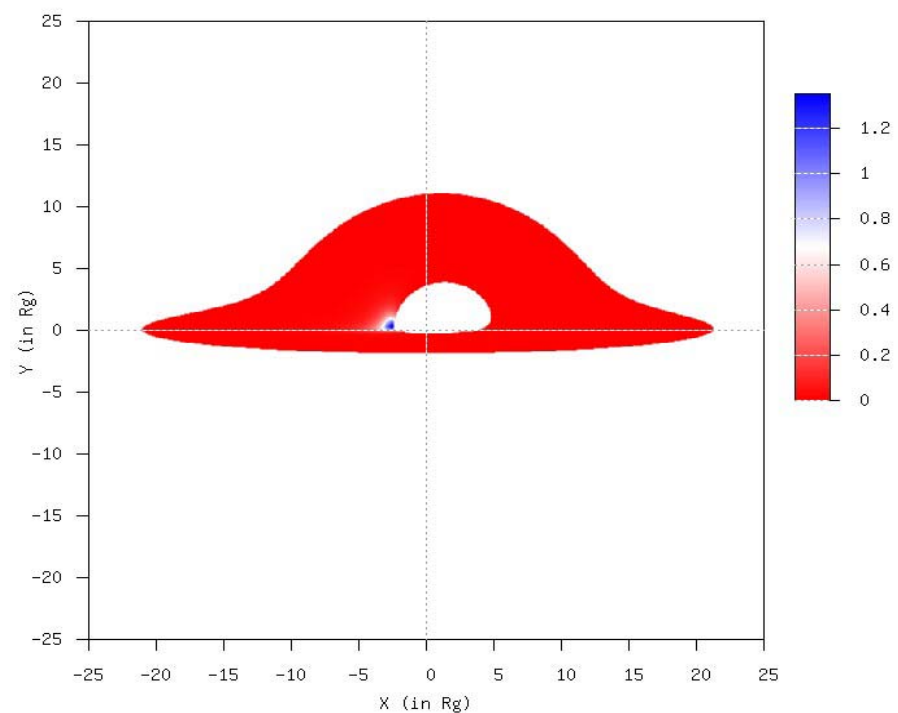
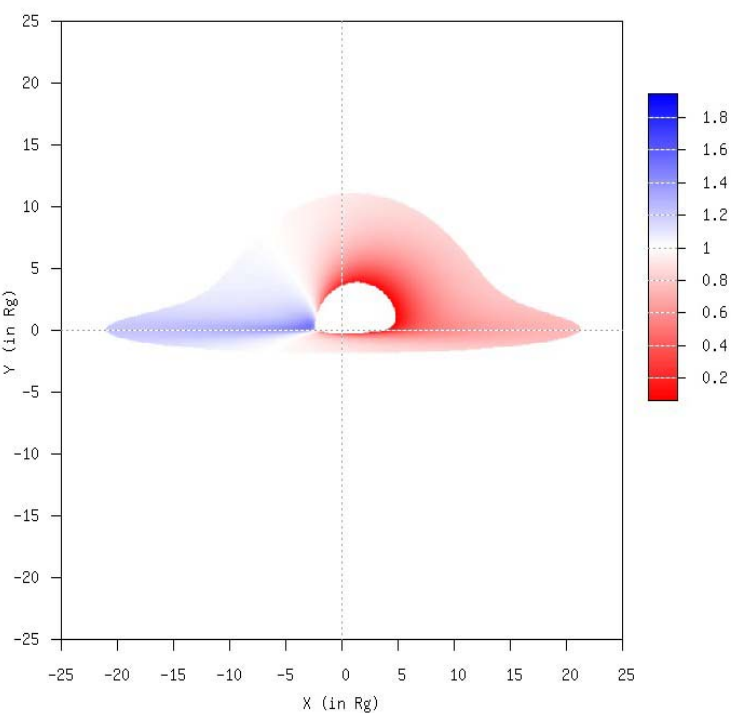
- Intensity map



# Kerr black hole images ( $a=0.99$ ): $\theta=85$ deg

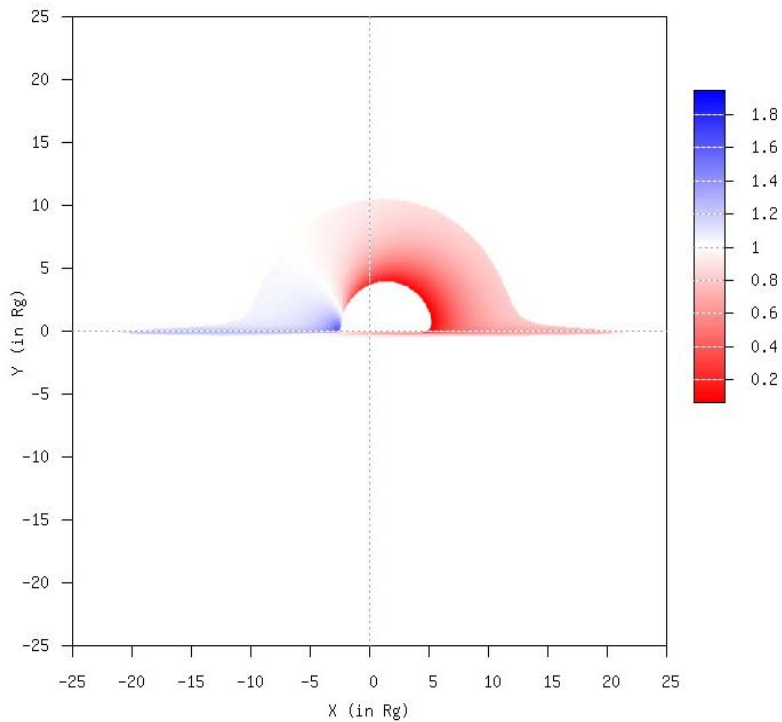
- Redshift map

- Intensity map

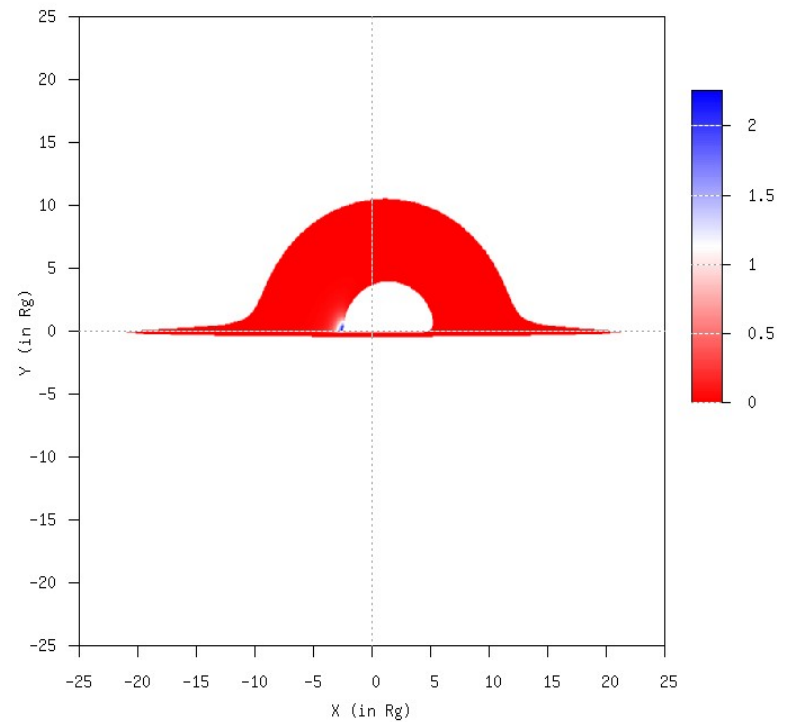


# Kerr black hole images ( $a=0.99$ ): $\theta=89$ deg

- Redshift map



- Intensity map



## • Conclusions

- Radioastron (or/and other VLBI systems in mm and sub-mm bands or MAXIM) could detect mirages (“faces”) around black holes.
- Shapes of images give an important information about BH parameters

- Thanks for your kind attention!

- The report is based on joint works with
- S.V. Repin (IKI RAN);
- F. De Paolis, G. Ingrosso, A.A. Nucita (Lecce University, Italy);
- Z. Ma (NAOC, Beijing, China);
- P. Jovanovic (Astronomical Observatory, Belgrade, Serbia)

## Conclusions

- Now the detailed structure of accretion disks is still unknown (in particular we do not know a thickness of accretion disks).
- Therefore, there is a possibility to observe highly inclined accretion disks (about 1% of all AGNs should have such high inclination. The situation is much better for microquasars; because of possible precession of accretion disks (for example, SS433).

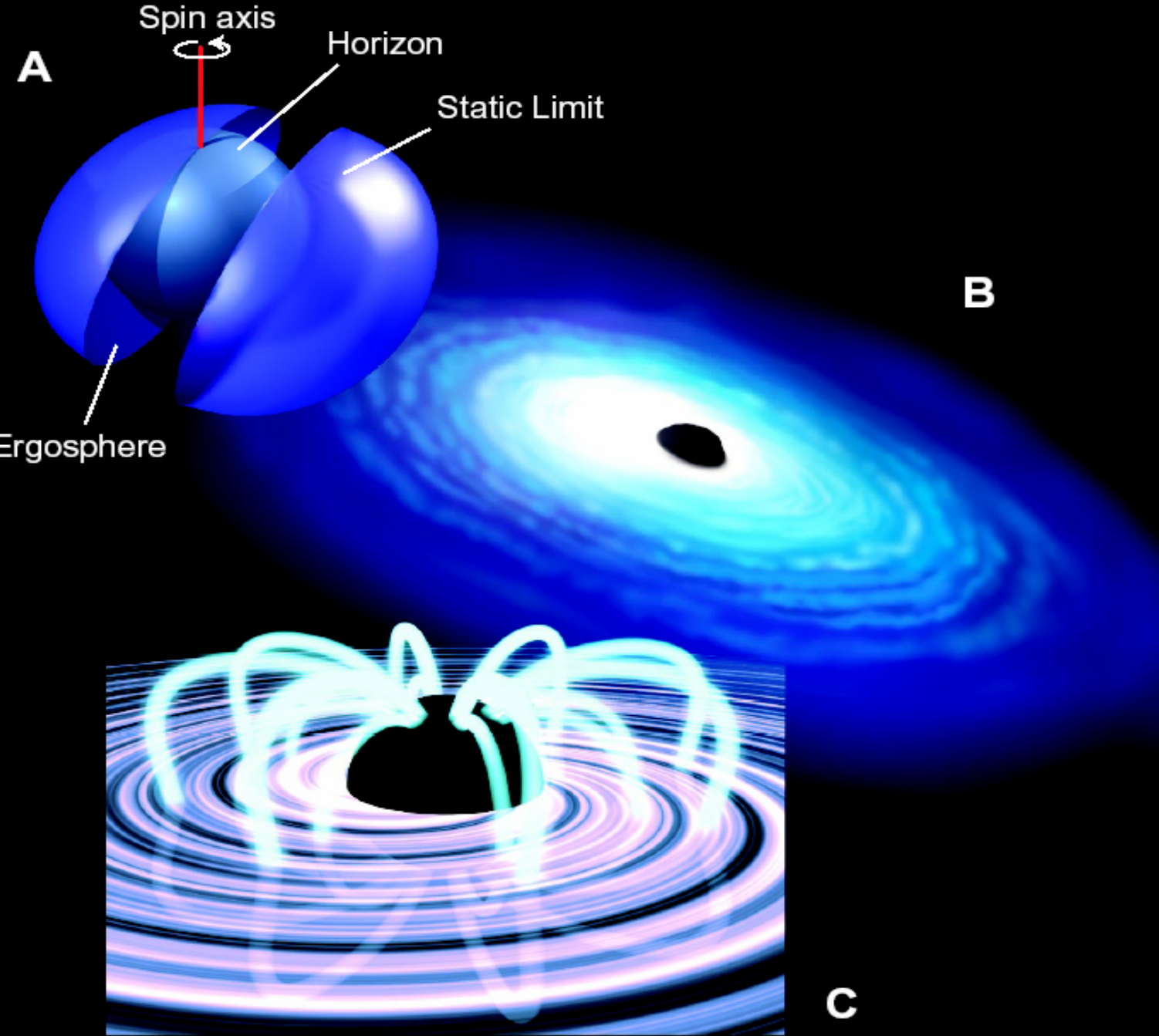
In this case this analysis could give us a useful tool for a determination of such high inclination angles, however another factors (which are behind of this simple model) could cause such line profiles.

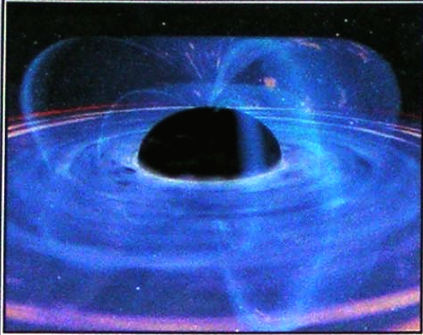
- Distortion of iron line profiles could give essential information about magnetic fields near BH horizons in AGNs and GBHCs.

**Searches for such features of spectral lines could be useful to realize using present and future spacecrafts such as**

**Chandra, XMM, Integral, Constellation.**

- [http://www.aire.org.cn/colloquia/upload\\_files/bh\\_evidence.ppt#21](http://www.aire.org.cn/colloquia/upload_files/bh_evidence.ppt#21)





# 学术报告

北京大学天文系  
北京天体物理中心

Prof. Alexander Zakharov

Institute of Theoretical and Experimental Physics,  
Moscow, Russia

## Measuring Parameters of Supermassive Black Holes with Present and Future Space Missions

时间： 2005年10月20日（星期四），下午3:30

地点： 北京大学理科二号楼2907（天文系会议室）

欢迎参加